NASA CR-169,984

NASA-CR-169984
19830010401

A Reproduced Copy

OF

NASA CR-169,984

Reproduced for NASA

by the

NASA Scientific and Technical Information Facility

FFNo 672 Aug 65

(NASA-CR-169984) PRESSURE INVESTIGATION OF NASA LEADING EDGE VORTEX FLAPS ON A 60 DEG DELTA WING Semiannual Progress Report (Virginia Polytechnic Inst. and State Univ.) 90 p HC A05/MF A01 CSCL 01A G3/02

N83-18672

Unclas 02973

Semi-Annual Progress Report

on

AN EXPERIMENTAL STUDY OF PRESSURES ON 60° DELTA WINGS WITH LEADING EDGE VORTEX FLAPS

(NAG-1-274)

by

J. F. Marchman, III
Denise Donatelli
James R. Terry

Aerospace and Ocean Engineering Department
Virginia Polytechnic Institute and State University
Blacksburg, VA

February 28, 1983

N83-18672 #

PRESSURE INVESTIGATION OF NASA LEADING EDGE VORTEX FLAPS ON A 60° DELTA WING

by
James f. Marchman, III,
Denise Donatelli and James Terry

Virginia Polytechnic Institute and State University

ABSTRACT

Pressure distributions on a 60° Delta Wing with NASA designed leading edge vortex flaps (LEVF) were found in order to provide more pressure data for LEVF and to help verify NASA computer codes used in designing these flaps. These flaps were intended to be optimized designs based on these computer codes. However, the pressure distributions show that the flaps were not optimum for the size and deflection specified. A second drag-producing vortex forming over the wing indicated that the flap was too large for the specified deflection. Also, it became apparent that flap thickness has a possible effect on the reattachment location of the vortex. Research is continuing to determine proper flap size and deflection relationships that provide well-behaved flowfields and acceptable hinge-moment characteristics.

This work supported by NASA Langley under Grant No. NAG - 1 - 274

ORIGINAL PAGE IS
OF POOR QUALITY

LIST OF SYMBOLS

α angle of attack (degrees)

δ_f flap deflection (degrees)

C_p pressure coefficient $\left(\frac{p - p_\infty}{q_\infty} \right)$

C_L lift coefficient $\left(\frac{L}{q_\infty S} \right)$

C_m moment coefficient $\left(\frac{M}{q_\infty SC} \right)$

L/D lift to drag ratio

p local static pressure

p_∞ freestream static pressure

q_∞ freestream dynamic pressure $\left(\frac{1}{2} \rho V_\infty^2 \right)$

L lift force (lb)

M pitching moment (ft-lb)

C root chord (ft)

S planform area (ft^2)

ρ density $\left(\frac{slug}{ft^3} \right)$

V_∞ freestream velocity $\left(\frac{ft}{sec} \right)$

LIST OF FIGURES

TABLE OF CONTENTS

INTRODUCTION

During the last few years, many studies have been conducted to develop the concept of and demonstrate the effectiveness of leading edge vortex flaps (LEVF) on highly swept delta wings.[1-5] The design of the LEVF allows the flow to separate at the leading edge and roll up into a vortex over the upper surface of the flap (Figure 1). Because of the downward deflection of the flap, the low pressures developed by the vortex produce a thrust component on the flap. If the vortex travels inboard onto the wing, the low pressures produce a force which contributes to the drag. Therefore, the reattachment of the flow must be as close as possible to the wing-flap junction in order to confine the vortex to the flap surface. This resulting thrust component effectively reduces drag and give higher lift-to-drag ratios to improve subsonic performance capabilities.

Force tests conducted at Virginia Tech have indicated this significant improvement of the drag characteristics of these wings with LEVF.[1] There is now a need for pressure surveys to understand more about the vortex formation on the wing and flap. Since there is very little existing pressure data for LEVF,[6-7] the present investigation has a dual purpose: 1) to obtain these local pressures, and 2) to verify the validity of computer codes written by NASA Langley with this experimental pressure distribution data. If the validity of computer codes that predict vortex flap aerodynamics can be confirmed, expensive wind tunnel testing can be reduced by using these codes for optimization of the flap design.

The LEVF used in the studies performed in Virginia Tech's Stability Wind Tunnel were designed by a classified computer code at NASA Langley. These flaps were tested on a 60° half delta wing mounted on the wind tunnel floor as shown in Figure 2. By using a semi-span wing, a larger model could be built, allowing a greater number of pressure parts to be installed on the flap and wing. Since delta wings tend to be relatively thin (i.e., small surface curvatures), a flat plate approximation was assumed in the construction of the wing. The NASA flaps were tested with and without an idealized fuselage scaled to represent an F-106 since current NASA plans call for testing of LEVF on an F-106 delta wing aircraft. The purpose of the fuselage tests was to determine if the presence of the fuselage significantly affects the flowfield over the wing. The experiment was then expanded to include pressure and force data comparisons with other LEVF previously tested at Virginia Tech[3] and attempts were made to further improve the flap's effect on the flowfield.

TEST PROCEDURE

For the pressure investigation, a wing model of 50 inch root chord and 29 inch semi-span was constructed from two sheets of 3/4" plywood laminated togetner. Four channels were routed out spanwise in the center of the wing for pressure tubing. Four rows of copper tubing were inlaid in the surface of the wing. Each tube was inlaid such that the rows of taps could be drilled to lie either perpendicular to the root chord or perpendicular to the leading edge as shown in Figure 3.

Two flaps designs were provided by NASA, a full span flap (VPI-8) and a part span flap (VPI-10) (Figure 4). The VPI-8 flap spans the entire leading edge of the wing model while the VPI-10 is specially scaled to allow the addition of a fuselage to the same wing model. Each NASA flap was cut from a single fir two-by-four and pressure taps were aligned with those rows on the wing perpendicular to the root chord (a NASA specification). Two sets of flaps were made, one with a 15^{o} and the other a 30^{o} chordline deflection. All the wooden surfaces were sanded and sealed.

The fuselage model was made from a 10 foot long styrofoam half-cylinder (5.75 inch radius) with one end shaped into a nose. The fuselage radius was selected to simulate an F-106 fuselage. The styrofoam was covered with layers of putty and epoxy to give a smooth, hard surface. The wing was mounted vertically on a turntable which, when rotated, gave the desired angles of attack (Figure 2).

Tests were conducted in the six-by-six foot straight test section of Virginia Tech's Stability Wind Tunnel. This tunnel was originally the NACA Stability Tunnel at Langley Field and is a continuous flow, subsonic facility with a freestream turbulence of less than 0.05%. Testing was usually done at a Reynolds number of 2.2×10^{6} and the angles of attack ranged from 0^{o} - 10^{o} in 2^{o} increments and 11^{o} - 15^{o} in 1^{o} increments. Pressure data was collected by a Hewlett-Packard (HP) 9825A Data Acquisition system from a Scanivalve pressure scanning manifold and a Setra Systems transducer (range: 0 to $\pm$ 0.25 psig). Also read by the system were the tunnel static and dynamic pressures and temperature from which Reynolds number, velocity, density, viscosity, and pressure coefficients were calculated. The measured pressure coefficients were then plotted on a scale drawing of the wing according to pressure port location.

The force testing was achieved by scaling down the NASA flaps to fit a 60^{o} delta wing that had a 3 foot wing span and 2.667 foot root chord. Two flaps were cut from sheet metal, deflected to 30^{o}, and attached to the leading edges of the wing by small bolts and tape. The tunnel was run at a dynamic pressure of 3.0 inches of water and the angles of attack ranged from 0^{o} - 40^{o} in 5^{o} increments. Forces and moments were measured by strut mounting the wing on a six-component strain gage balance system as shown in Figure 5. This data was collected by the HP Data Acquisition system and reduced to the aerodynamic coefficients which were then printed out and plotted.

Some yawhead pressure probe tests were conducted on the wing at the two center row stations. The yawhead probe used was a five hole pitot probe from which velocity magnitude and direction could be measured. The probe was mounted on a traverse which enabled it to be moved vertically and horizontally along a row of pressure ports (Figure 6). These pressures were collected by the HP Data Acquisition system and the tunnel was run at a Reynolds number of 2.2×10^{6}. The purpose of these tests was to obtain a physical picture of the direction of the flow over the wing and the flap.

Finally, tuft and smoke flow visualizations were done. Both the force and pressure wing models were tufted with 1 inch pieces of yarn and pictures were taken at various angles of attack (Figure 7). The smoke tests were accomplished by using smoke bombs and kerosene smoke.

RESULTS

Force Data Comparison

Force data for flap designs previously tested at Virginia Tech showed that cropped, constant chord flaps (CCCF) and fully tapered flaps (FTF), both at 30^{o} deflections, gave the highest lift-to-drag ratios.[1] Since the NASA flap design appears to be a hybrid combination of the CCCF and FTF, it was suspected that the NASA design would perform as well as the previous designs. The force data taken for the NASA VPI-8 flap (full span) showed that this was true. Figure 8 shows that the NASA flap is a good compromise between the CCCF and the FTF, incorporating the higher lift-to-drag ratio of CCCF while maintaining the desirable pitching properties of the FTF. The reduced pitch-up tendency of the NASA flap is due to the smaller flap area near the nose of the delta wing. Yet, even with the smaller flap design, the NASA flap's low drag and high lift-to-drag ratio is some evidence of the flap's ability to maintain a vortex over the majority of its length.

Pressure Analysis

In modeling the wing and flap for surface pressure measurements, appreciable thickness was added to the model for structural strength. The flap model for the force measurements had essentially no thickness (sheet metal construction) and while the delta wing had some thickness, its thickness ratio was approximately three times smaller than that for the wing pressure model.

Since the NASA computer code used to predict surface pressures over the wing-flap system does not take into account flap or wing thickness, questions about the validity of comparing the computer and force results to the measured pressure results arise. If a valid comparison can be made, the primary questions become: 1) how should thickness be accounted for and 2) how should the flap deflection be defined on the model with thickness?

At first, the flap angle was defined from the flap surface and tested at 30^{o} surface deflection for both the CCCF and the VPI-8. Data for these VPI 8 flaps are shown in Figures 21 to 31. At angles of attack from 0^{o} to 2^{o}, no vortex had appeared on either of the flaps. Low pressures were seen at the flap wing hinge line due to local flow acceleration around the hinge line. At 4^{o} angle of attack, negative pressures began to appear on the flap. By 8^{o} angle of attack, strong negative pressures indicated a vortex on the flap. The design cruise angle of attack for the test system is approximately 11^{o} according to NASA and the pressure distribution for this angle of attack for the VPI-8 is shown in Figure 27. Two problems are evident from Figure 27; first, the reattachment line for the vortex washes over onto the wing and secondly, the vortex as a whole moves off the flap and onto the wing just on the aft portion of the wing. Both of these actions do not allow the full effect of the vortex to be used and also results in excess drag. As angle of attack is increased further, both of these effects grow worse. A more optimal angle of attack appears to be around 10^{o} (Figure 26). Here, the reattachment is along the hinge line and the vortex movement off the flap is minimal. Also, several runs were made at different Reynolds numbers (2.2×10^{6}, 2.8×10^{6}, and 3.7×10^{6}) and the pressures proved to be independent of Reynolds number in the range tested.

Due to the size of the CCCF, reattachment washover was not a problem, but the CCCF are apparently too large since the reattachment line is on the flap. The results for these flaps are shown in Figures 12 to 20. However, the problem of vortex movement onto the wing was also seen on the CCCF.

A comparison between the 30^{o} surface deflection data and the NASA computational results showed that the two did not agree. This disagreement led NASA to suggest a redefinition of the flap angle as the centerline or chordline deflection, thus a surface deflection of 45^{o} was used. Testing of the VPI-10 and the VPI-8 with a 30° chordline deflection also included fuselage tests with the VPI-10 flaps. The pressure distributions at this 30° chordline deflection for the VPI-8, as shown on Figures 32 to 41, were found by NASA to agree with their computational results. Since the NASA results have not yet been released for publication, a comparison cannot be included in this report.

If the flap chordline is the important reference line for the system, then Figure 9 shows how thickness can affect the location of the reattachment line of the vortex. If the thickness is too small for a given deflection, the vortex will reattach or impact over the wing which results in inefficient use of the vortex and added drag. A wing that is too thick causes the vortex to impact too early on the flap resulting in a non-optimized flap design due to excess flap area. Also, if the hinge line is sharp enough, the reattached flow could separate again at the hinge line and create a drag producing vortex over the wing.

Figure 38 shows the pressure distribution for the VPI-8 flap at 11° angle of attack and a 30° chordline deflection. On the forward half of the flap, the flow reattachment line is on the flap itself and a second vortex appears to have been formed as just described by the flow separating at the hinge line. This second vortex is present at angles of attack greater than 4° and has also been observed in some NASA tests. The problem of the vortex moving off the flap onto the wing appears to have been eliminated with these flaps as the NASA design shows one flap vortex maintained over the full length of the flap.

The early impact of the vortex on the VPI-8 flap tends to indicate that the flap is oversized (chordwise). Yet, as already stated, this early impact could also be due to excessive model thickness. If the thickness ratio was scaled down to a more realistic size, the impact point may be closer to or even be at the hinge line, eliminating the second vortex found on the wing.

When the pressure results from the VPI-8 flap at the two different deflections are compared with the force data results of the same flap at a surface deflection of 30°, the pressure model at the same surface deflection (i.e., 15° chordline deflection) showed the best correlation. The maximum lift-to-drag ratio was achieved around 7° to 8° as shown in Figure 8. The 15° chordline deflected flap showed a much better pressure distribution than the 30° chordline deflected flap at this angle of attack (Figures 25 and 36). The 30° case only shows a second vortex over the wing and does not devel[illegible] a substantial flap vortex until 11°. Even then, the second vortex is still present, so a maximum lift-to-drag ratio could not be achieved until at least 11° angle of attack. The 15° case, however, shows its best pressure distribution in the 8° - 10° angle of attack range.

Smoke, tuft and yawhead probe flow visualizations were conducted in order to find the extent and origin of the second vortex. Smoke tests proved inconclusive due to the smoke stream being larger than the vortex and, therefore, covering the details of the flow. The tufts and yawhead probe results, however, indicated that the second vortex formed due to the flow separation at the hinge line. Both the flow visualizations showed the flow accelerating off the flap and over the hinge line. The yawhead tests verified this conclusion showing a circulating flow resulting from separation off the flap-wing hinge line (Figures 10 and 11).

It appears that in order to properly optimize a flap design the correct thickness ratio must first be modeled. Flap size and deflection can be optimized to provide the best compromise for the resulting thrust produced by the flap. The question which must be answered is, is it better thrust-wise and hinge moment-wise to have a higher flap deflection with a smaller vortex on a smaller flap or to have a less steep flap deflection with a larger vortex on a larger flap? It would also be advantageous to investigate how to eliminate or at least lessen the likelihood of the formation of the second vortex over the wing in the case of early vortex impact at some off-design condition. It is planned at Virginia Tech to see how the rounding of the hinge line will affect the formation of the second vortex. Also work will be attempted on actually optimizing the NASA flap size and deflection.

One simple modification was tested on the VPI-8 at a 30° surface deflection (15° chordline deflection). Since the only apparent problem at this flap deflection was vortex movement, a flap extension was added on to the rear portion of the original flap. Since this extension was made of metal (i.e., it had almost no thickness), it was tested at two different deflections: one at the surface deflection and the other at the chordline deflection of the flap. No appreciable difference was found in the pressure distribution, though, due to varying the deflection of the extension. It was hoped that the vortex formed by the extension would pull the original vortex back onto the flap. Figures 64 to 75 show that the extension does maintain the vortex over the original flap.

The VPI-10 tests with and without the fuselage showed that the fuselage had no significant effect on the flap-wing flowfield for the zero yaw case (Figures 42 to 63).

CONCLUSIONS

Both goals of this investigation were met: the acquisition of pressure data for the LEVF-wing combination and the verification of NASA computer generated results for a given NASA flap design.

In obtaining this data, several optimization problems became evident. First of all, the problem of thickness and its possible effect on the position of the flow reattachment became apparent. Also, the tradeoffs between flap size and deflection need to be more thoroughly examined in order to achieve the best compromise between thrust and hinge moments generated.

REFERENCES

1. Marchman, J. F., "Effectiveness of Leading Edge Vortex Flap on 60 and 75 Degree Delta Wings," J. of Aircraft, Vol. 18, April 1981, pp. 280-286.

2. Marchman, J. F., and Thomas, R. H., "Effect of Yaw on Leading Edge Vortex Flap Aerodynamics,: AIAA Paper 81-1660, AIAA, Aug. 1981.

3. Yip, L. P., and Murri, D. G., "Effect of Vortex Flaps on the Low Speed Aerodynamic Characteristics of an Arrow Wing," NASA TR 1914, Sept. 1981.

4. Runyan, J. L., Middleton, W. D., and Paulson, J. A., "Wind Tunnel Test Results of a New Leading Edge Flap Design for Highly Swept Wing - A Vortex Flap,: NASA CP 2108, "Supersonic Cruise Research '79," Nov. 1979, pp. 131-147.

5. Campbell, J. F. and Huffman, J. K., "Experimental Results of a Leading Edge Vortex Flap on a Highly Swept Cranked Wing," NASA CP 2162, pp. 563-580, October 1981.

6. Rao, D. M., and Tingas, S. A., "Subsonic Balance and Pressure Investigation of a 60-Degree Delta Wing with Leading-Edge Devices (Data (Report)," NASA CR 165806, Nov.1981.

7. Wentz, W. H., Jr., "Effects of Leading-Edge Camber on Low-Speed Characteristics of Slender Delta Wings," NASA CR-2002, October 1972.

Figure 1 Formation of Vortex on Leading Edge Vortex Flap and Resultant Force(1)

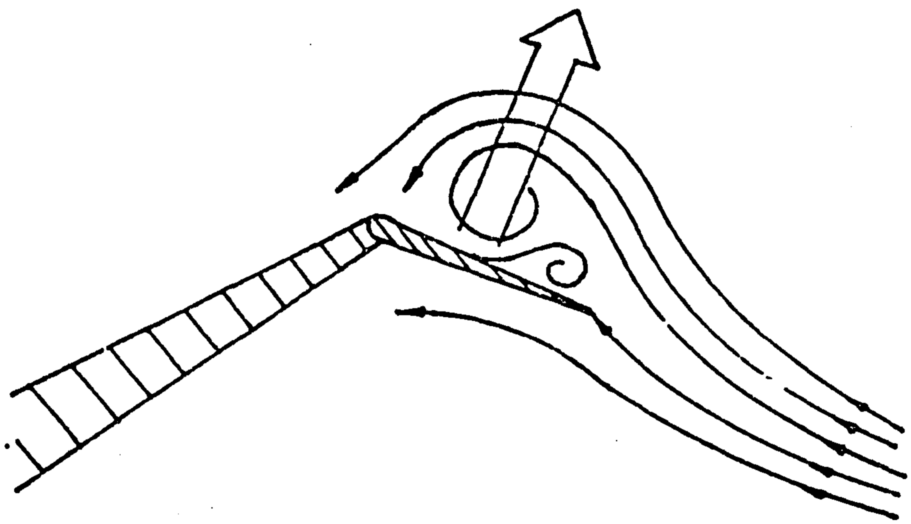

Figure 2 Model Mounting in VPI 6' x 6' Stability Wind Tunnel (Configuration Shown is VPI-10 Flap with Fuselage).

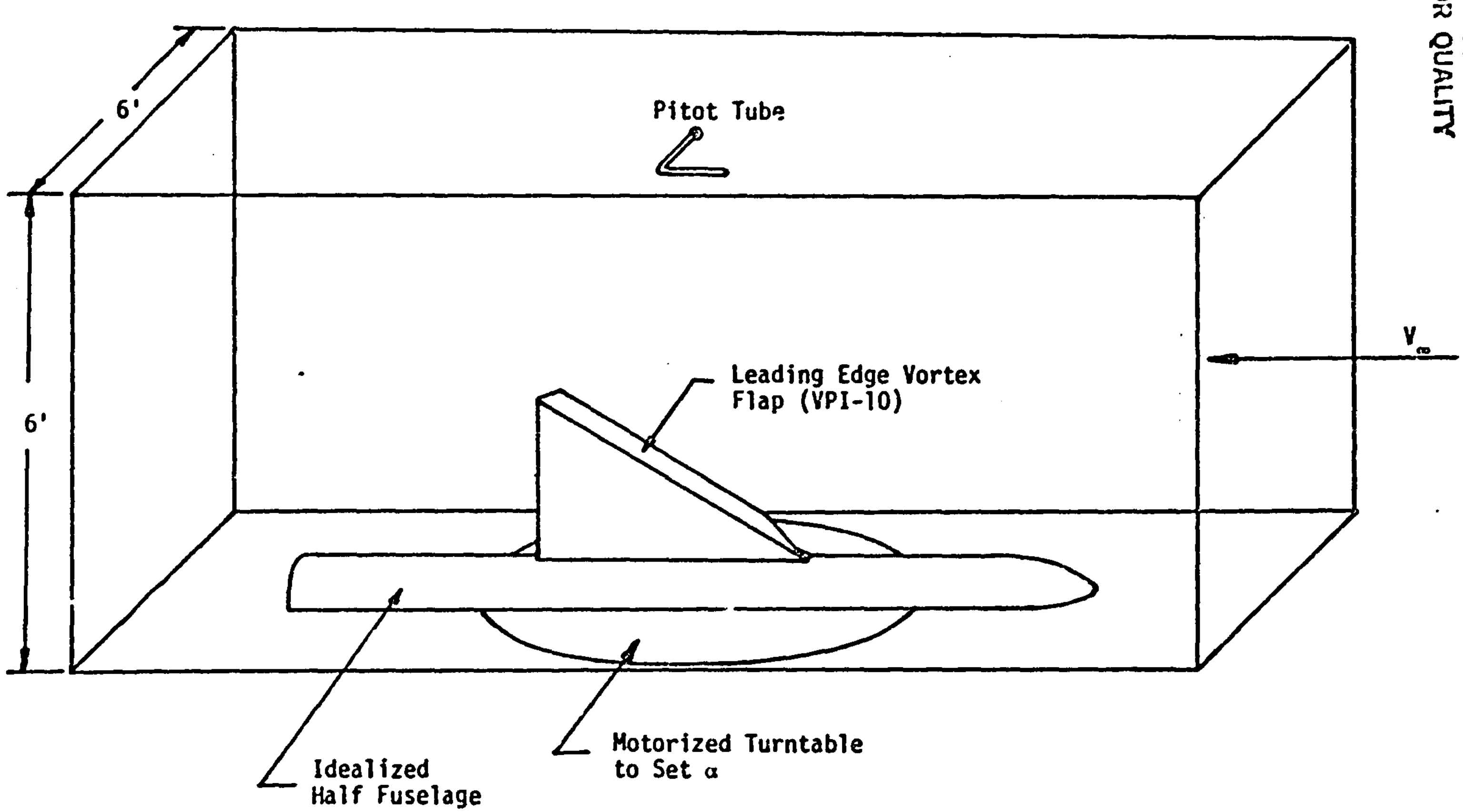

Figure 3 60 Degree Wing Model Dimensions and Port Locations (without flap)

Note: Wing Secured to Turntable by Steel "L" Brackets Inlaid Into Both Wing and Turntable

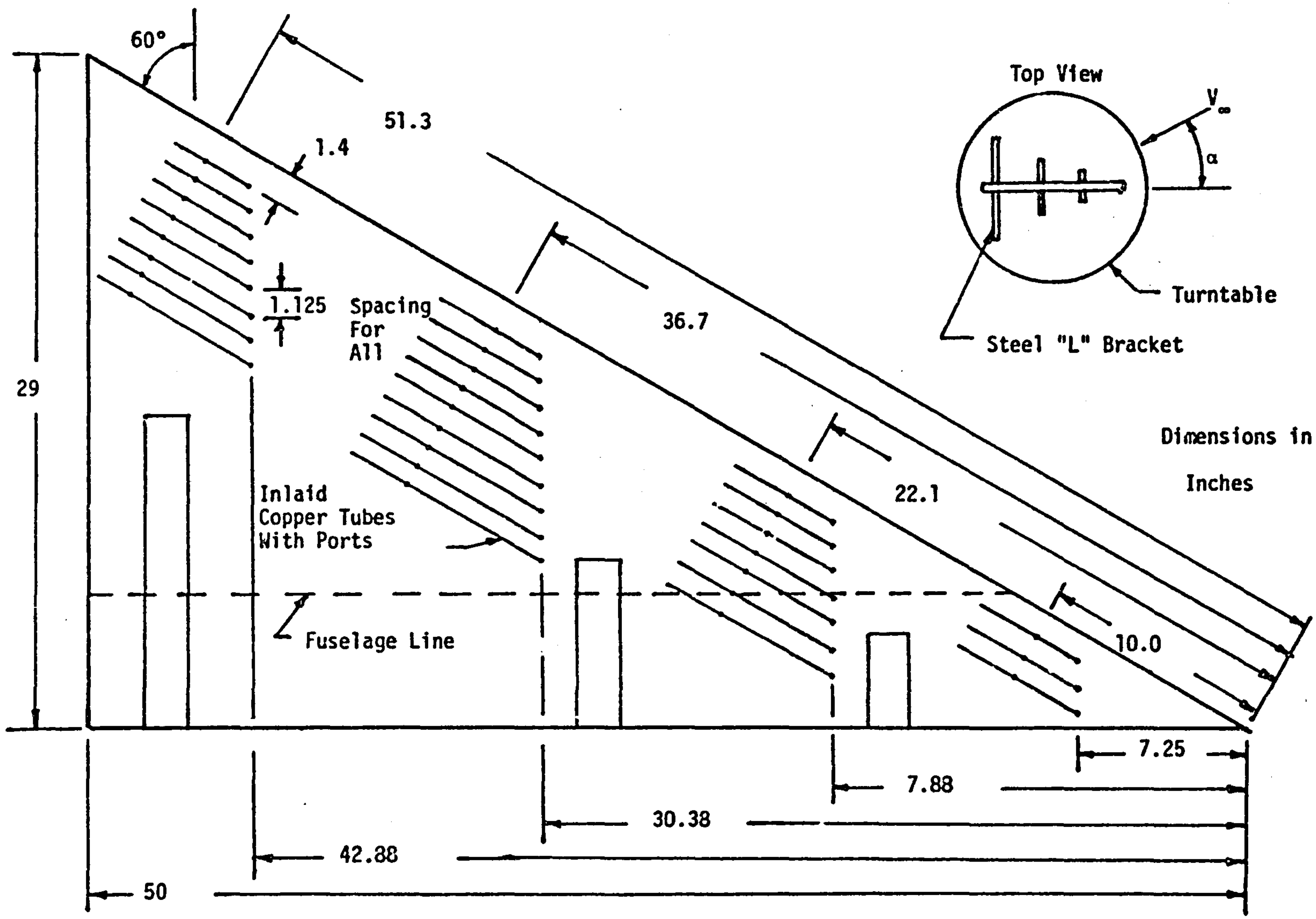

Figure 4 Pressure Flap Model Configurations and Port Locations

All Ports Equally Spaced

Dimensions in Inches

VPI-8: Port Rows Align With Wing Port Rows Perpendicular to Root Chord

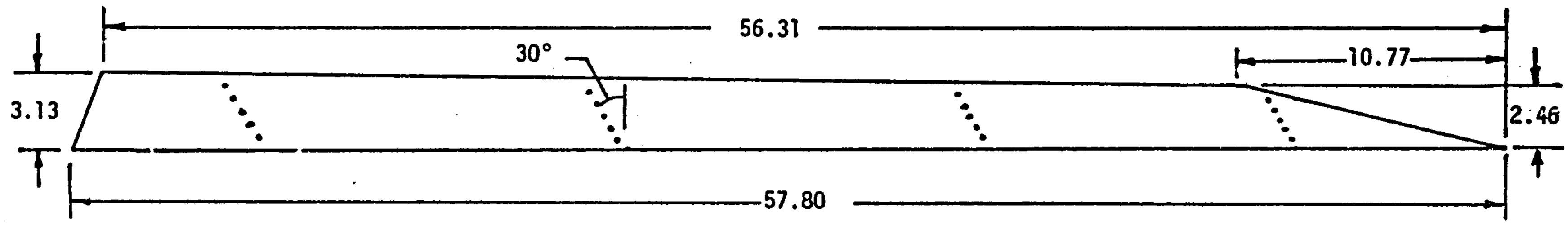

VPI-10: Port Rows Align With Wing Port Rows Perpendicular to Root Chord

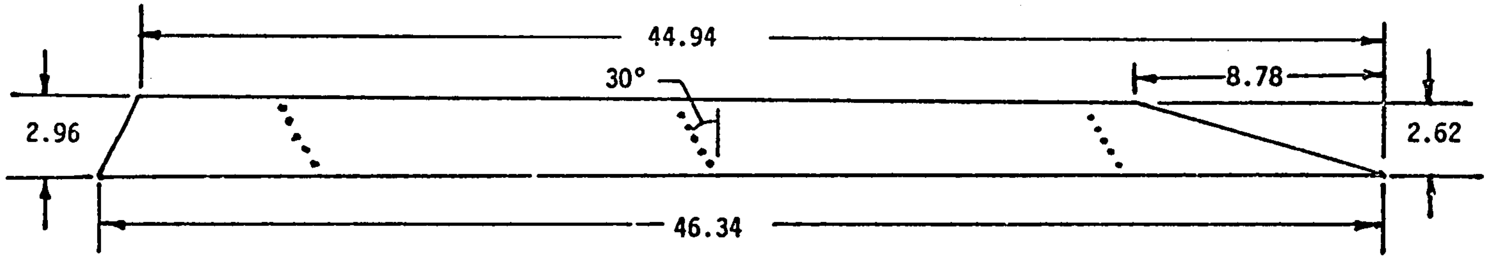

CCCF: Port Rows Align With Wing Port Rows Perpendicular to Leading Edge

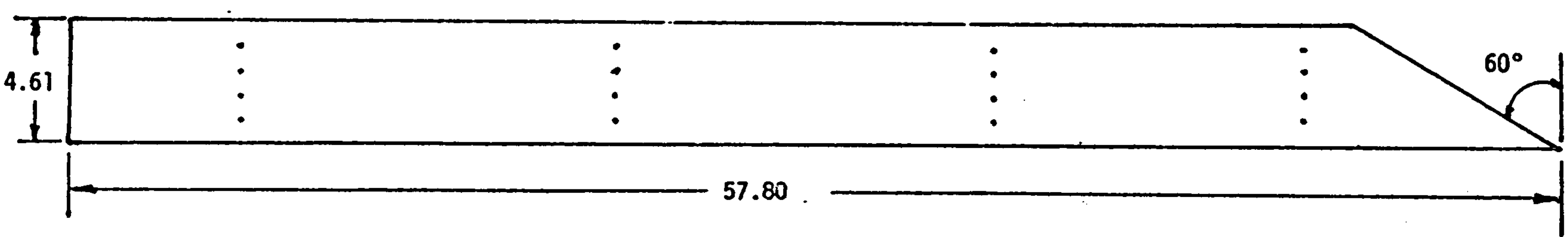

ORIGINAL PAGE IS
OF POOR QUALITY

Figure 5 Strut Mounted 60° Delta Wing with VPI-8 LEVF.

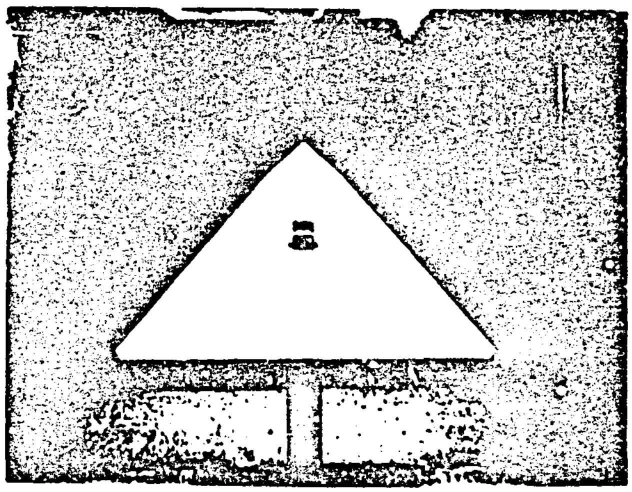

ORIGINAL PAGE IS
OF POOR QUALITY

Figure 6 Yaw Head Probe Setup on 60° Half Delta Wing with VPI-8 LEVF.

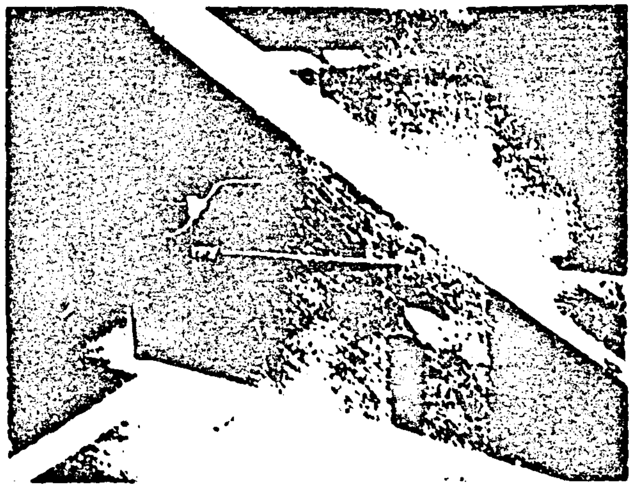

Figure 7 Tufted 60° Half Delta Wing with VPI-8 LEVF.

Figure 8 Performance of the NASA VPI-8 LEVF[1] Compared to Previously Tested LEVF

ORIGINAL PAGE IS OF POOR QUALITY

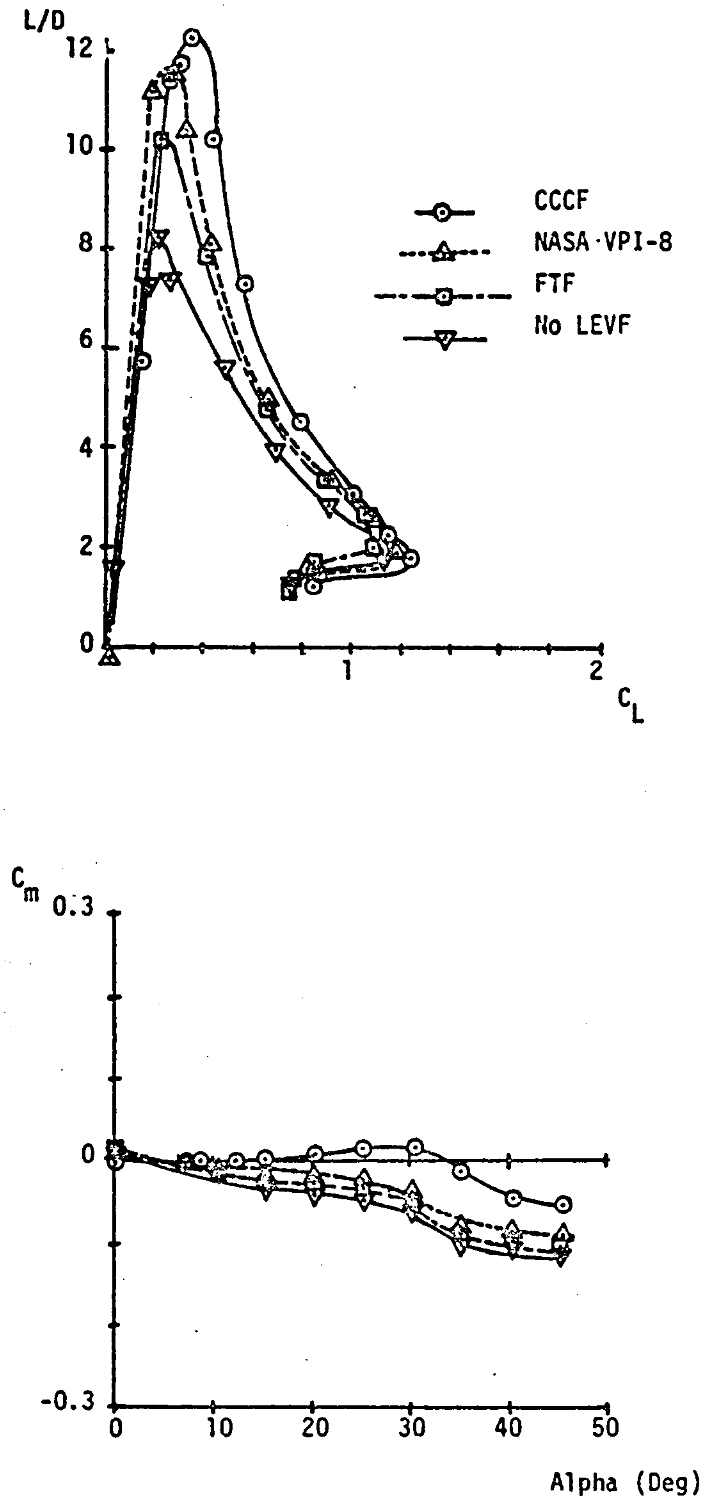

Figure 9 Possible Effect From Thickness Variation on Vortex Reattachment Position

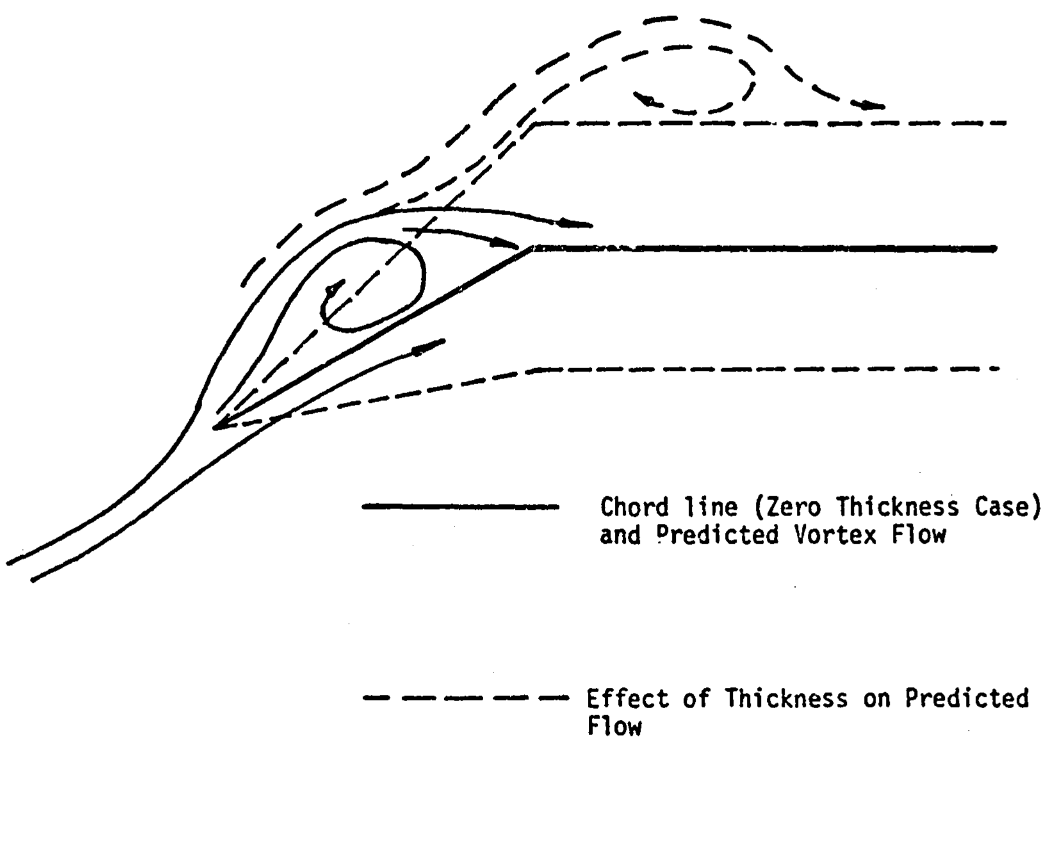

Figure 10 Yawhead Probe Results at Second Port Row (x = 17.88")
Cross Section is Perpendicular to Root Chord
Upstream is into Page.
Flap: VPI-8, $\delta_f = 30^0$.

ORIGINAL PAGE IS
OF POOR QUALITY

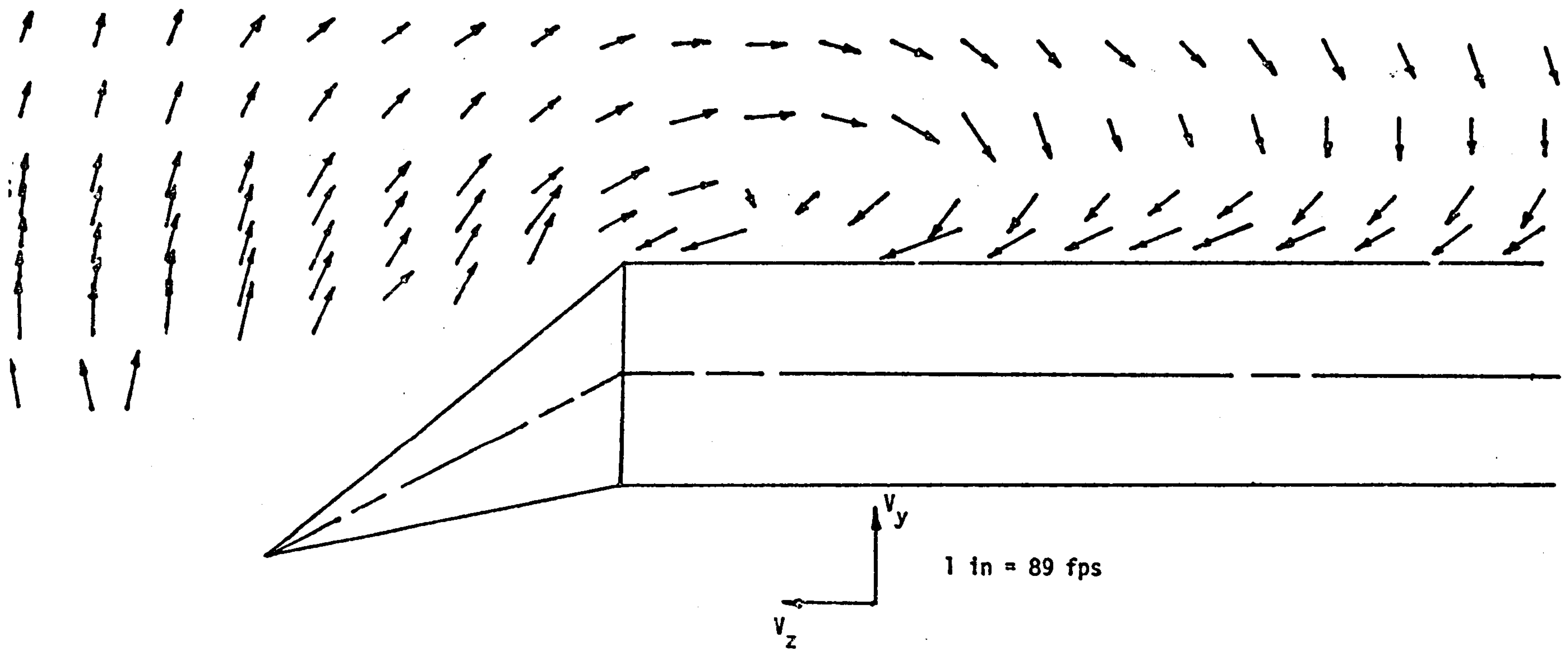

Figure 11 Yawhead Probe Results at Third Port Row (x = 30.38")
Cross Section is Perpendicular to Root Chord
Upstream is into Page.
Flap: VPI-8, $\delta_f = 30^0$

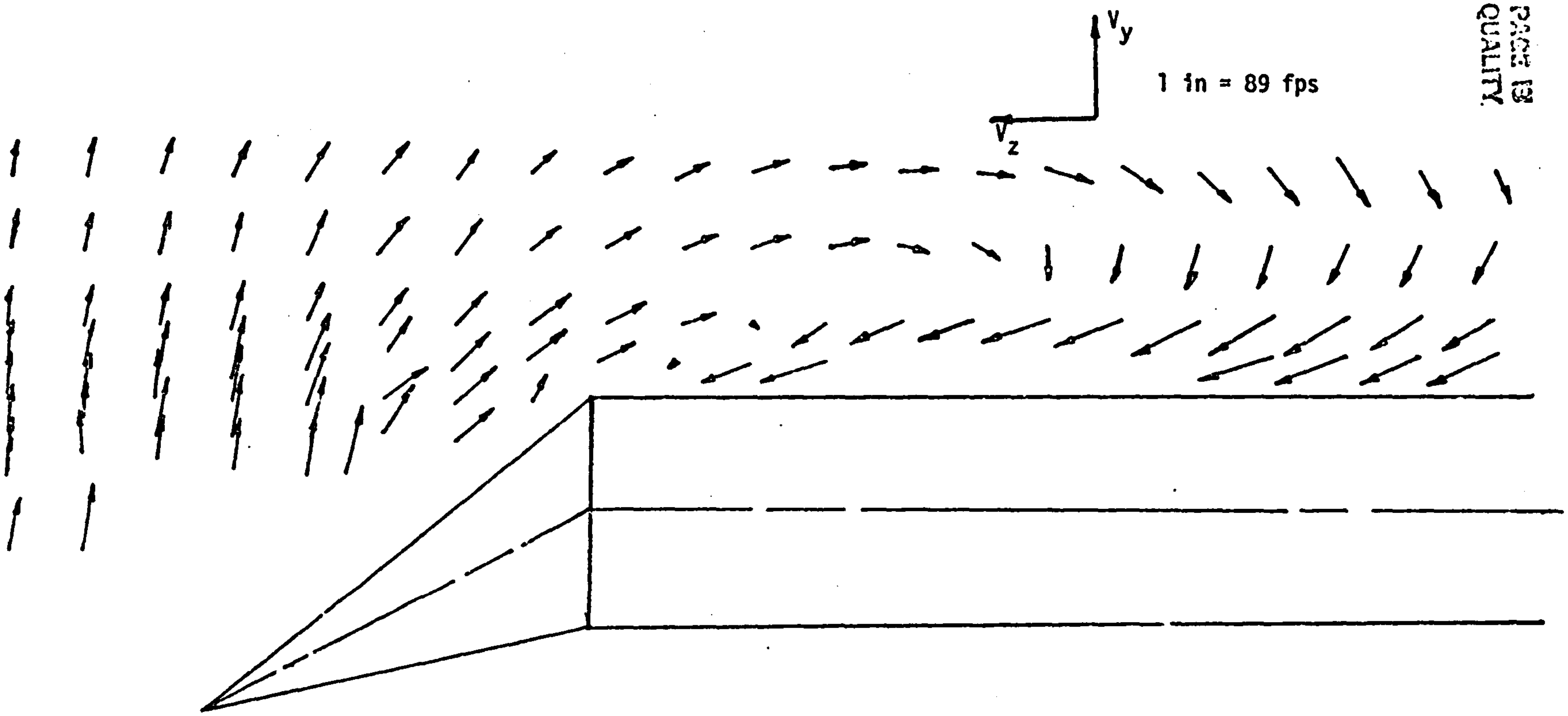

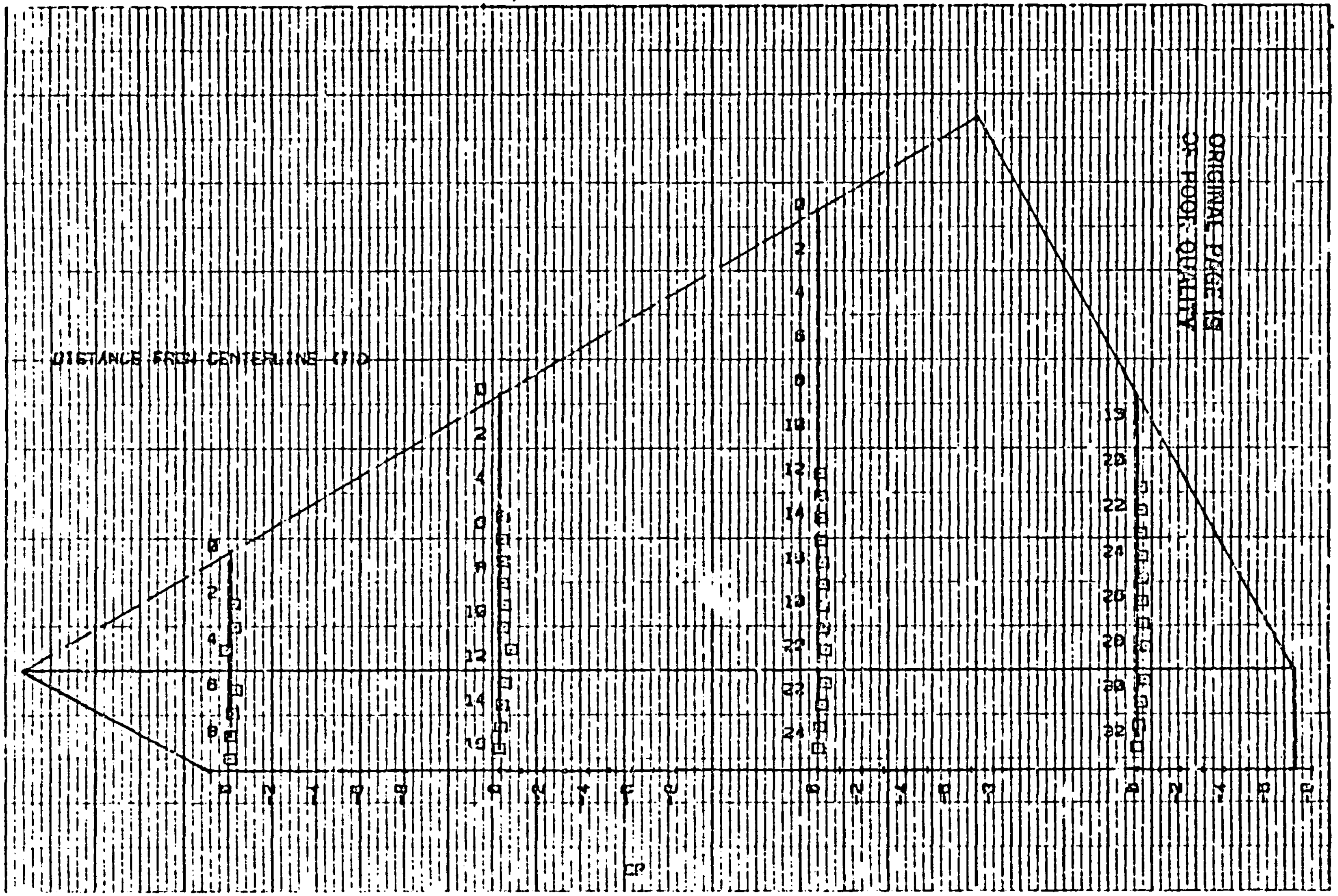

Figure 12 Pressures on CCCF
at $\alpha = 5^{o}$, $\delta_f = 15^{o}$.

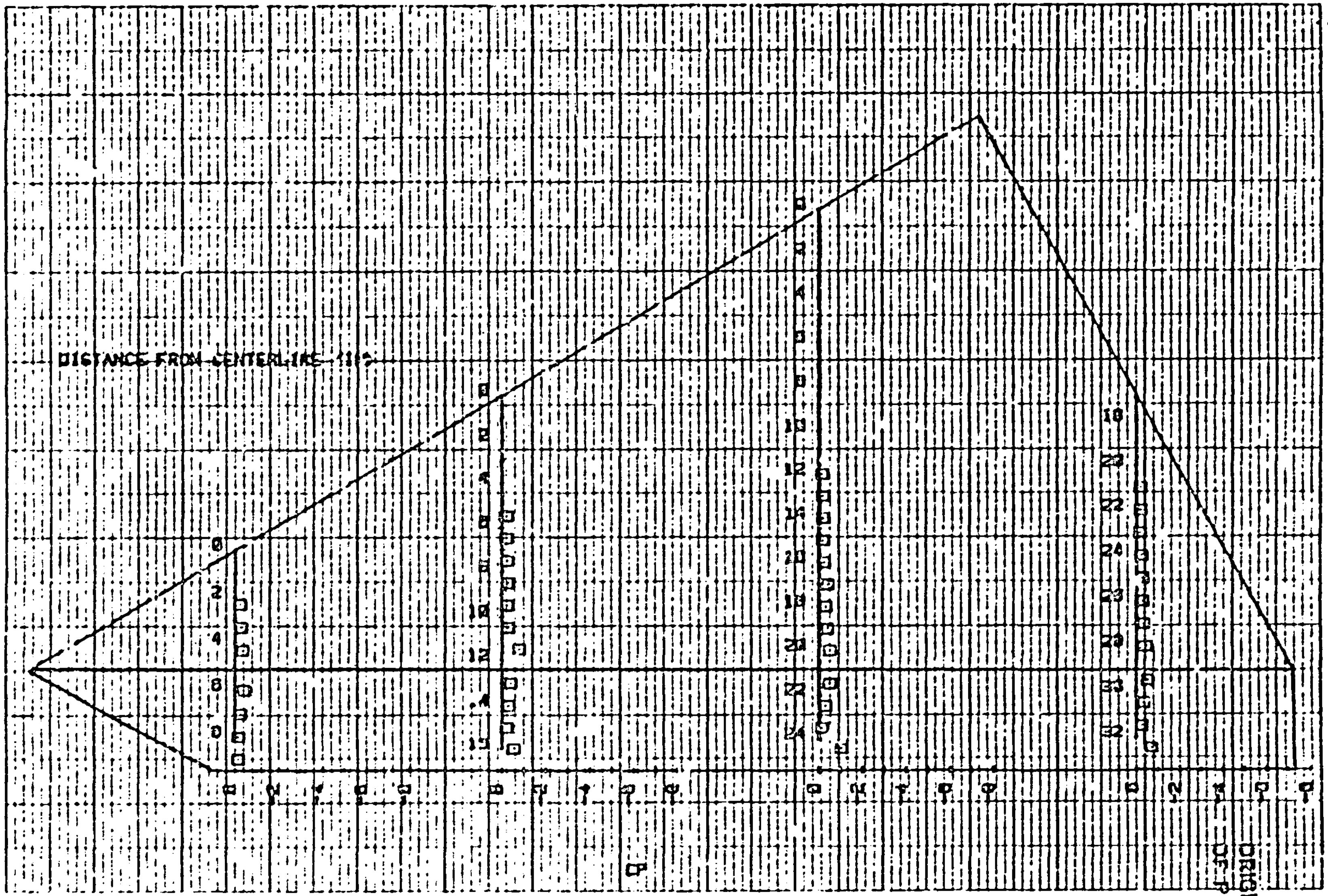

Figure 13 Pressures on CCCF at $\alpha = 10^{o}$, $\delta_f = 15^{o}$.

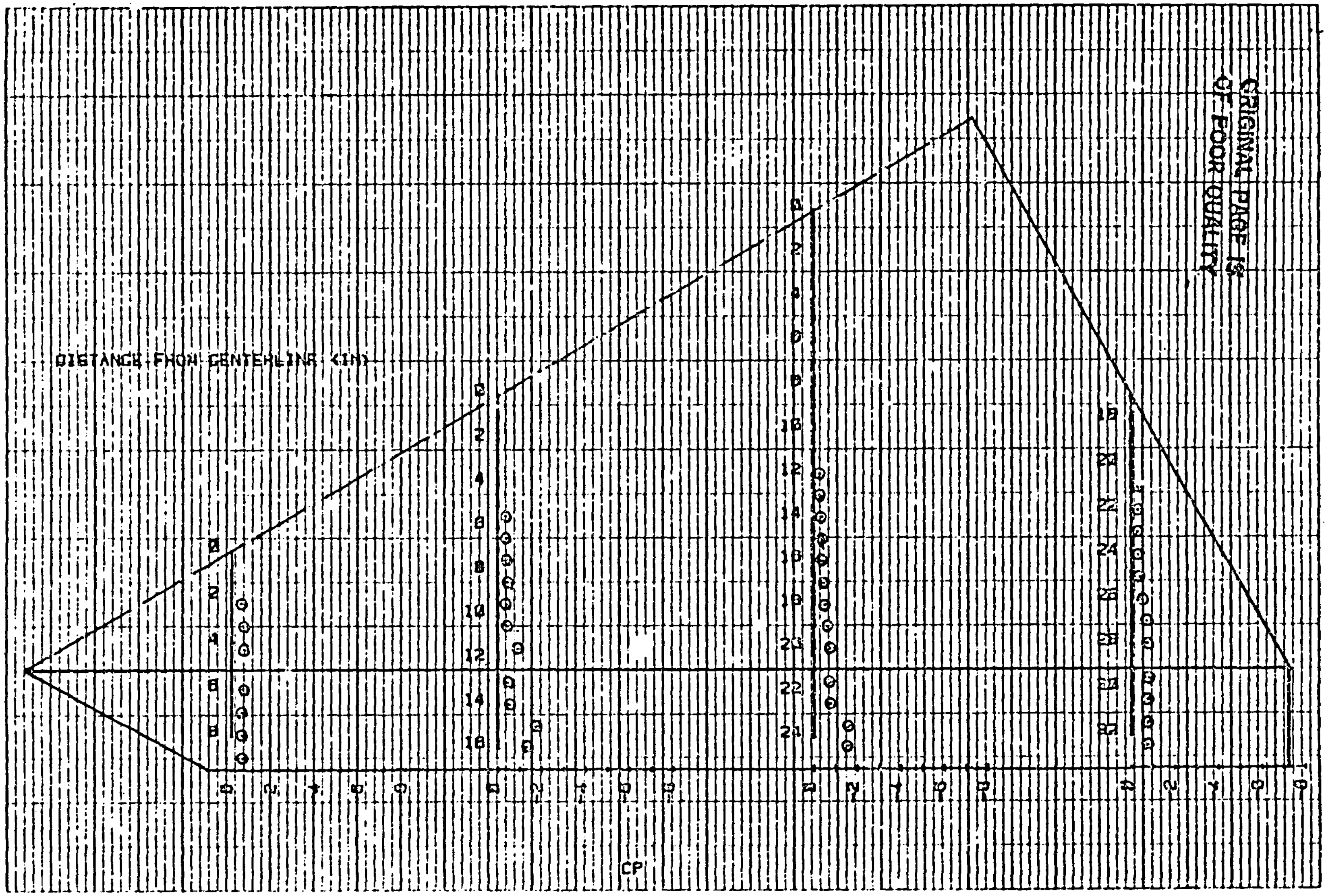

Figure 14 Pressures on CCCF
at α = 15^{o}, δ_f = 15^{o}.

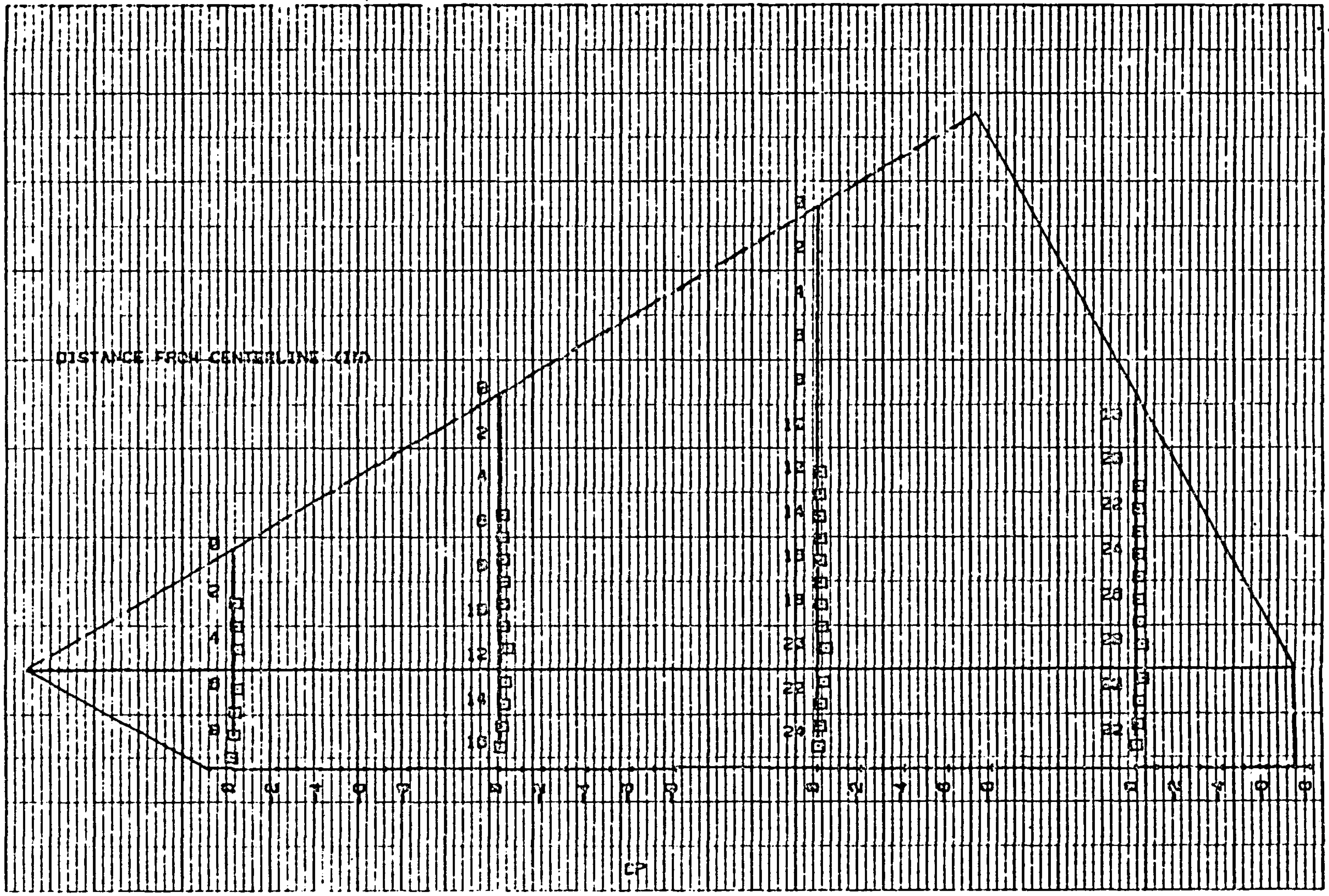

Figure 15 Pressures on CCCF at $\alpha = 5^0$, $\delta_f = 20^0$.

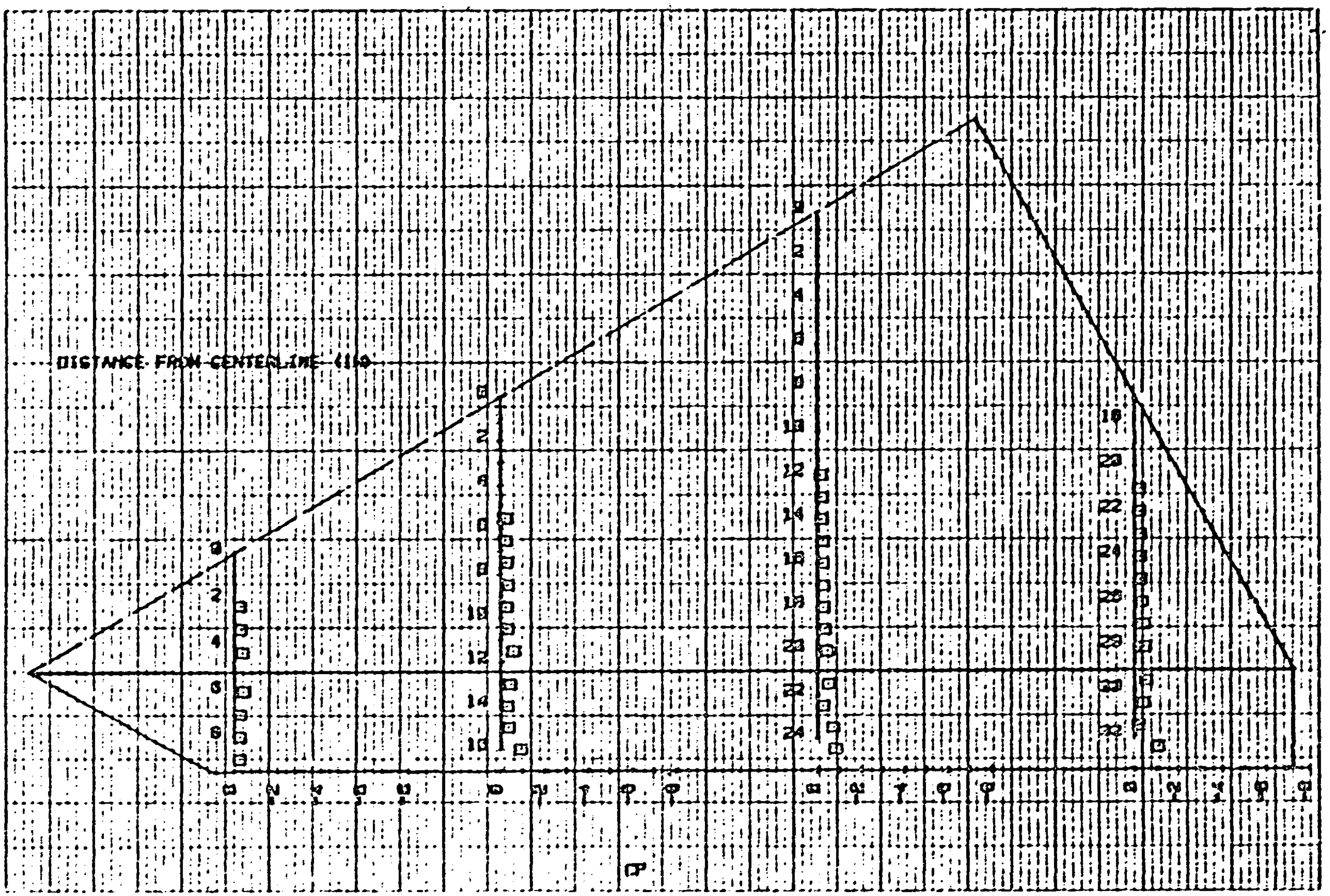

Figure 16 Pressures on CCCF
at α = 10^{0}, δ_{f} = 20^{0}.

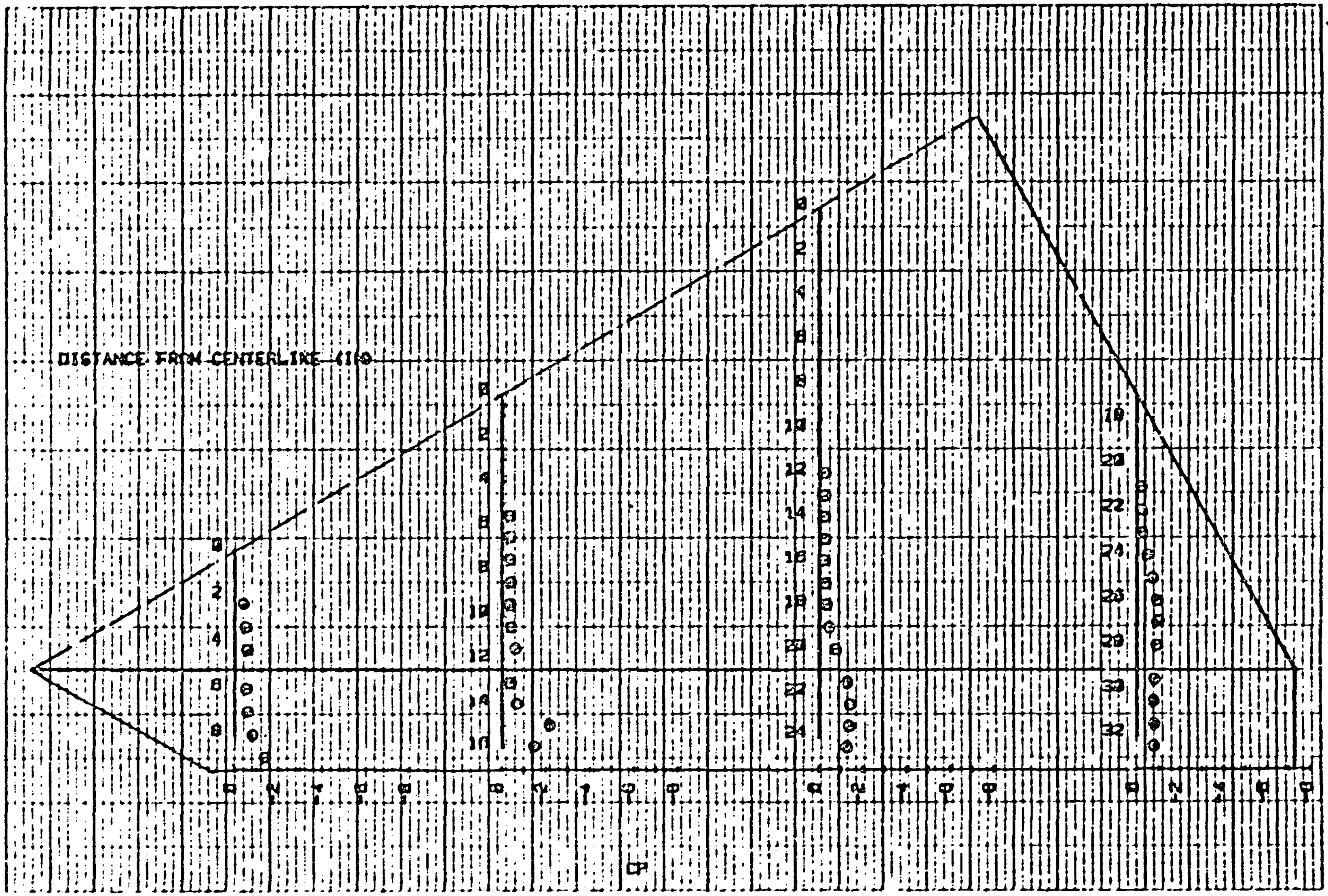

Figure 17 Pressures on CCCF at $\alpha = 15^{0}$, $\delta_f = 20^{0}$.

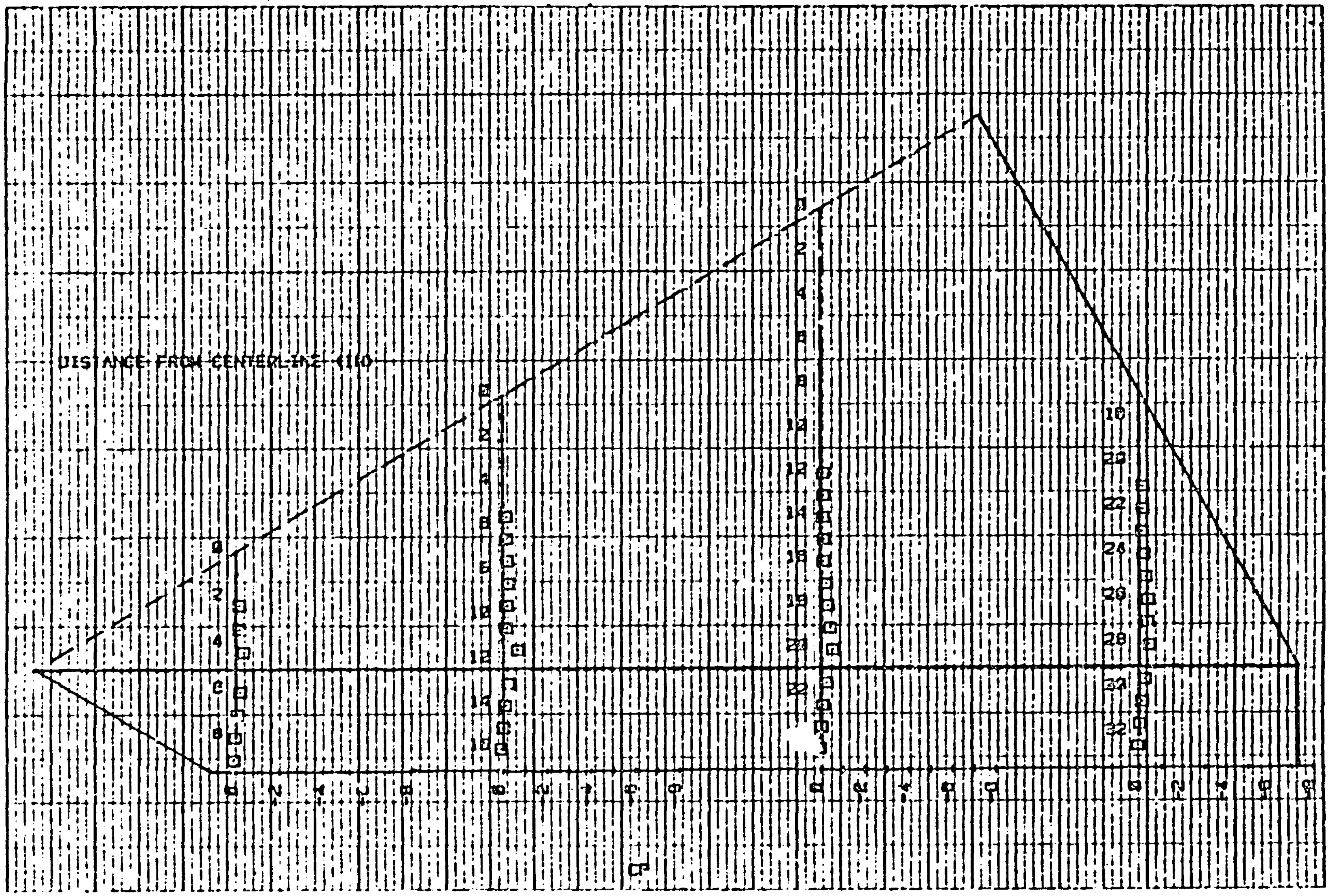

Figure 18 Pressures on CCCF
at $\alpha = 5^0$, $\delta_f = 30^0$.

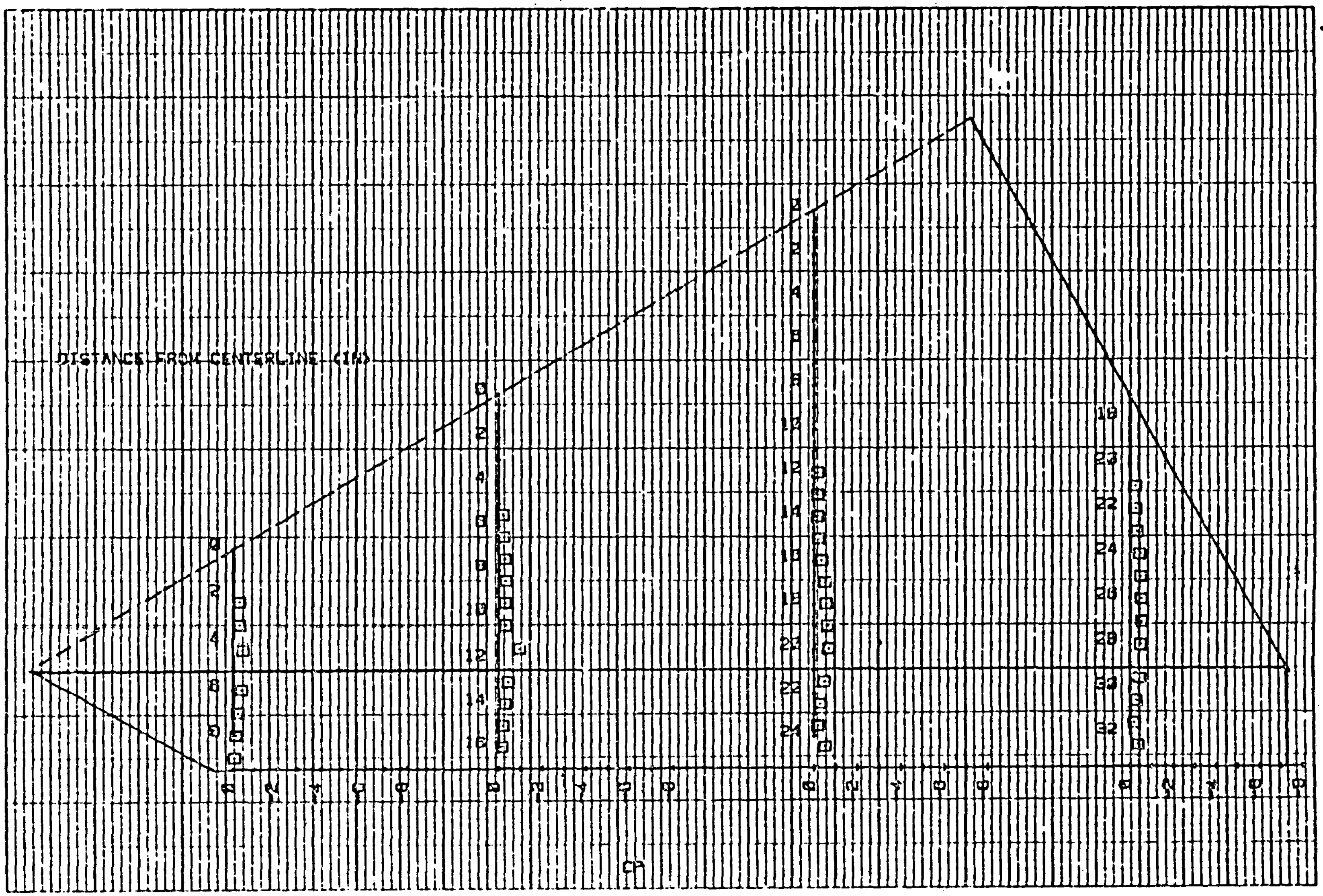

Figure 19 Pressures on CCCF
at $\alpha = 10^0$, $\delta_f = 30^0$.

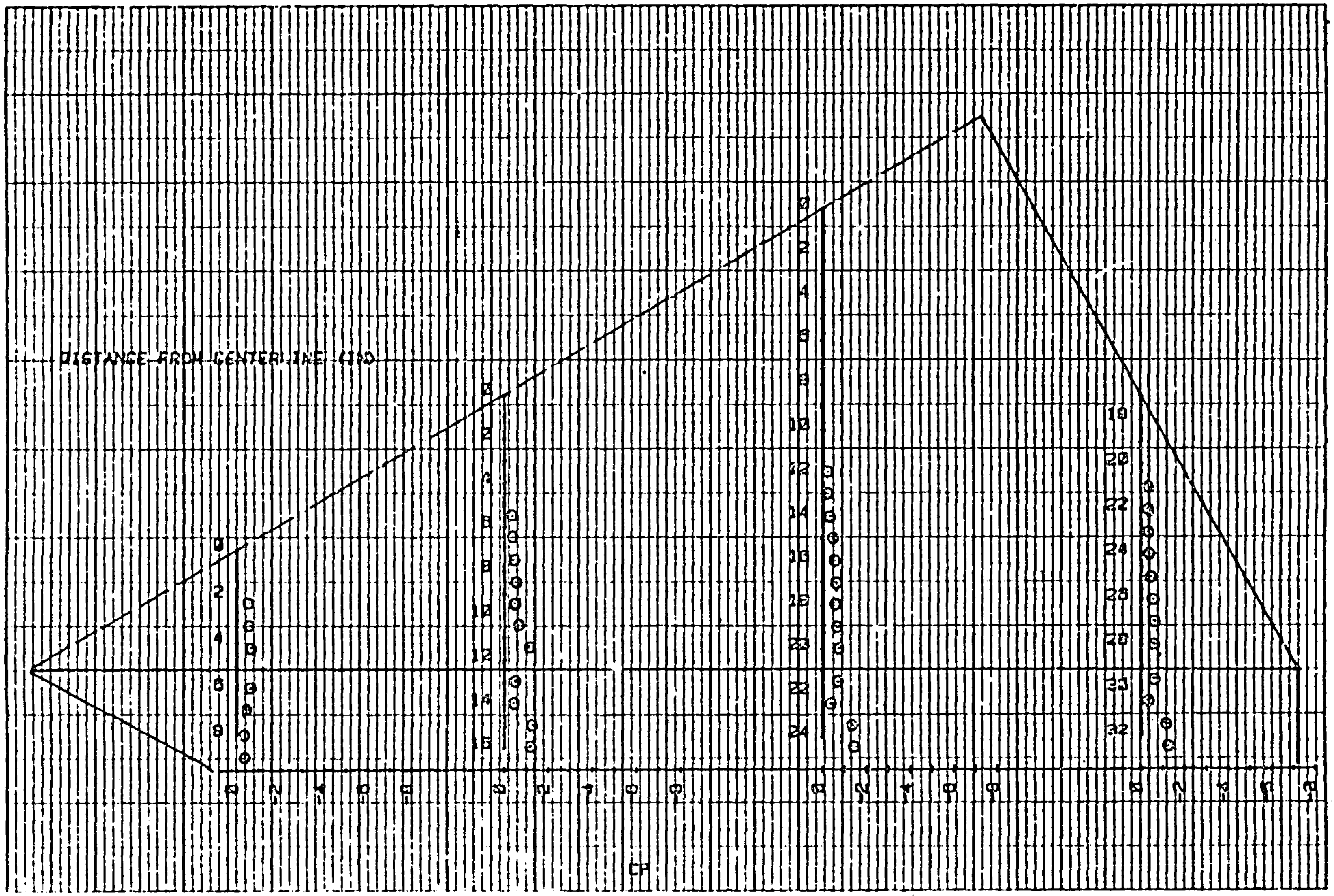

Figure 20 Pressures on CCCF at $\alpha = 15^0$, $\delta_f = 30^0$:

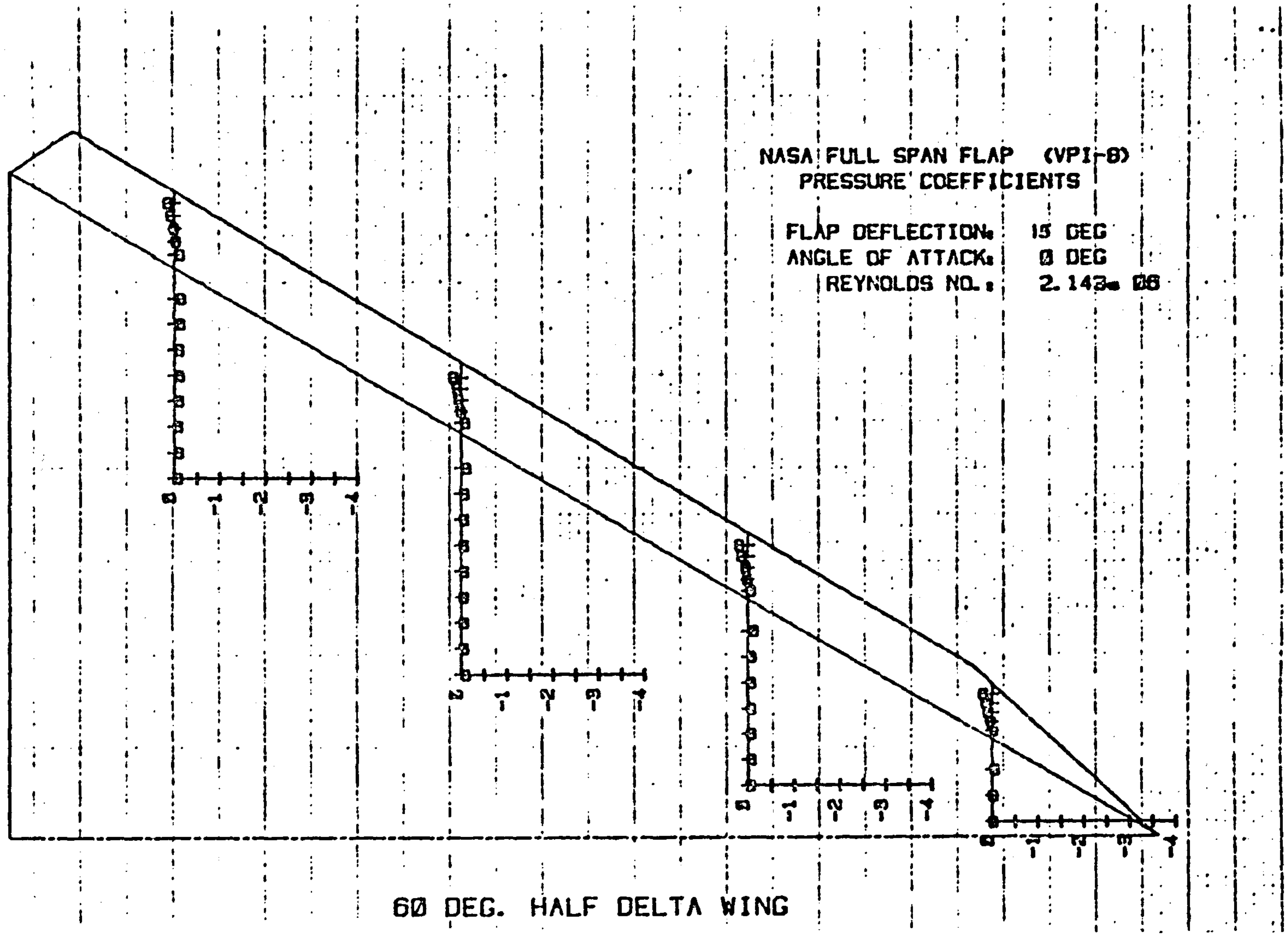

Figure 21 Pressures on VPI-8 at $\alpha = 0^0$, $\delta_f = 15^0$.

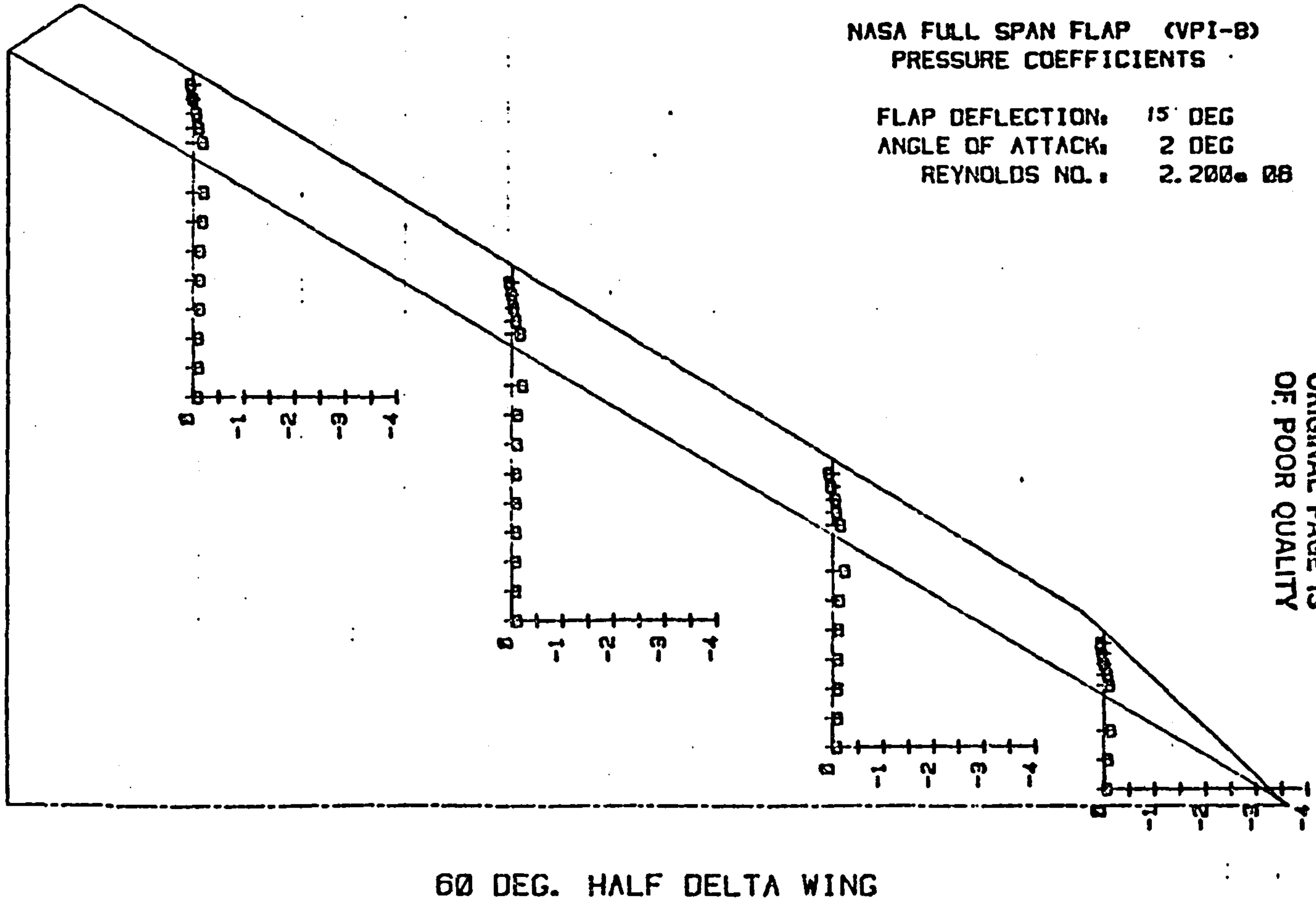

Figure 22 Pressures on VPI-8 at $\alpha = 2^{o}$, $\delta_f = 15^{o}$.

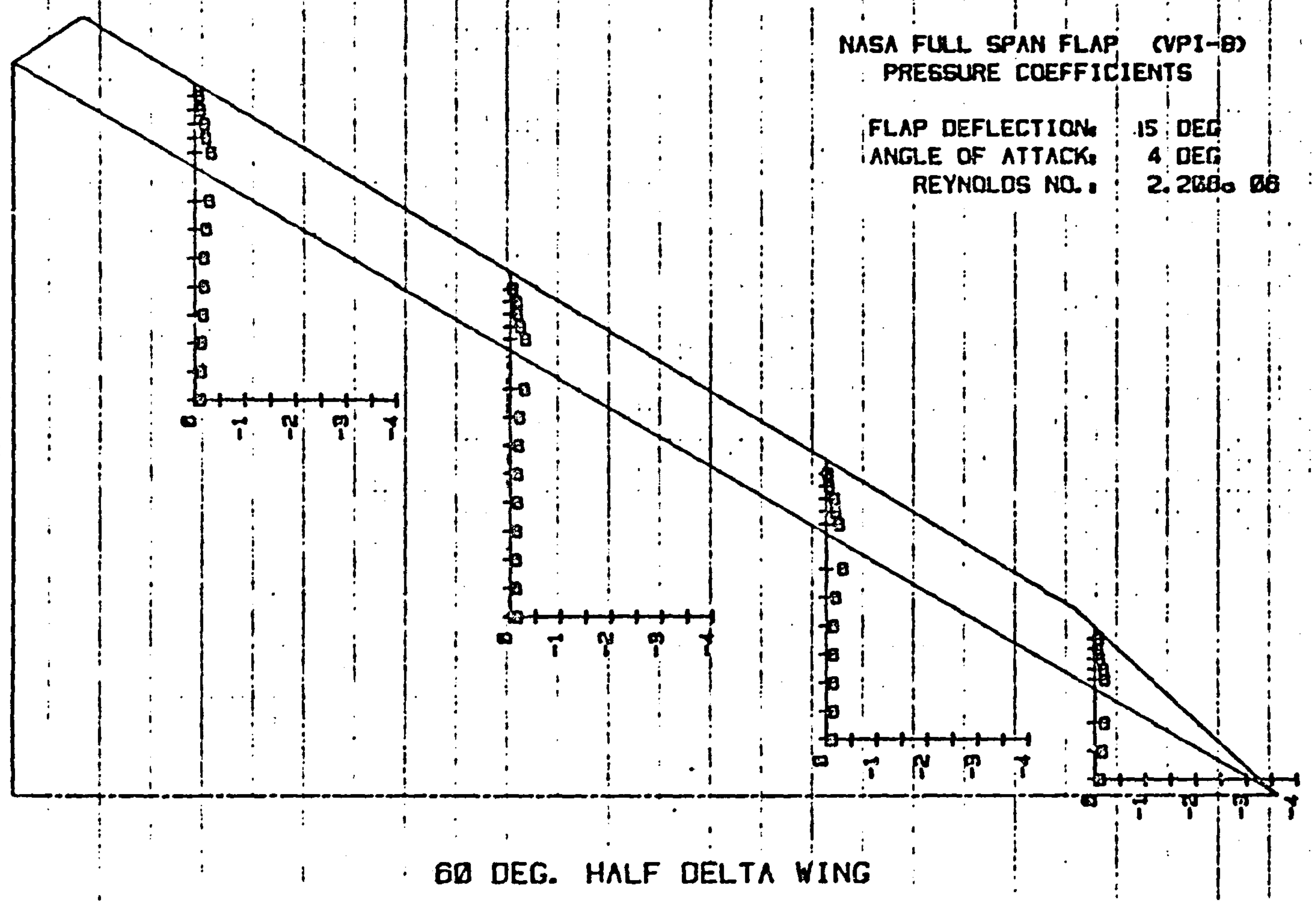

Figure 23 Pressures on VPI-8 at $\alpha = 4^{0}$, $\delta_f = 15^{0}$.

ORIGINAL PAGE IS OF POOR QUALITY

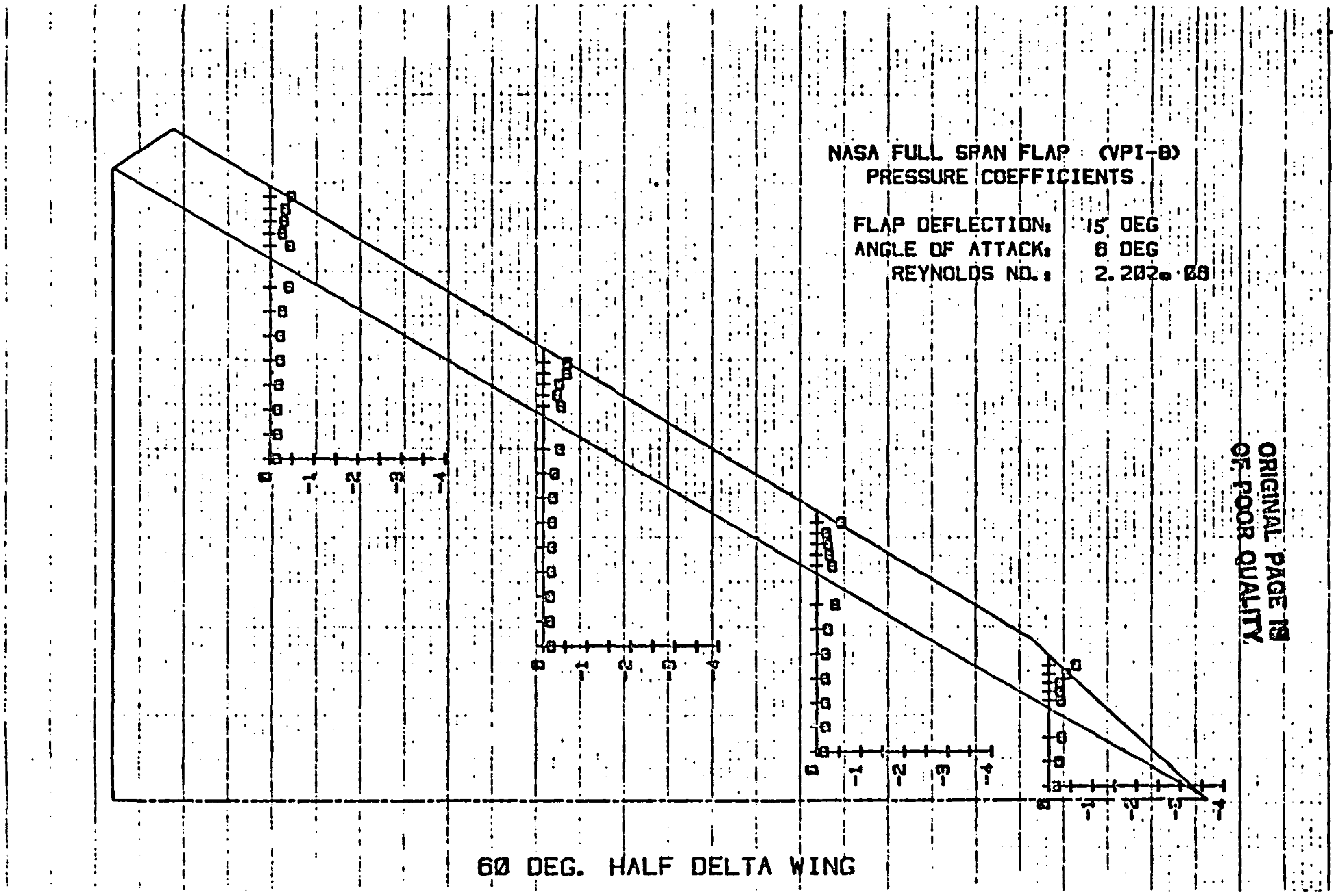

Figure 24 Pressures on VPI-8
at $\alpha = 6^0$, $\delta_f = 15^0$.

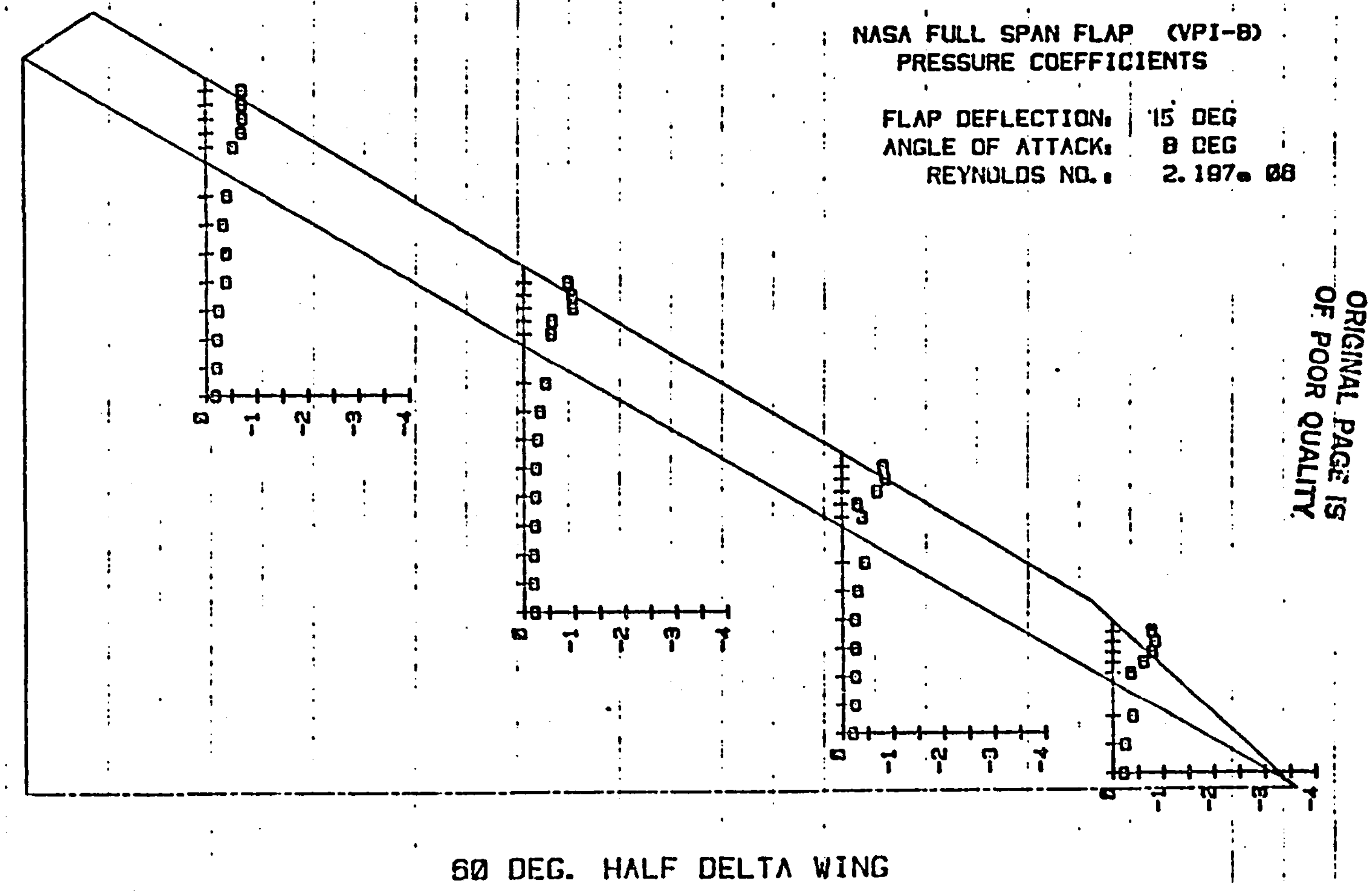

Figure 25 Pressures on VPI-8 at $\alpha = 8^{o}$, $\delta_f = 15^{o}$.

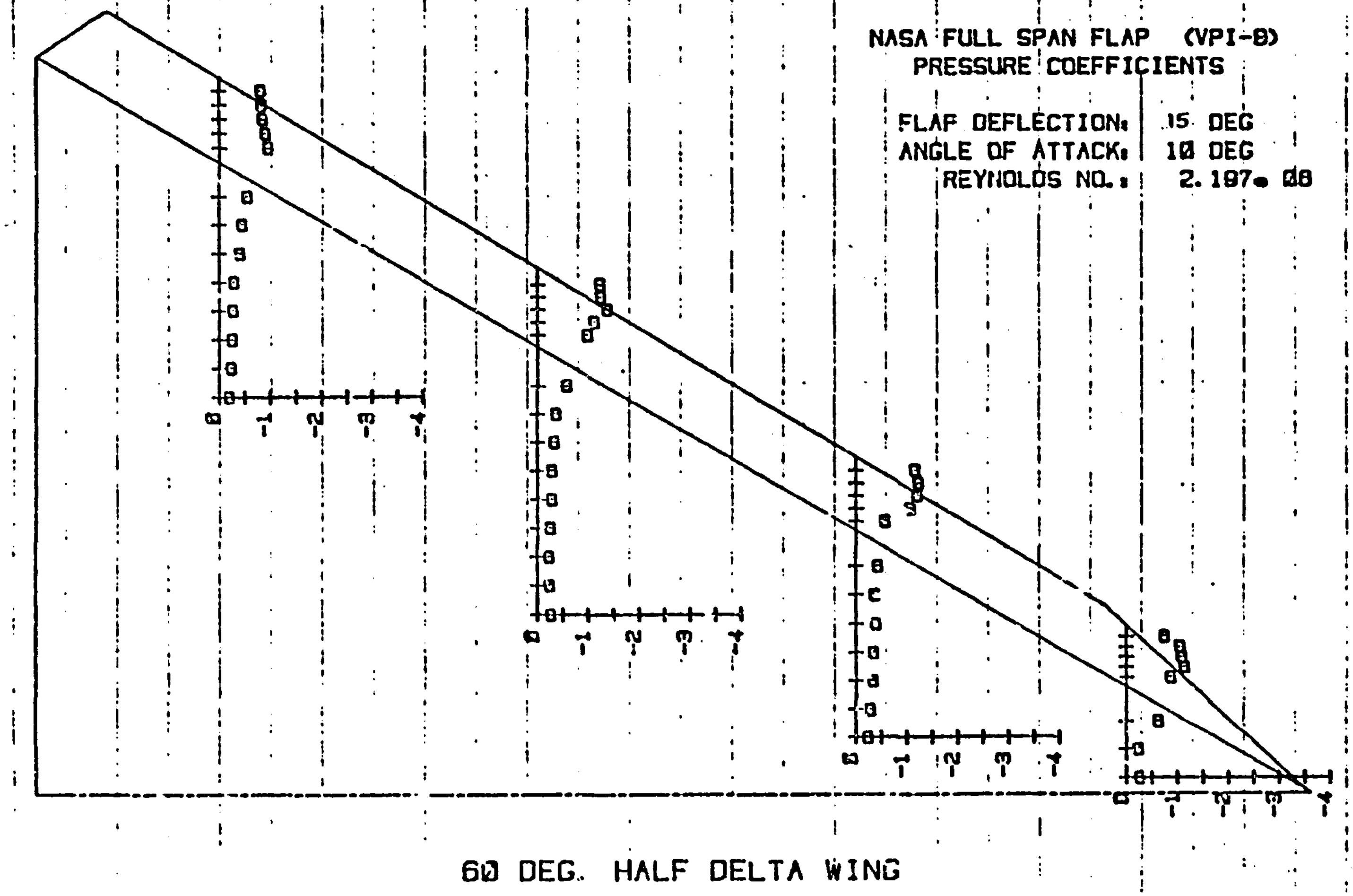

Figure 26 Pressures on VPI-8 at $\alpha = 10^0$, $\delta_f = 15^0$.

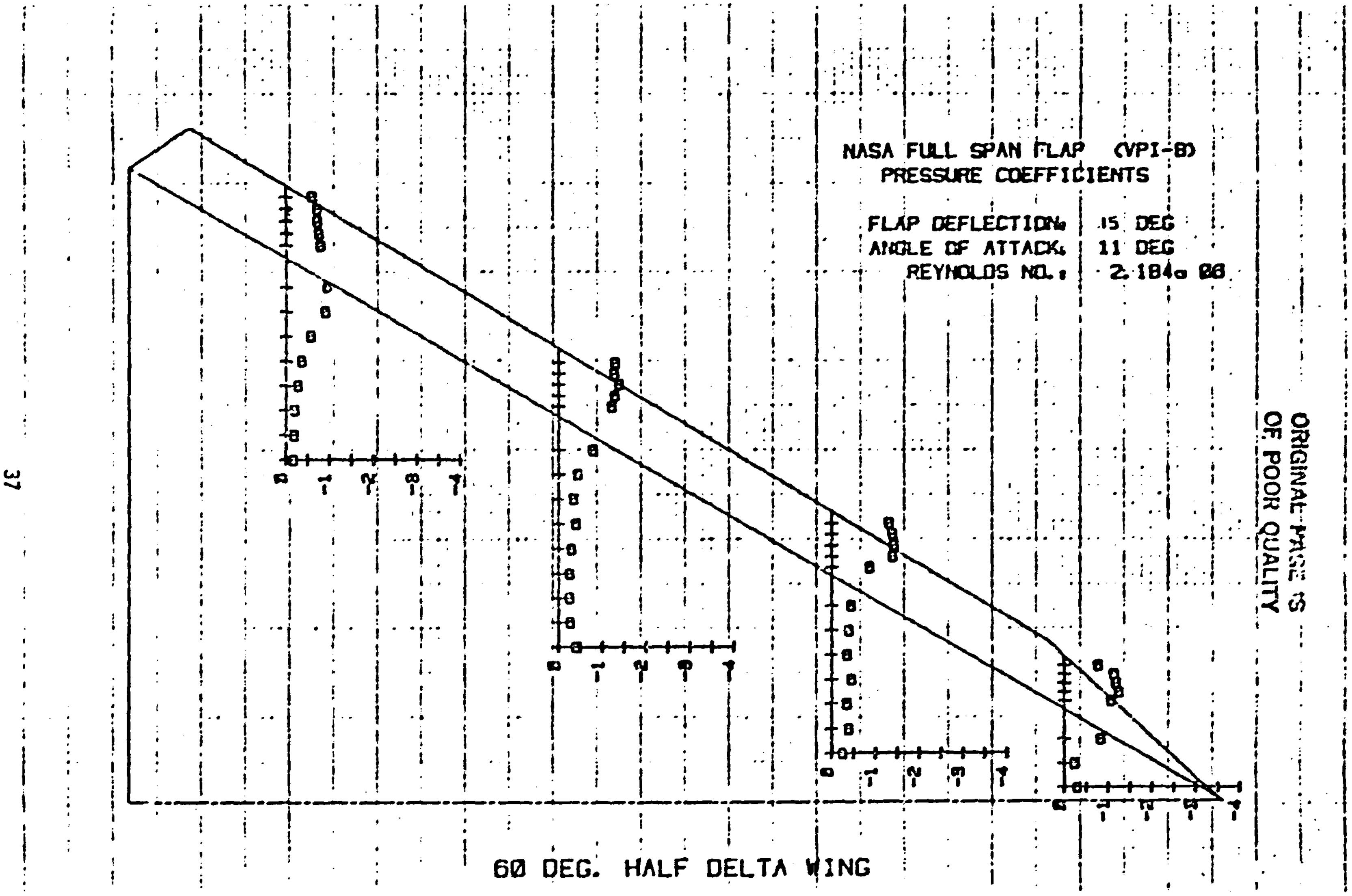

Figure 27 Pressures on VPI-8 at $\alpha = 11^{o}$, $\delta_f = 15^{o}$.

ORIGINAL PAGE IS OF POOR QUALITY

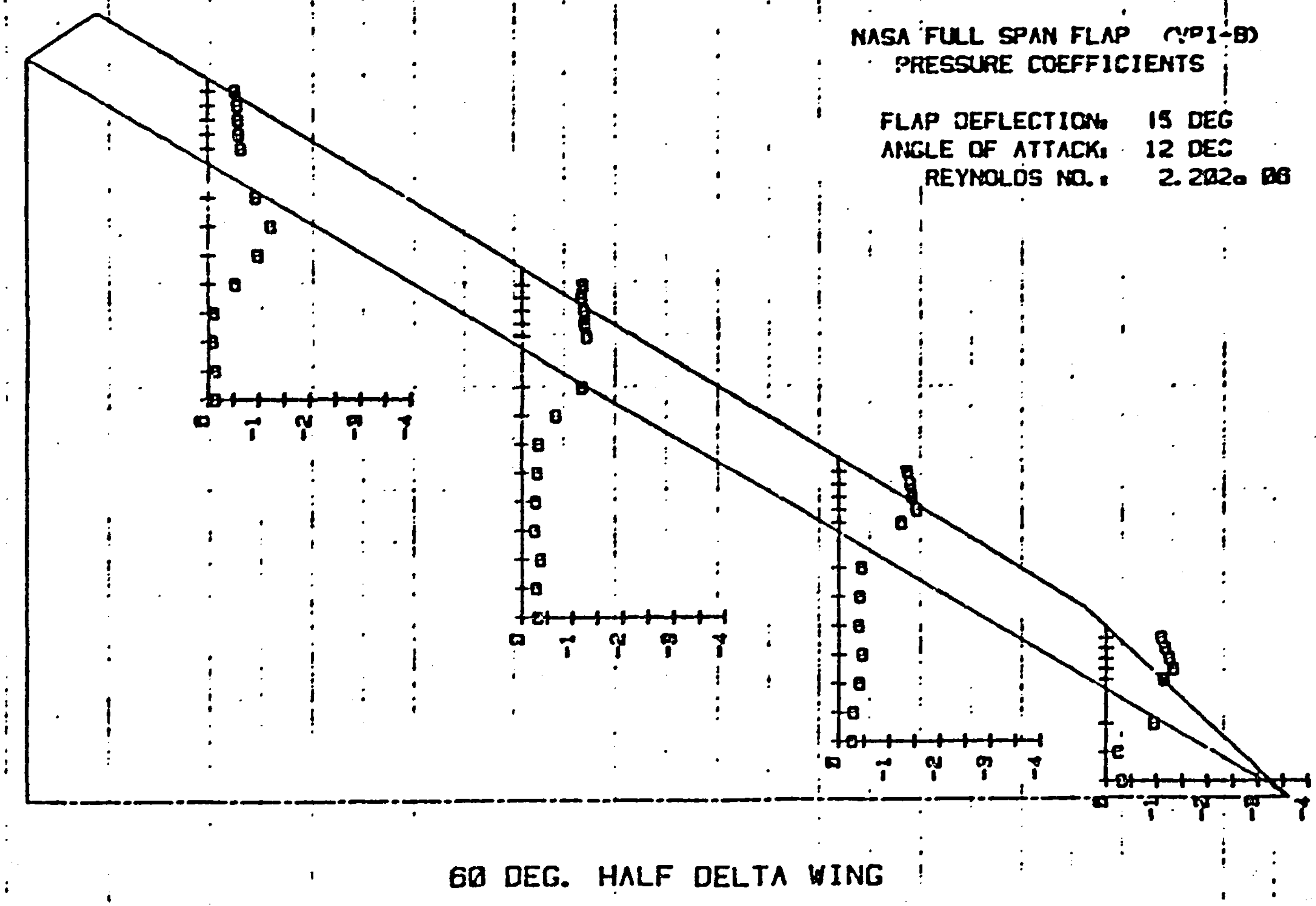

Figure 28 Pressures on VPI-8 at $\alpha = 12^{\circ}$, $\delta_f = 15^{\circ}$.

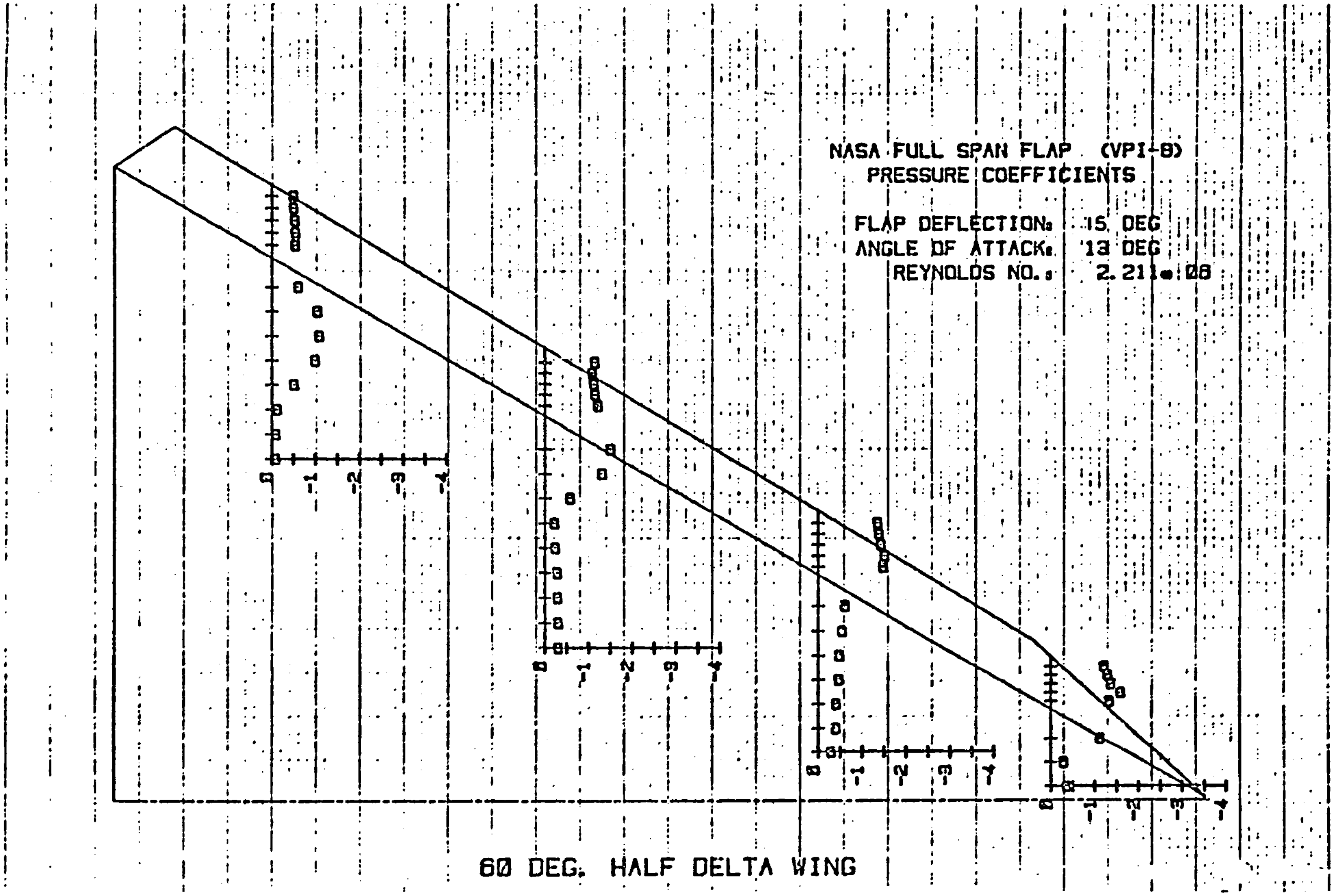

Figure 29 Pressures on VPI-8 at $\alpha = 13^o$, $\delta_f = 15^o$.

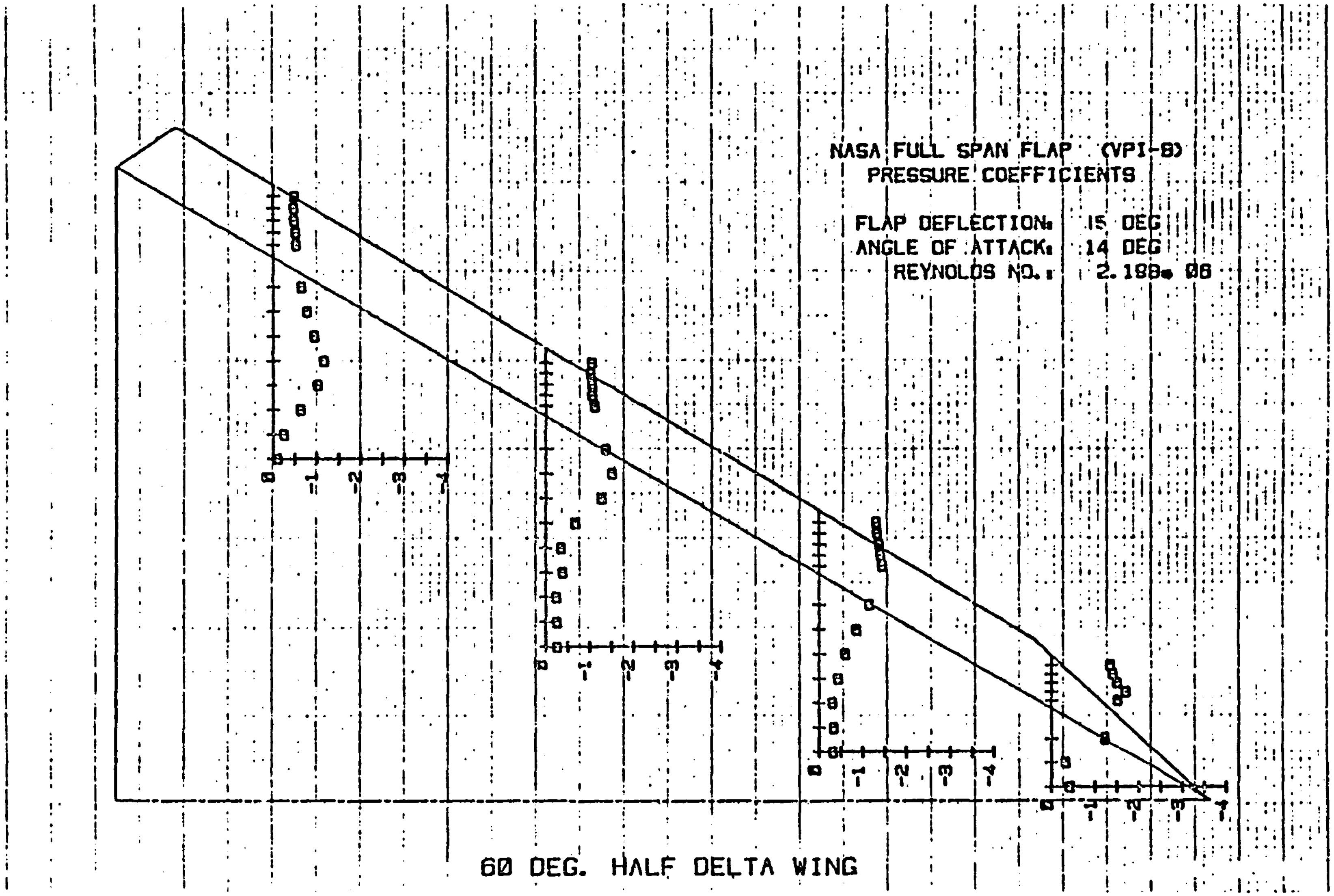

Figure 30 Pressures on VPI-8
at α = 14°, δ_f = 15°.

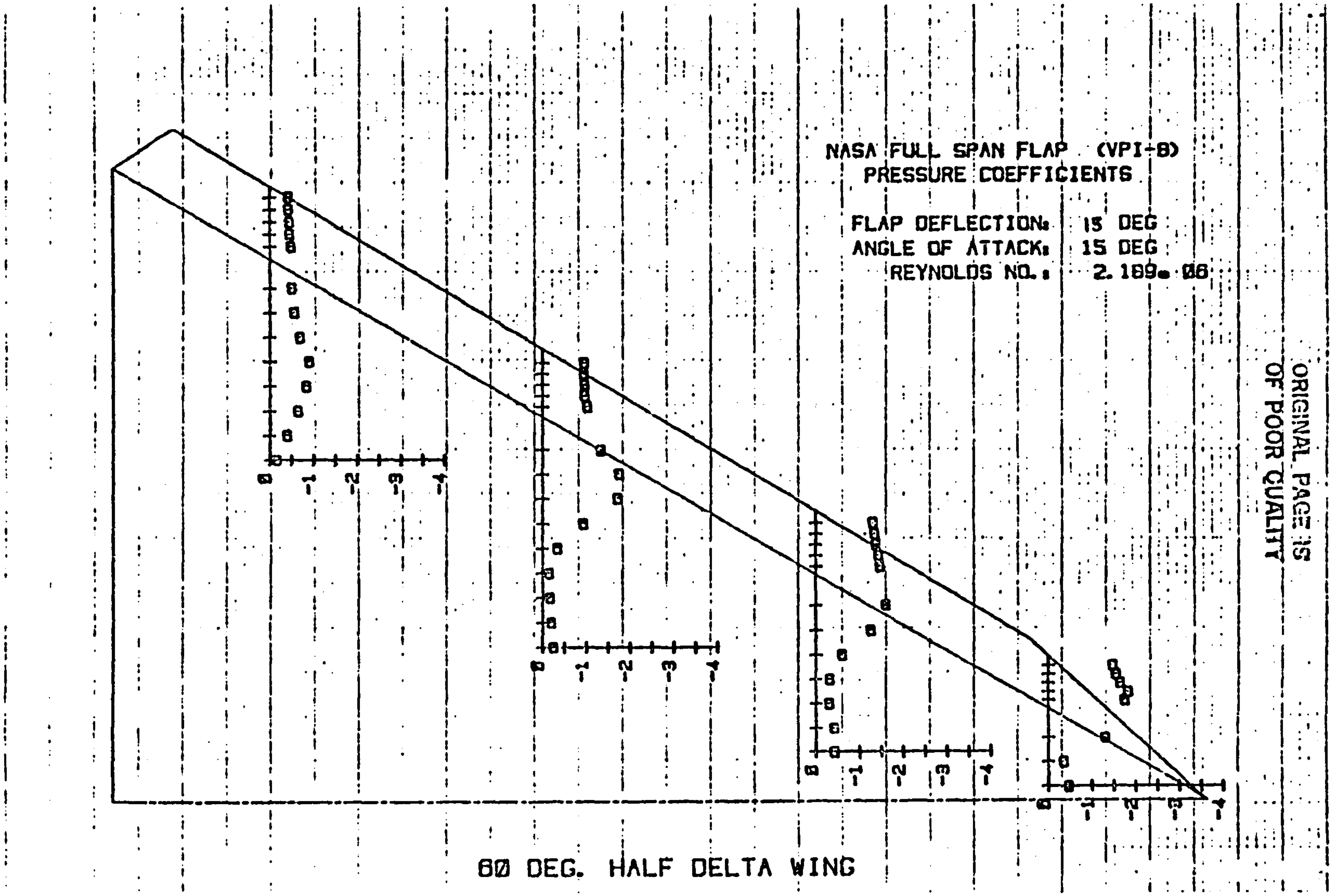

ORIGINAL PAGE IS
OF POOR QUALITY

Figure 31 Pressures on VPI-8
at $\alpha = 15^0$, $\delta_f = 15^0$.

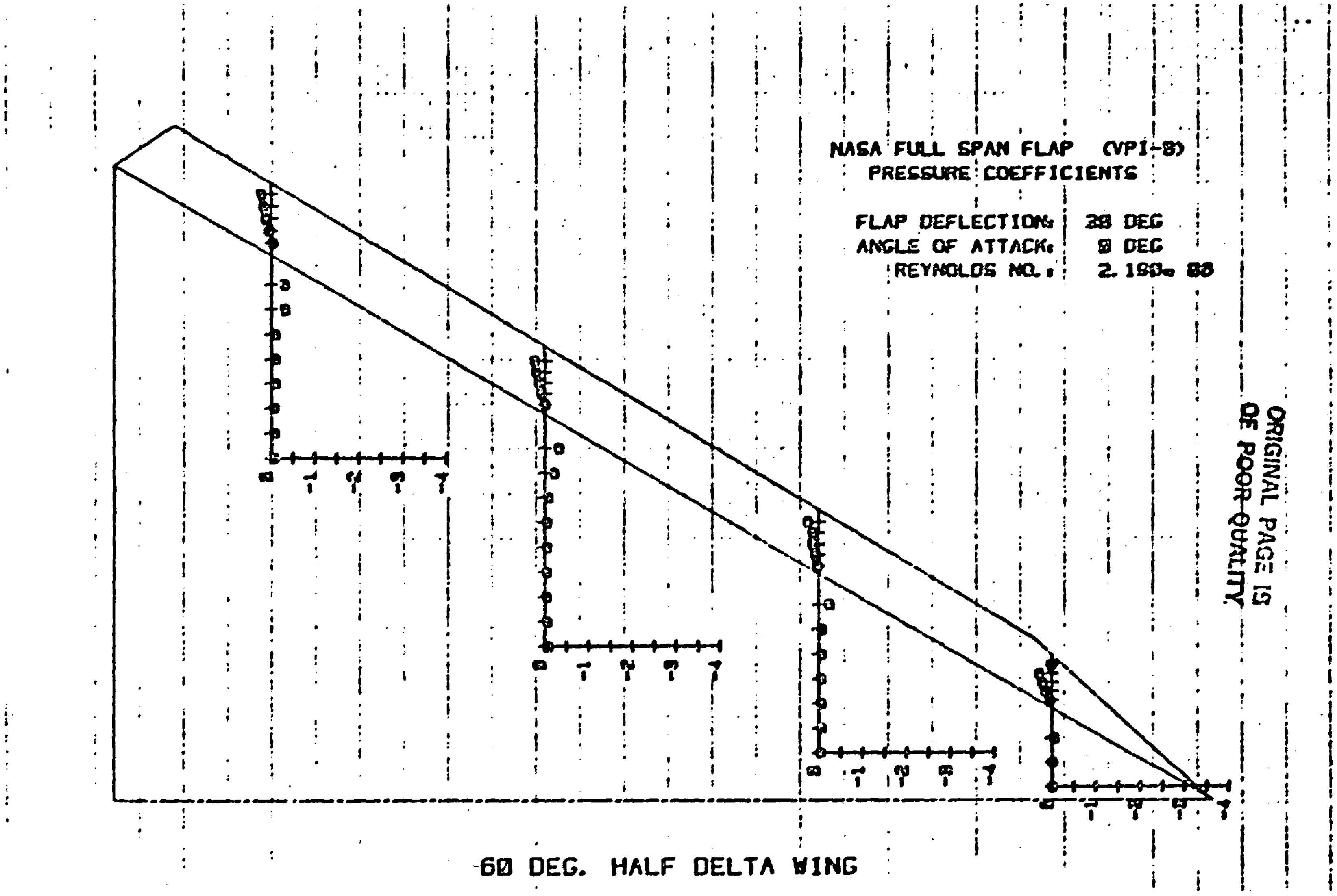

Figure 32 Pressures on VPI-8 at $\alpha = 0^o$, $\delta_f = 30^o$.

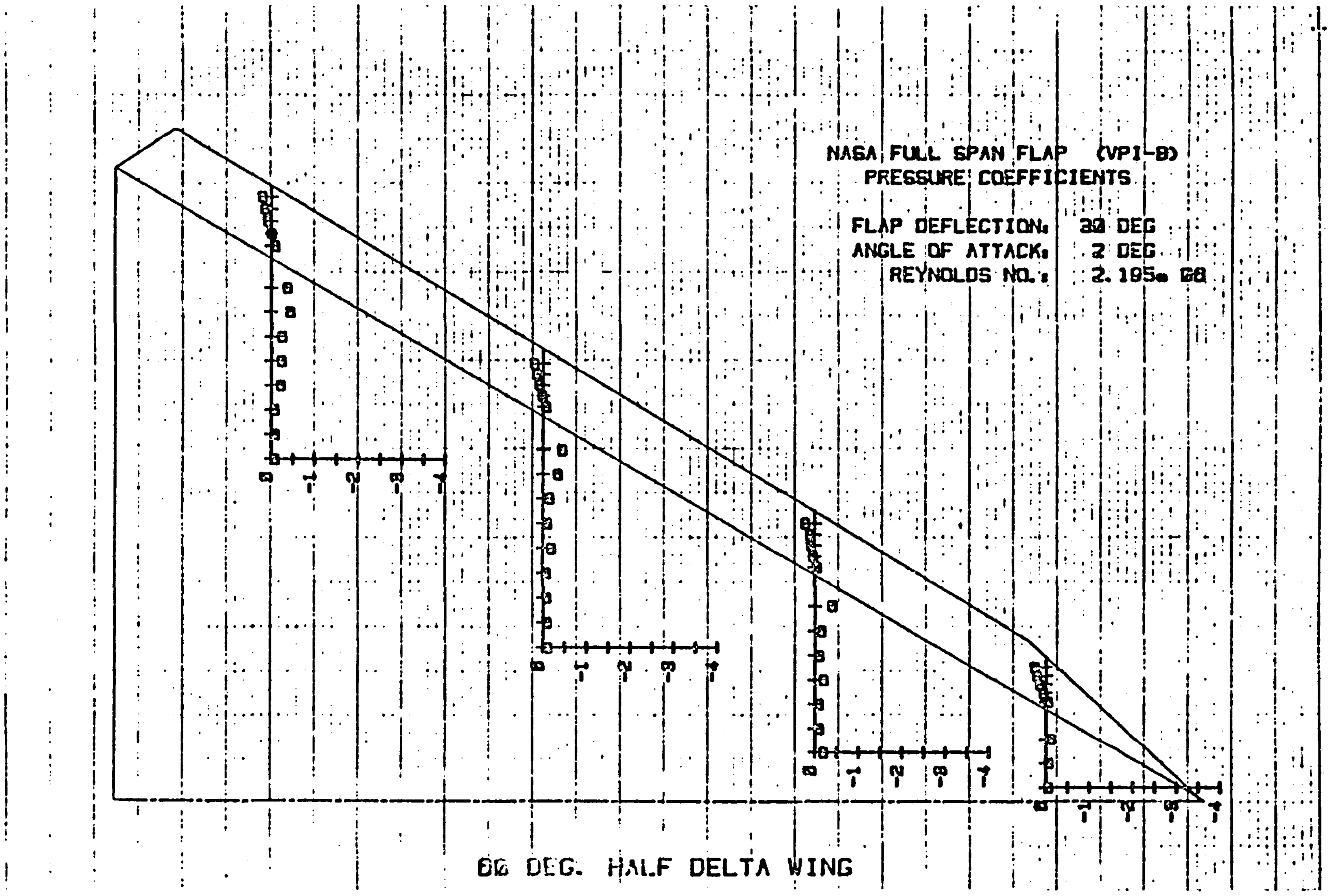

Figure 33 Pressures on VPI-8 at $\alpha = 2^{\circ}$, $\delta_T = 30^{\circ}$.

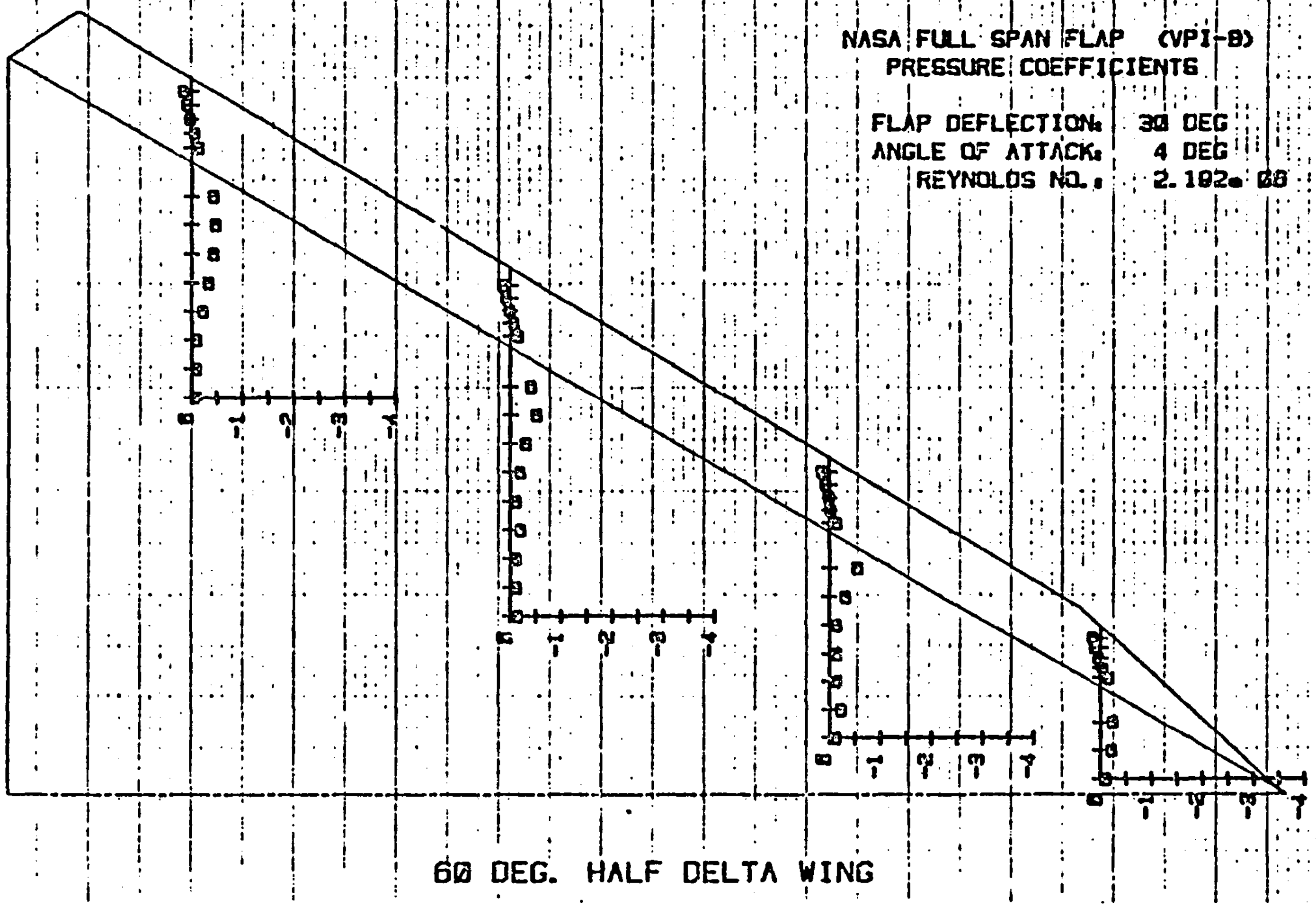

Figure 34 Pressures on VPI-8
at $\alpha = 4^{o}$, $\delta_f = 30^{o}$.

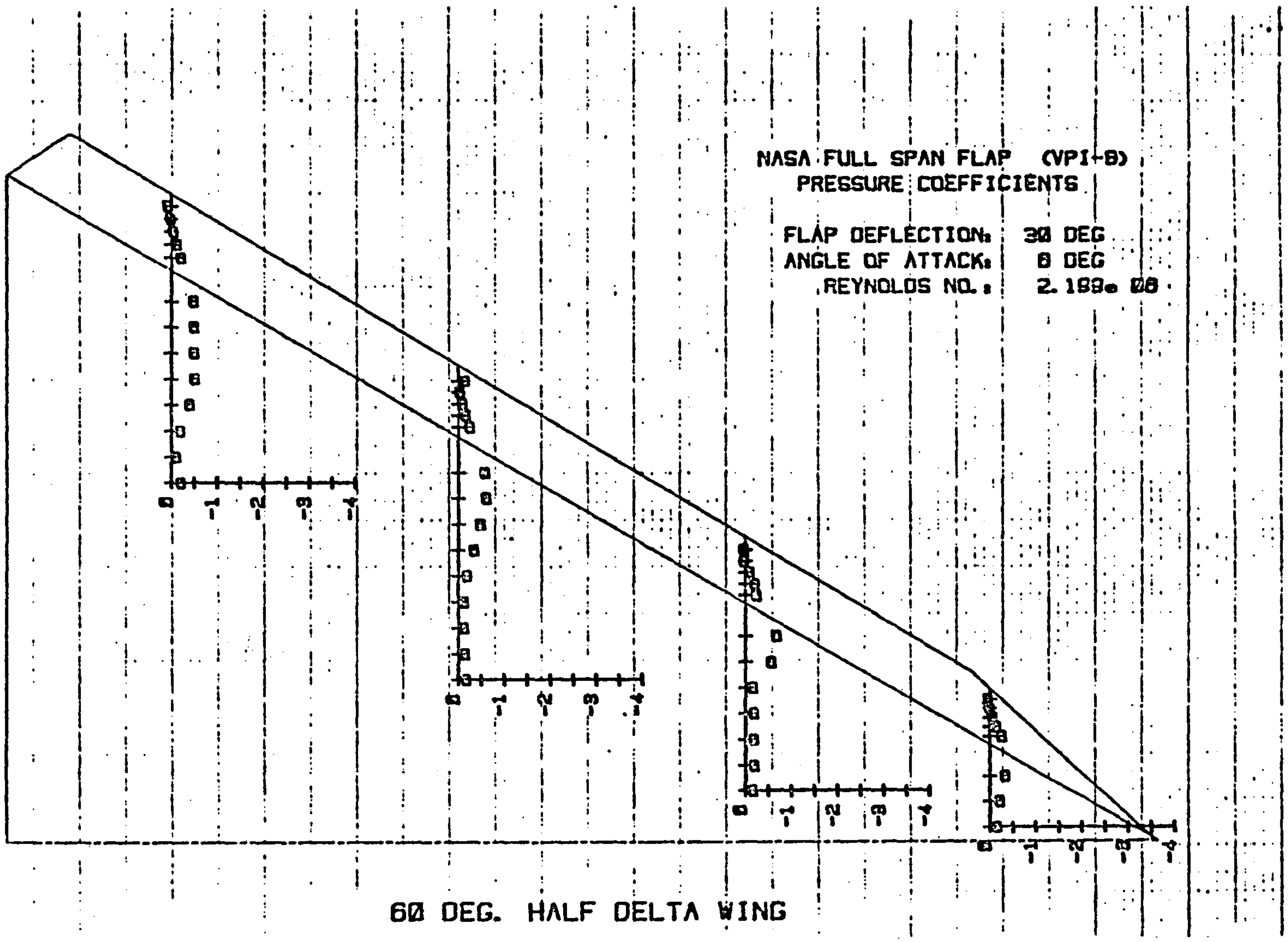

Figure 35 Pressures on VPI-8
at $\alpha = 6^0$, $\delta_f = 30^0$.

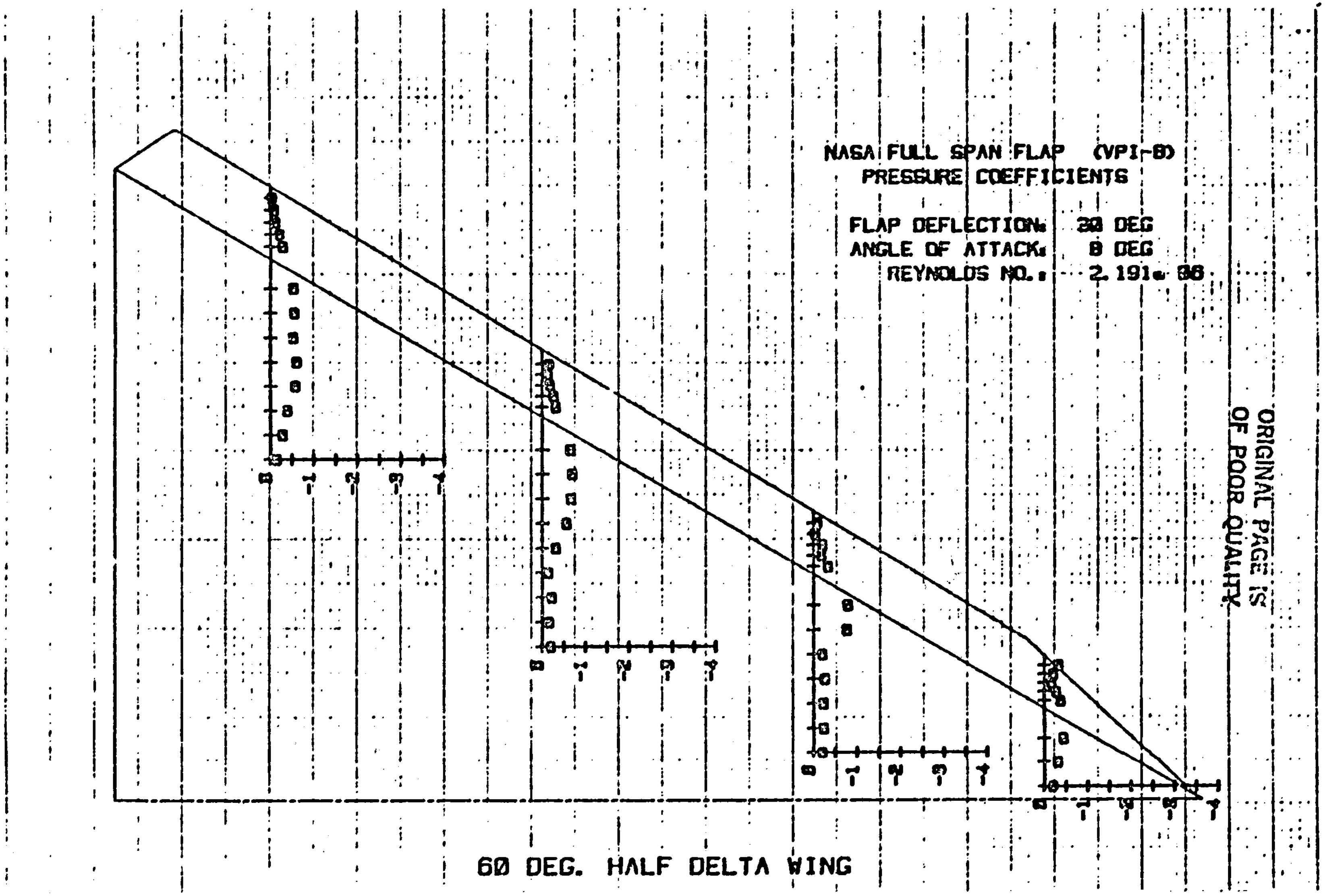

Figure 36 Pressures on VPI-8 at $\alpha = 8^0$, $\delta_f = 30^0$.

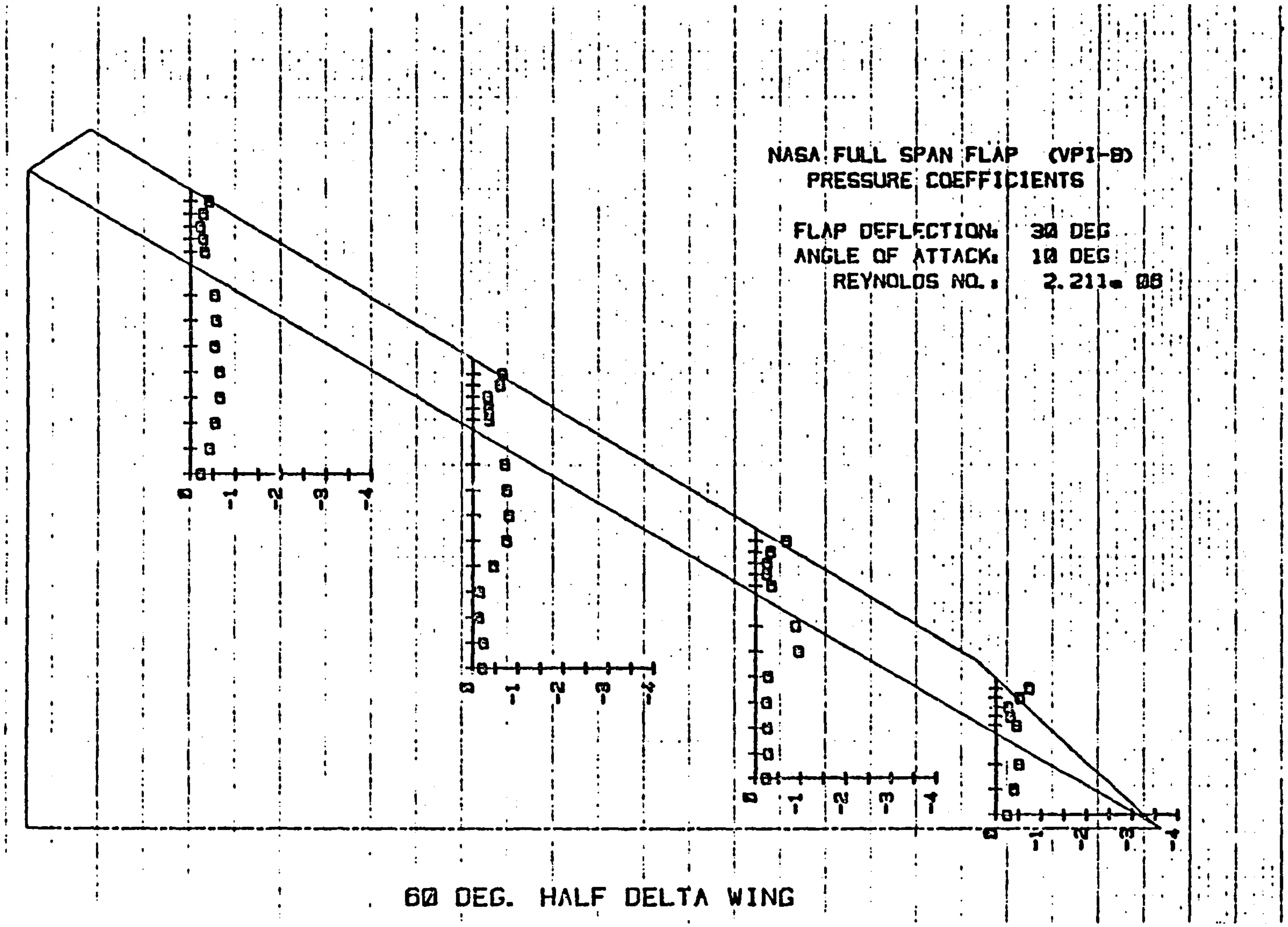

Figure 37 Pressures on VPI-8
at $\alpha = 10^0$, $\delta_f = 30^0$.

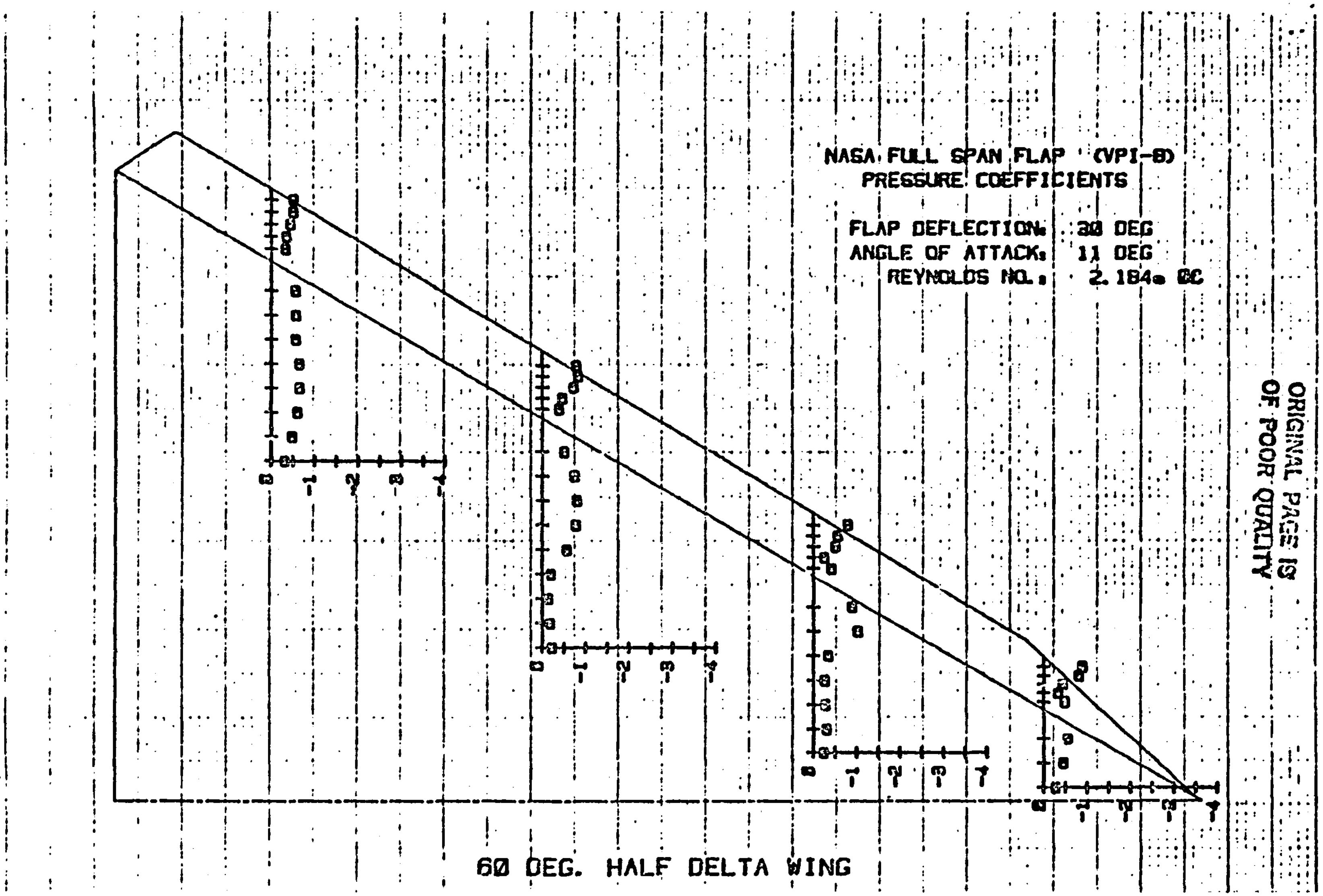

Figure 38 Pressures on VPI-8 at $\alpha = 11^{o}$, $\delta_f = 30^{o}$.

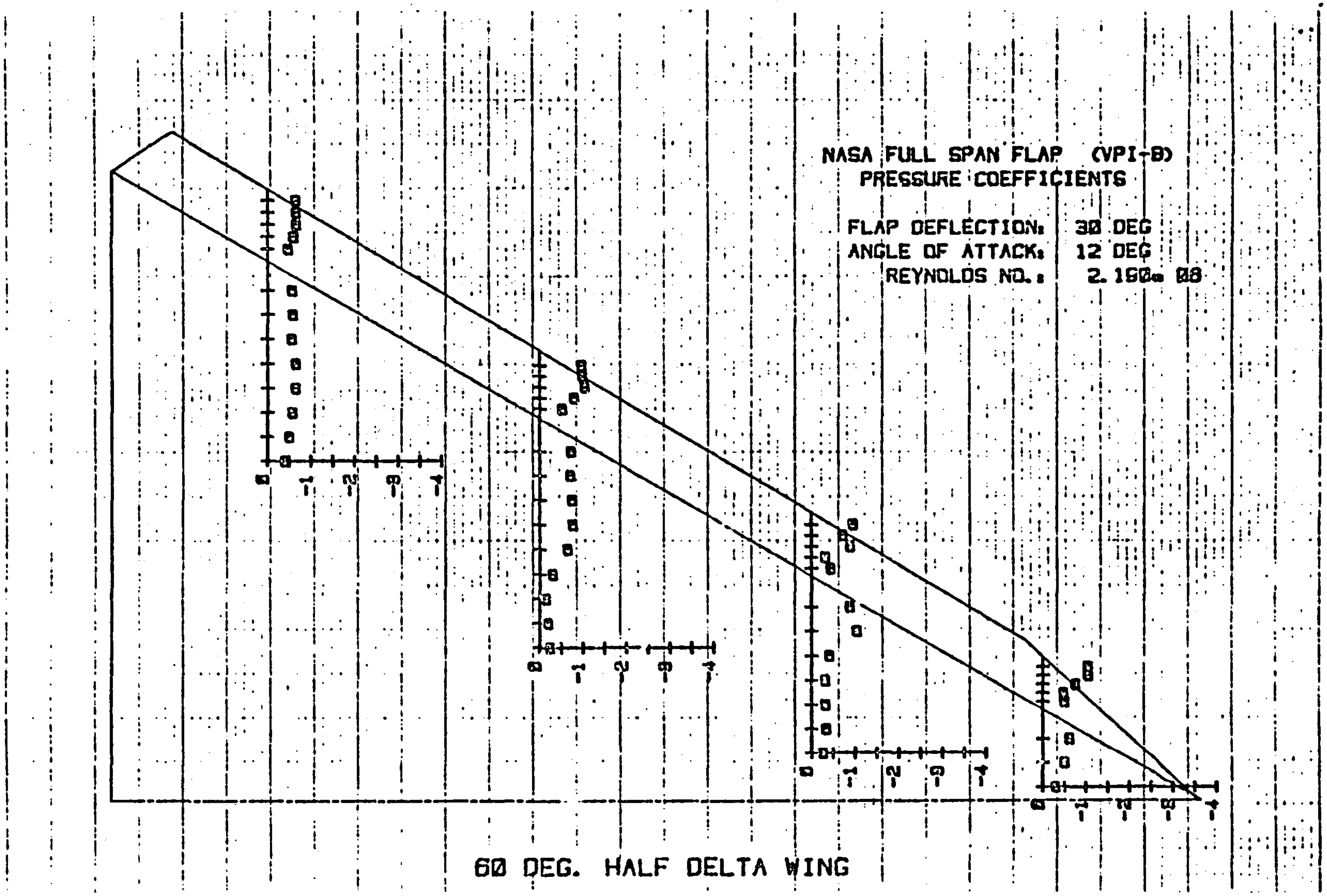

Figure 39 Pressures on VPI-8 at $\alpha = 12^{0}$, $-\delta_f = 30^{0}$.

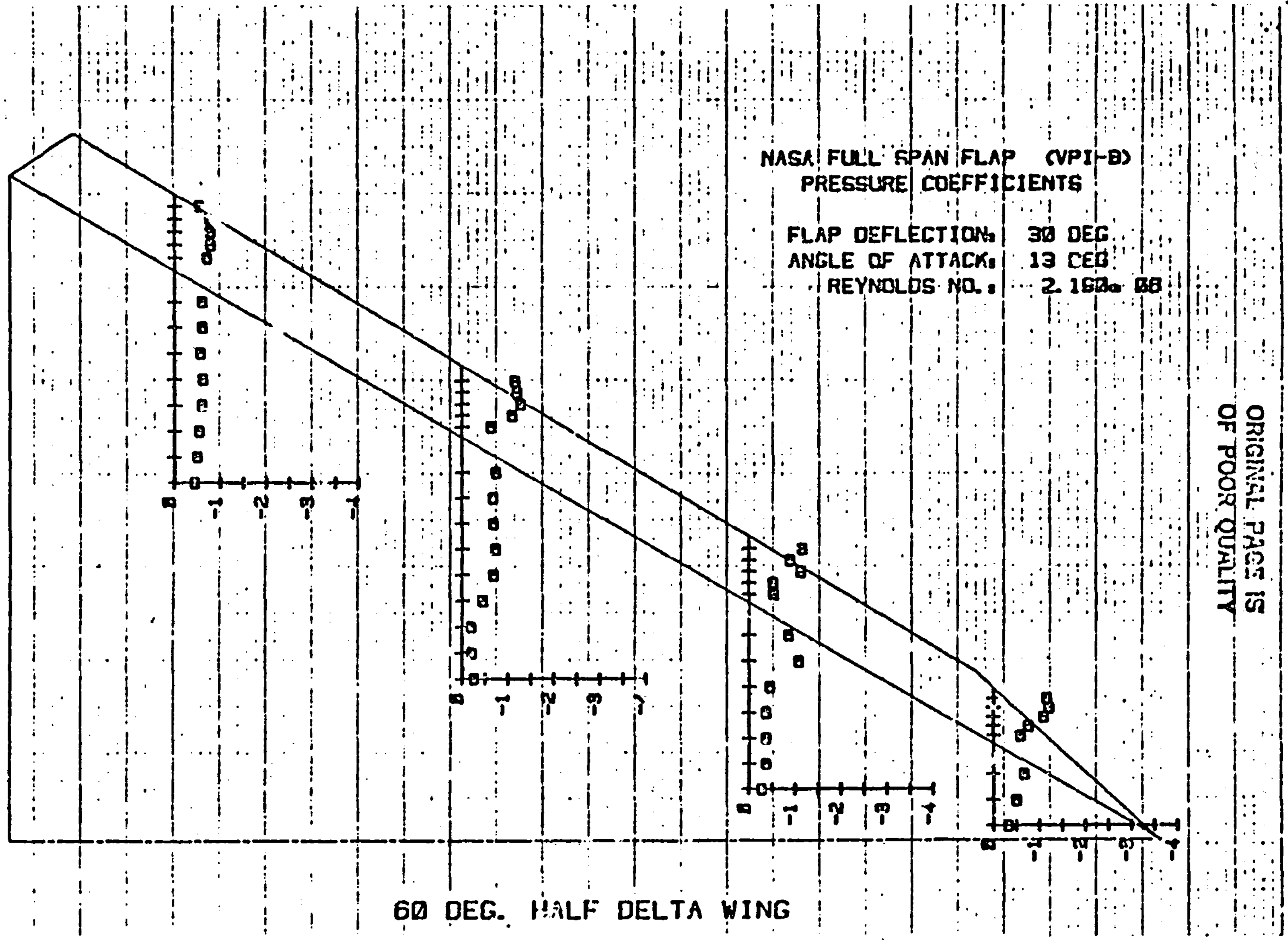

Figure 40 Pressures on VPI-8 at $\alpha = 13^o$, $\delta_f = 30^o$.

ORIGINAL PAGE IS OF POOR QUALITY

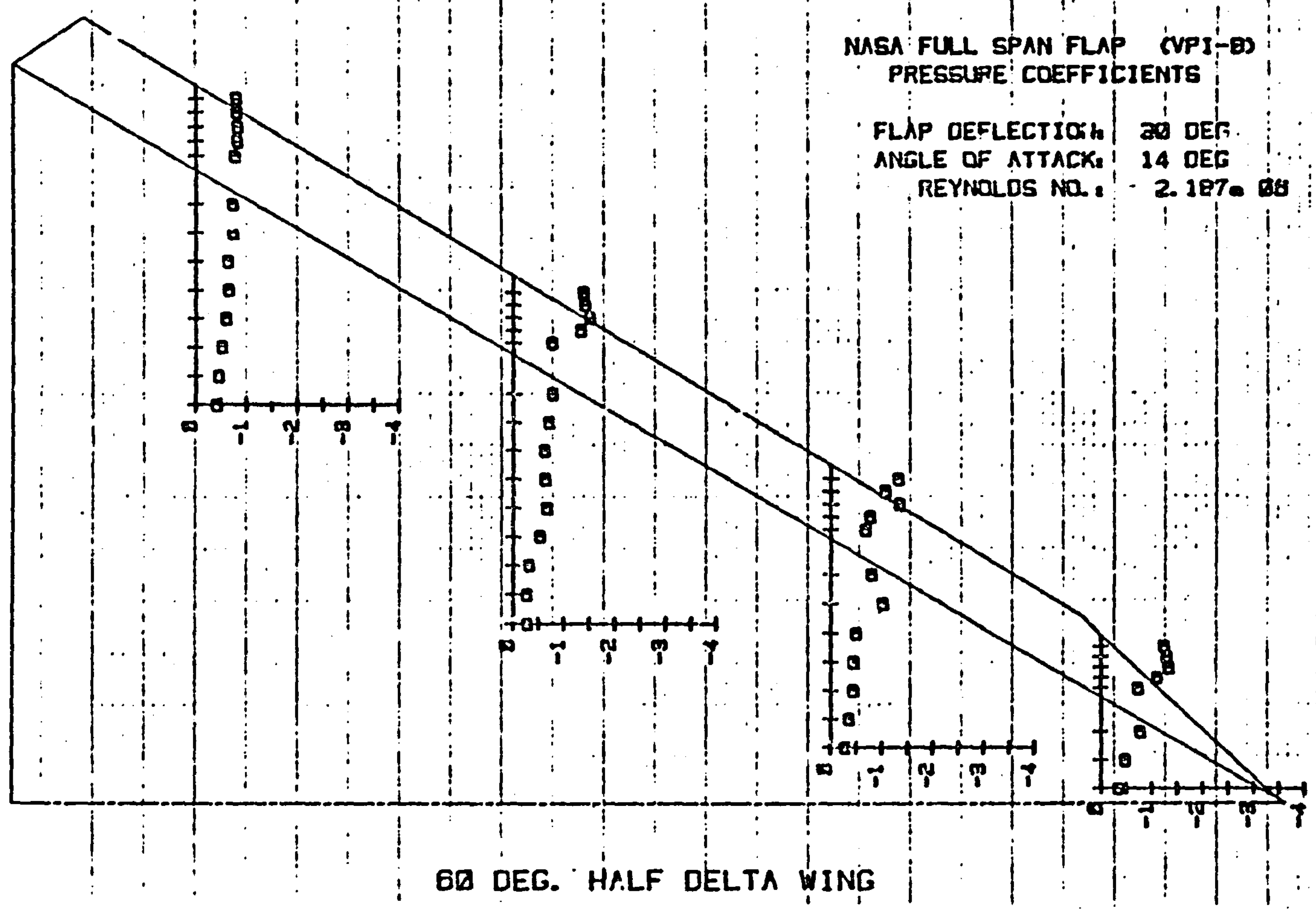

Figure 41 Pressures on VPI-8
at $\alpha = 14^{0}$, $\delta_f = 30^{0}$.

ORIGINAL PAGE IS
OF POOR QUALITY.

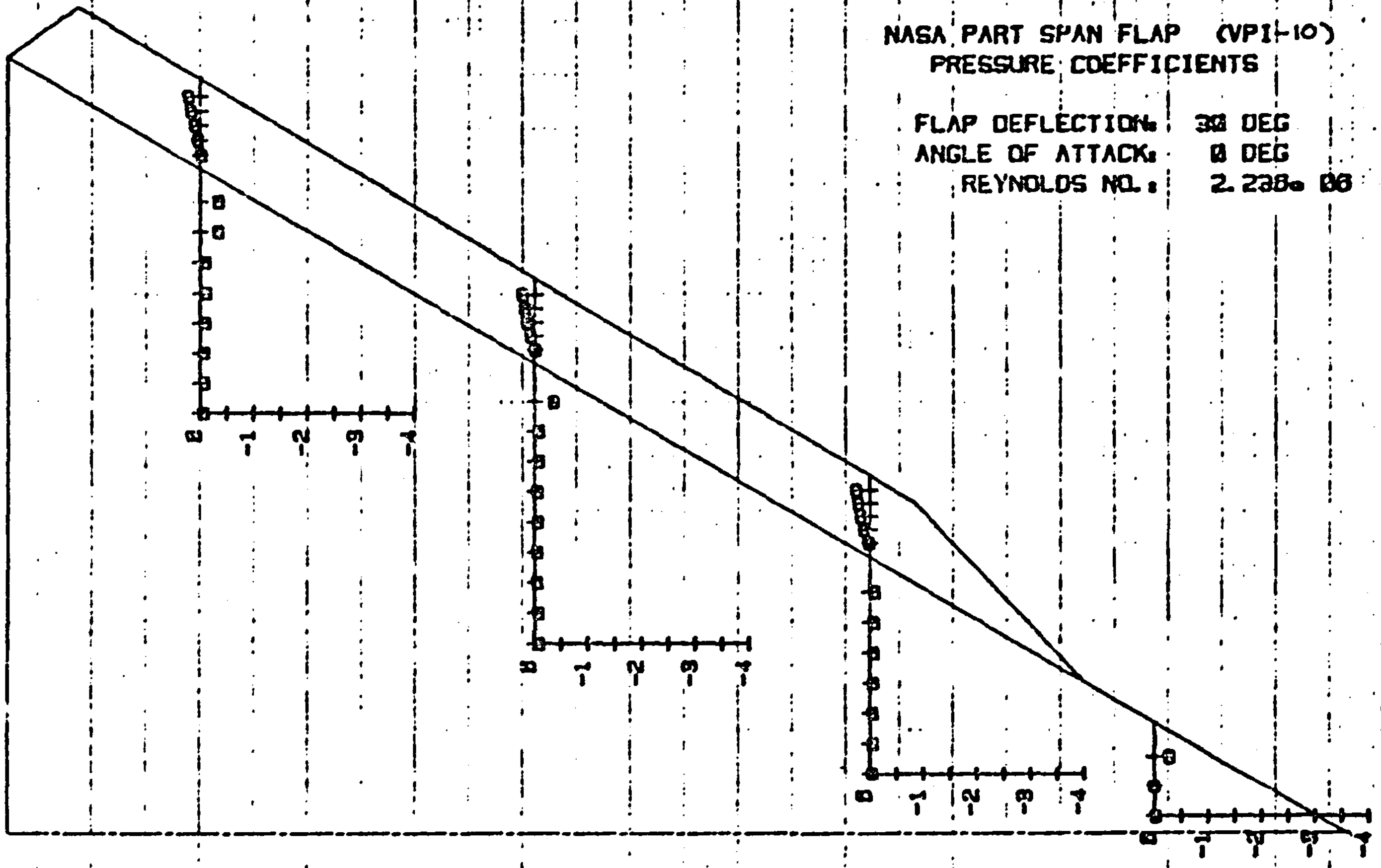

Figure 42 Pressures on VPI-10, No Fuselage, $\alpha = 0^{o}$, $\delta_f = 30^{o}$.

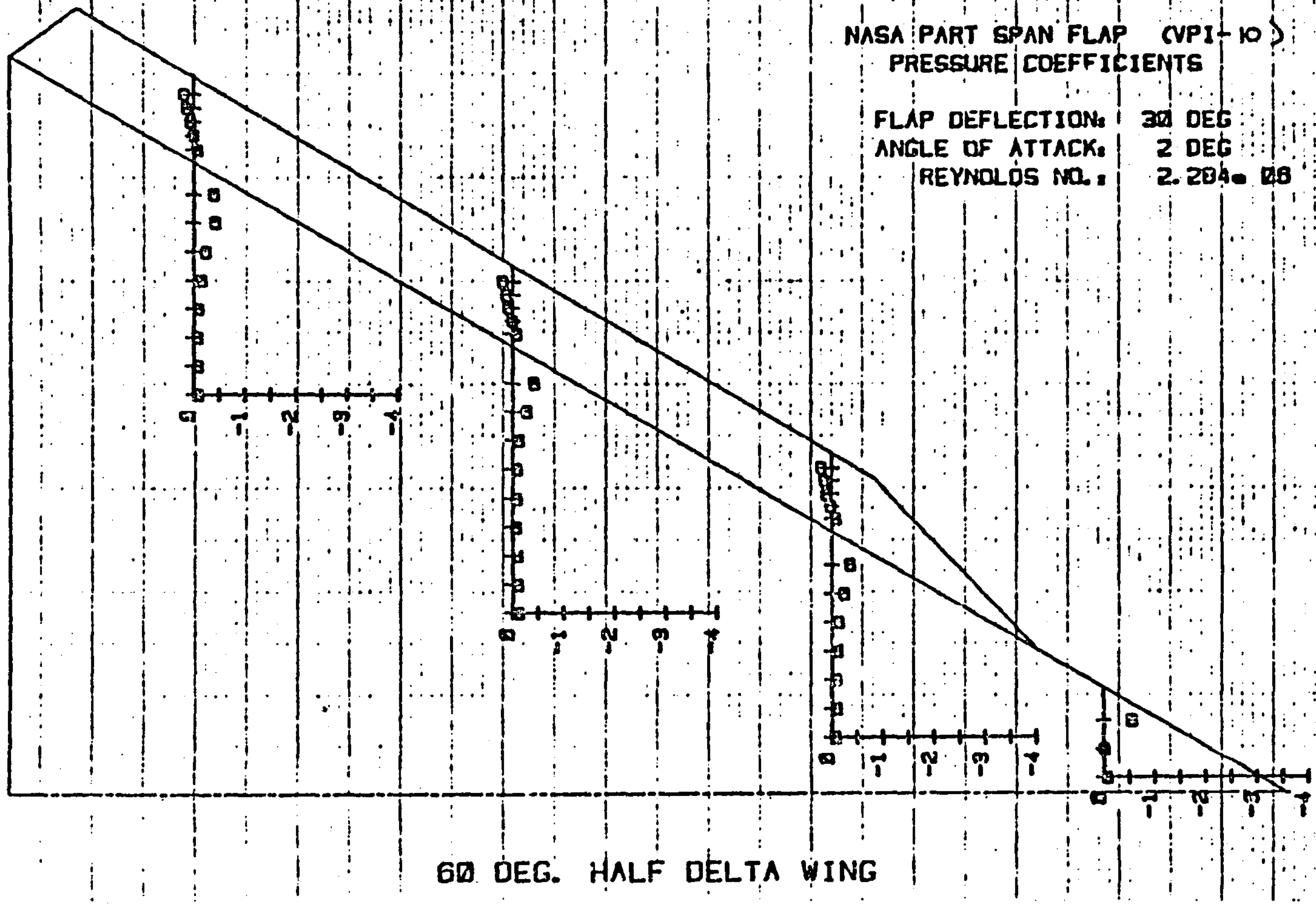

Figure 43 Pressures on VPI-10, No Fuselage, $\alpha = 2^0$, $\delta_f = 30^0$.

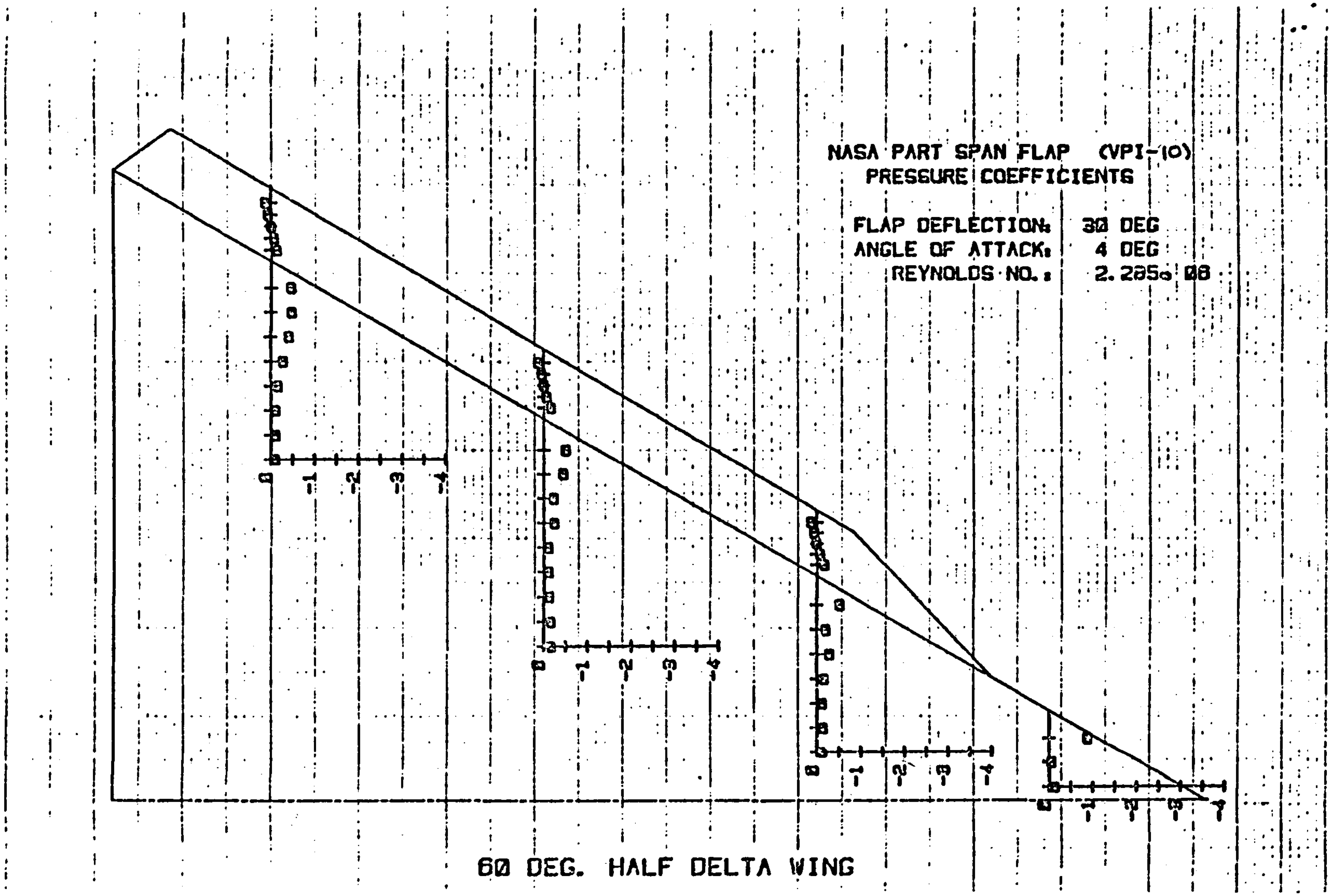

Figure 44 Pressures on VPI-10, No Fuselage, $\alpha = 4^0$, $\delta_f = 30^0$.

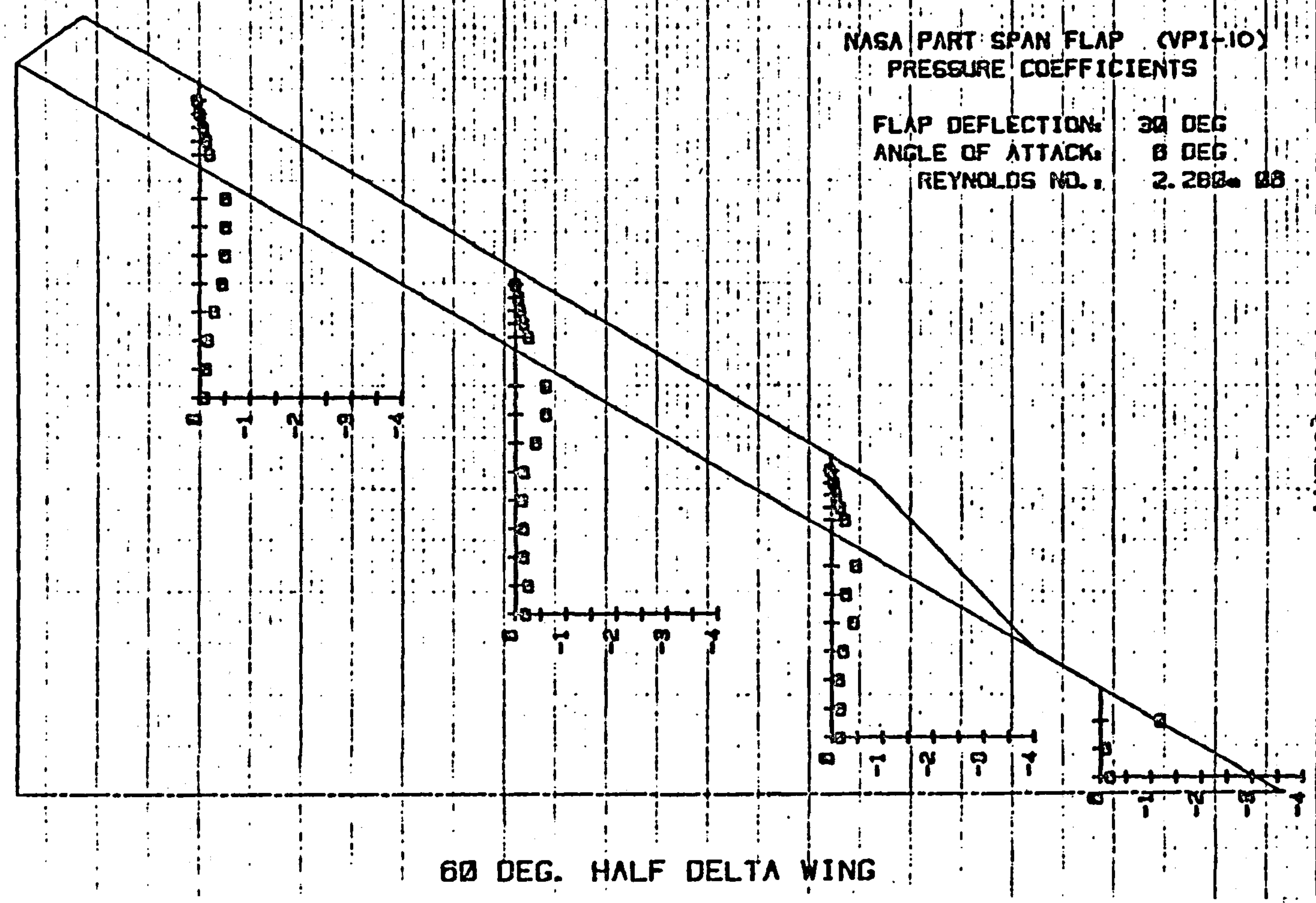

Figure 45 Pressures on VPI-10, No Fuselage, $\alpha = 6^0$, $\delta_f = 30^0$.

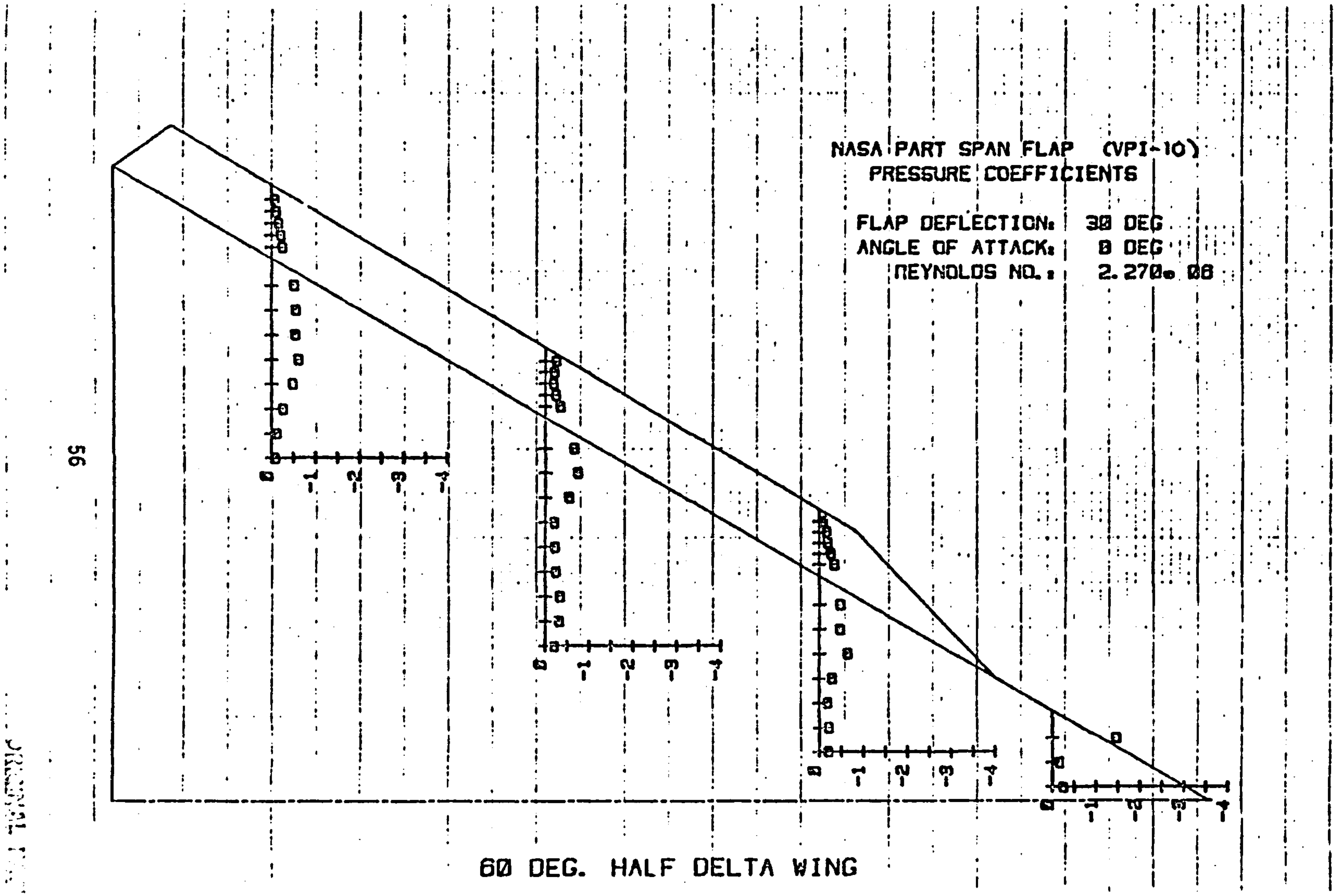

Figure 46 Pressures on VPI-10, No Fuselage, $\alpha = 8^0$, $\delta_f = 30^0$.

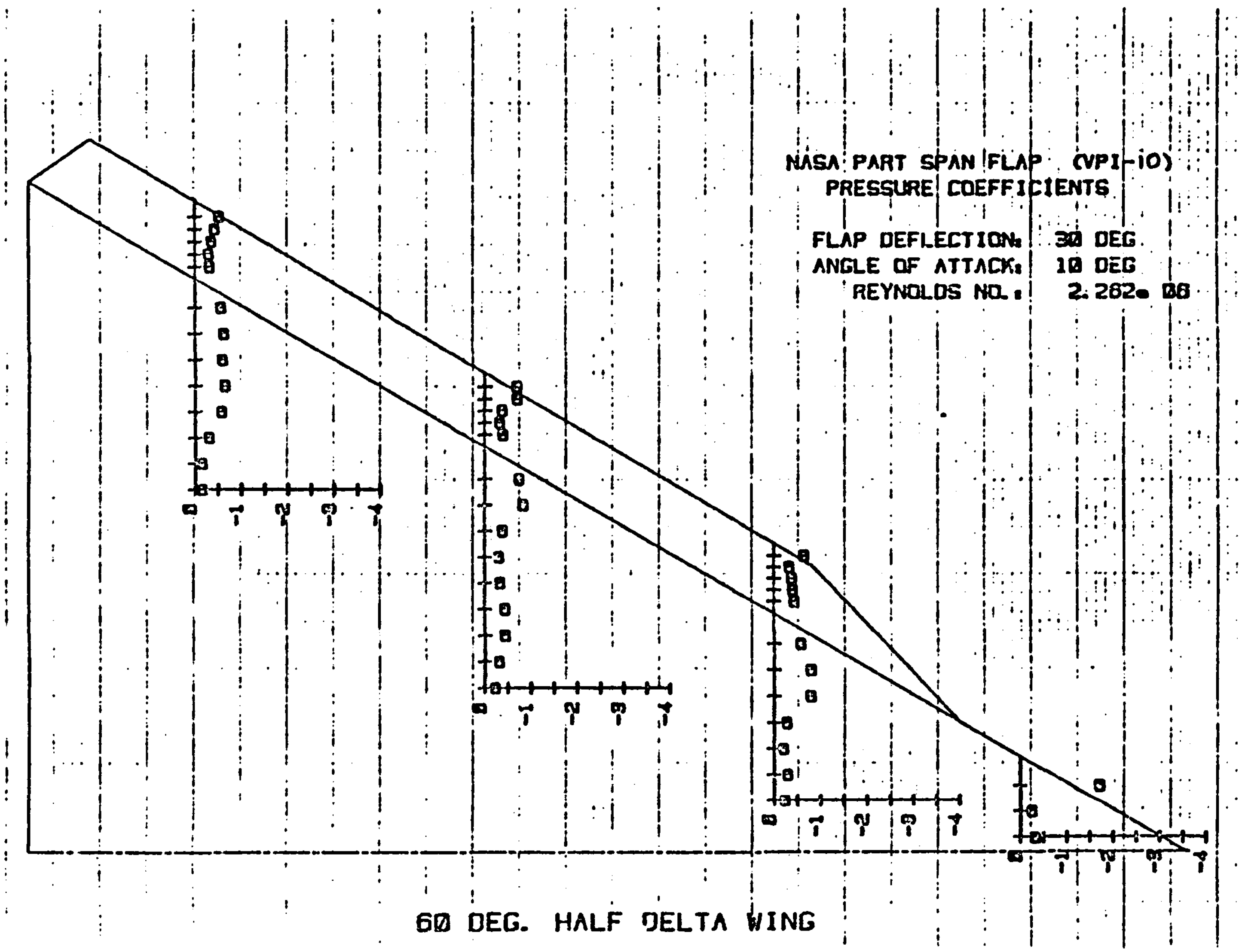

Figure 47 Pressures on VPI-10, No Fuselage, α = 10°, δ_f = 30°.

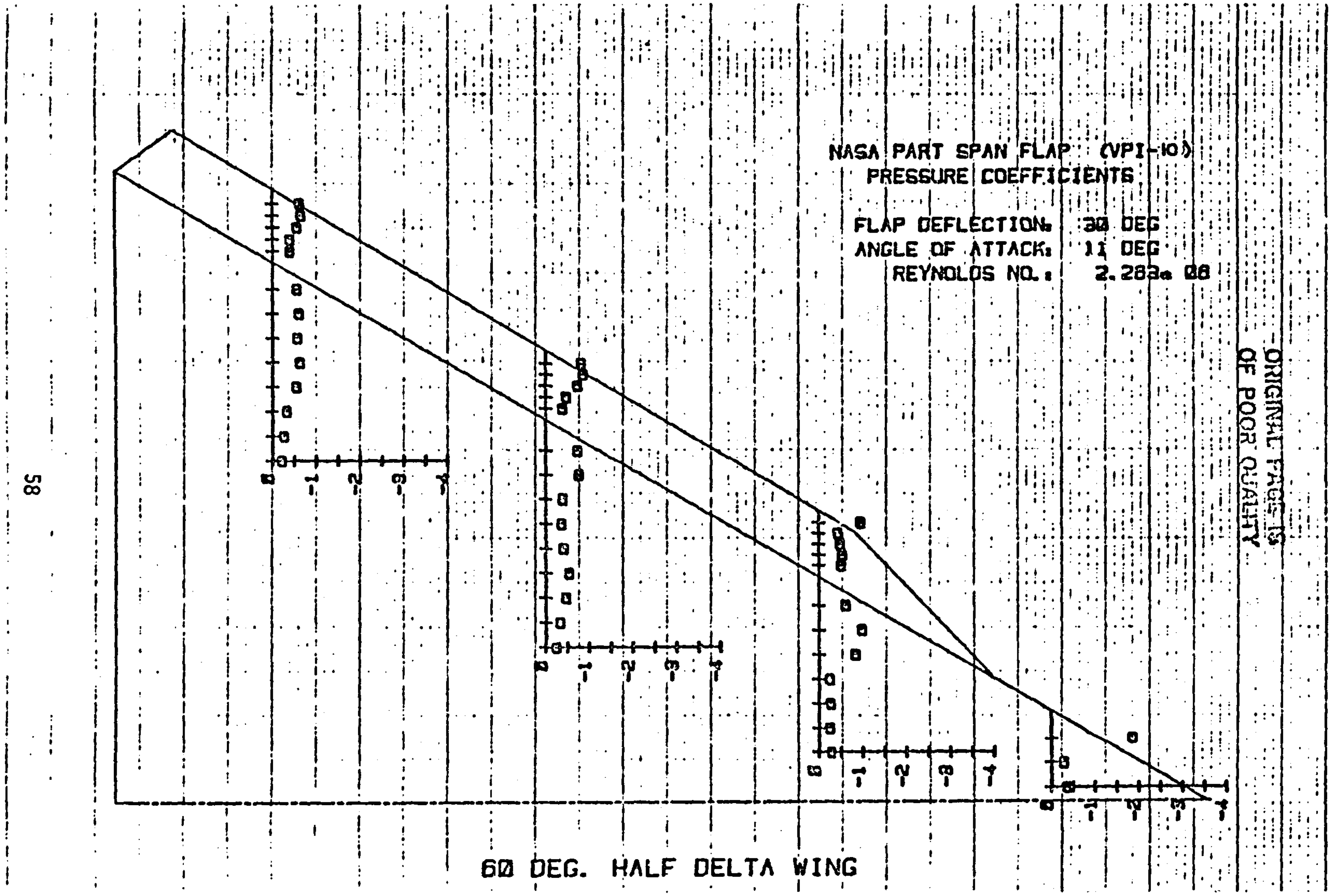

Figure 48 Pressures on VPI-10, No Fuselage, $\alpha = 11^0$, $\delta_f = 30^0$.

ORIGINAL PAGE IS OF POOR QUALITY

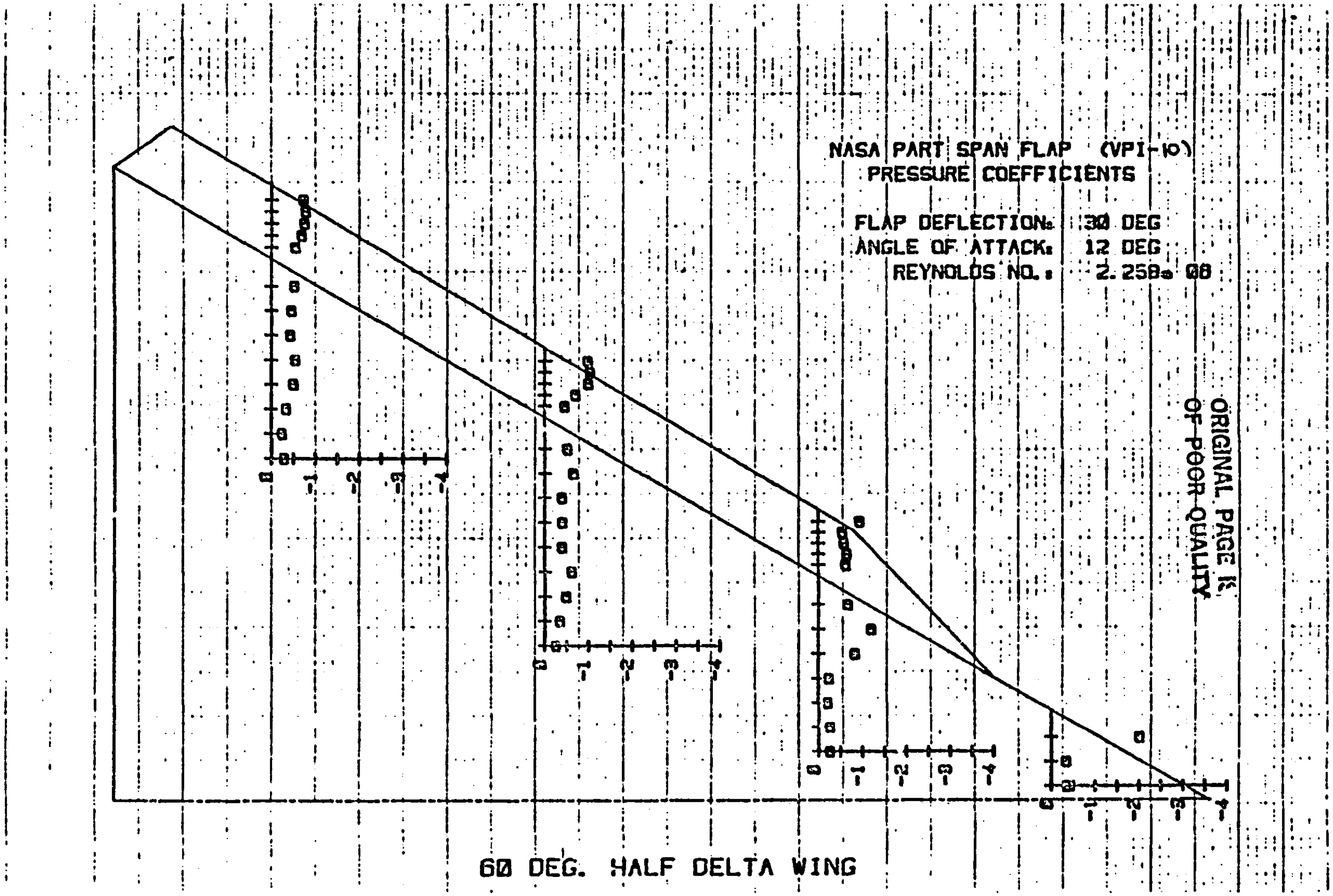

Figure 49 Pressures on VPI-10, No
Fuselage, α = 12^{o}, δ_{f} = 30^{o}.

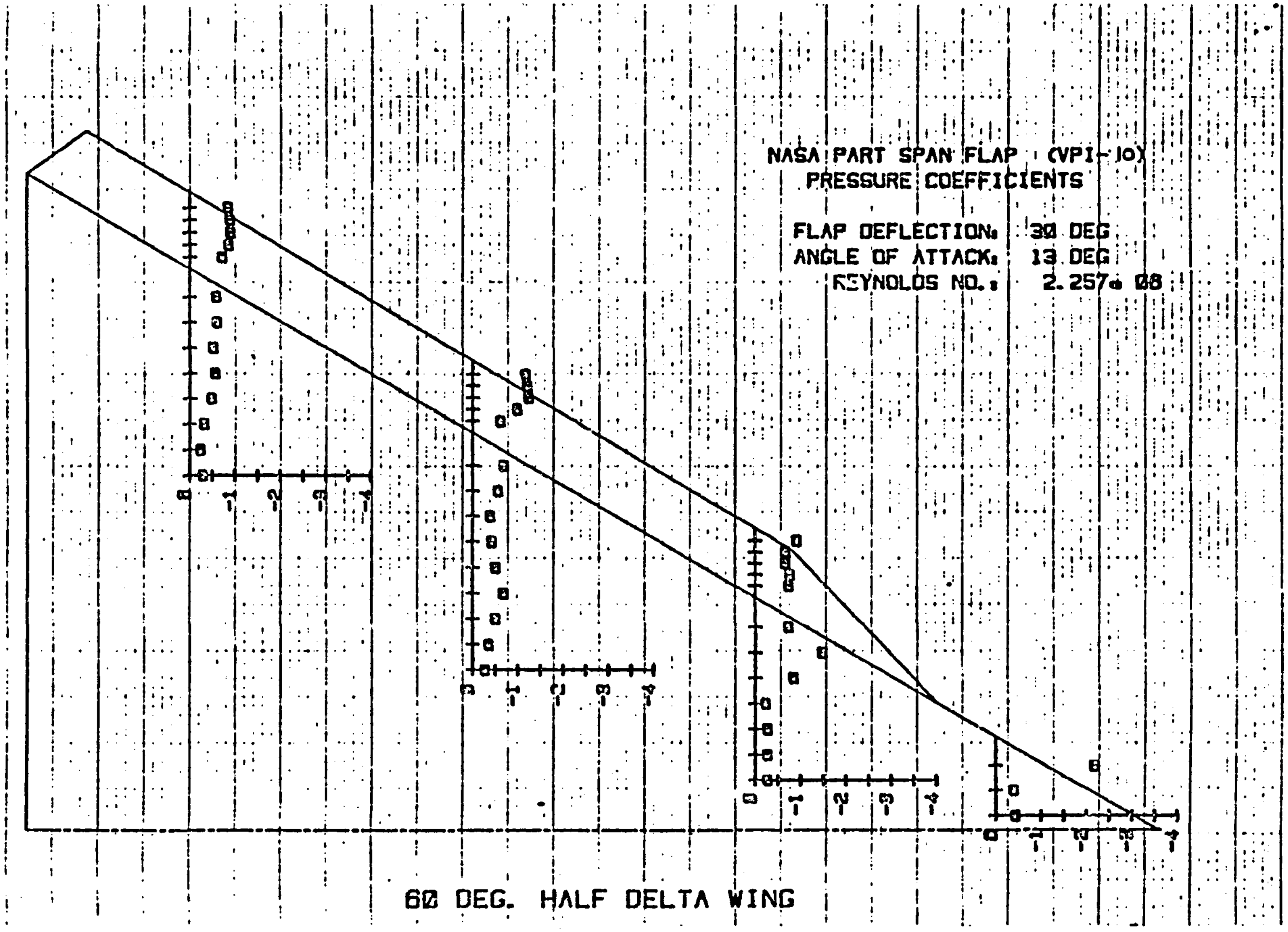

Figure 50 Pressures on VPI-10, No Fuselage, $\alpha = 13^0$, $\delta_f = 30^0$.

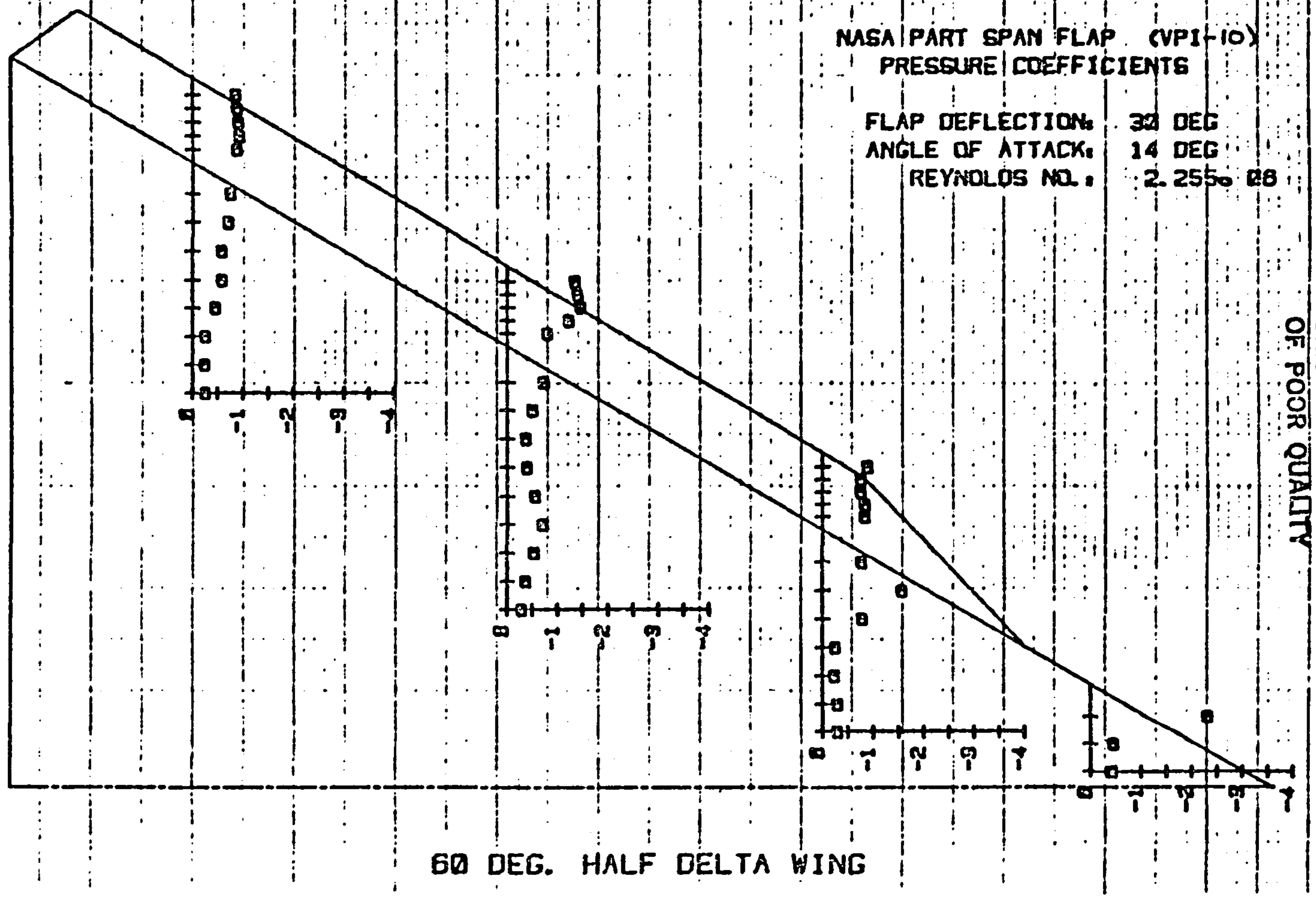

ORIGINAL PAGE IS OF POOR QUALITY

Figure 51 Pressures on VPI-10, No Fuselage, $\alpha = 14^{o}$, $\delta_f = 30^{o}$.

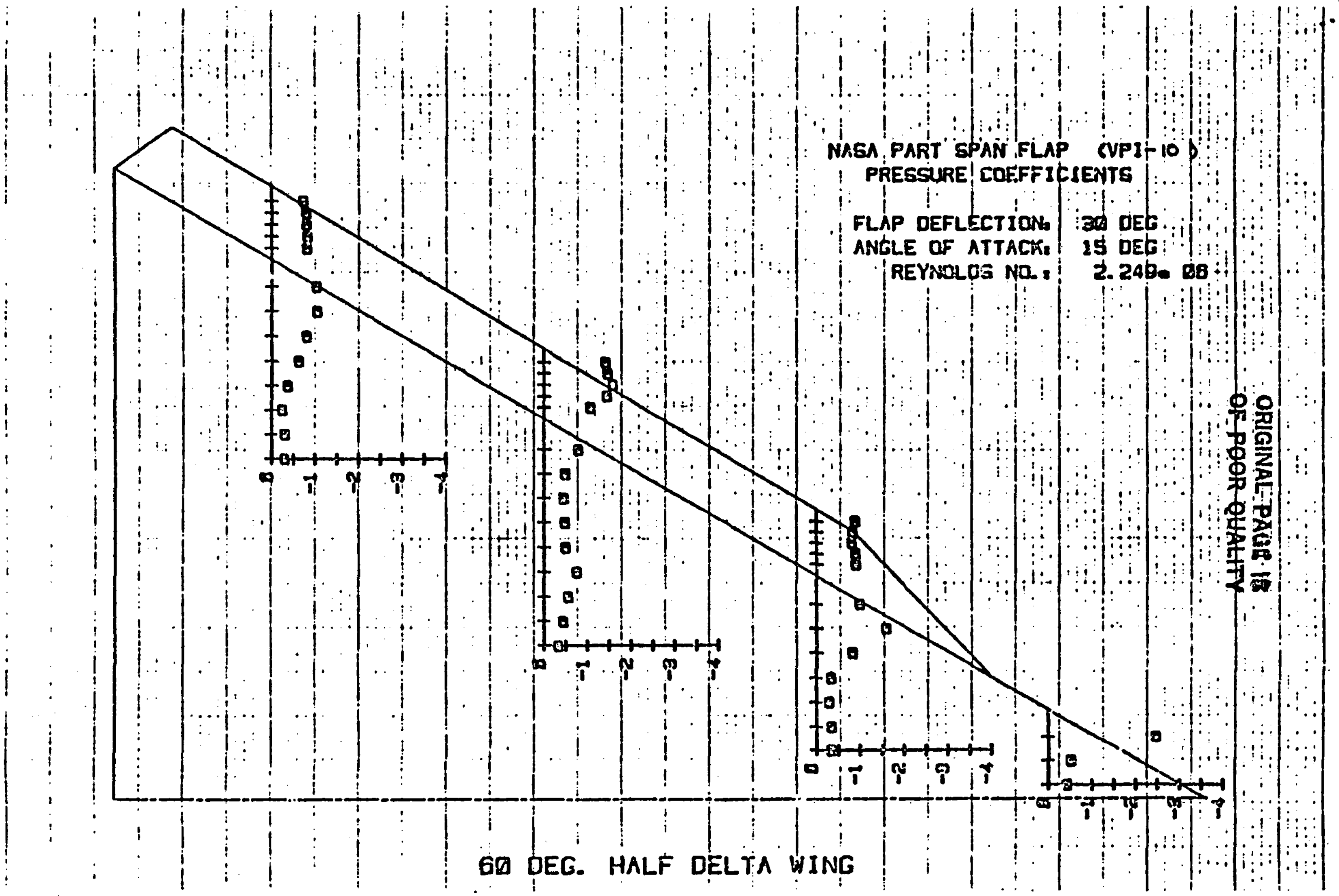

Figure 52 Pressures on VPI-10, No Fuselage, $\alpha = 15^{o}$, $\delta_f = 30^{o}$.

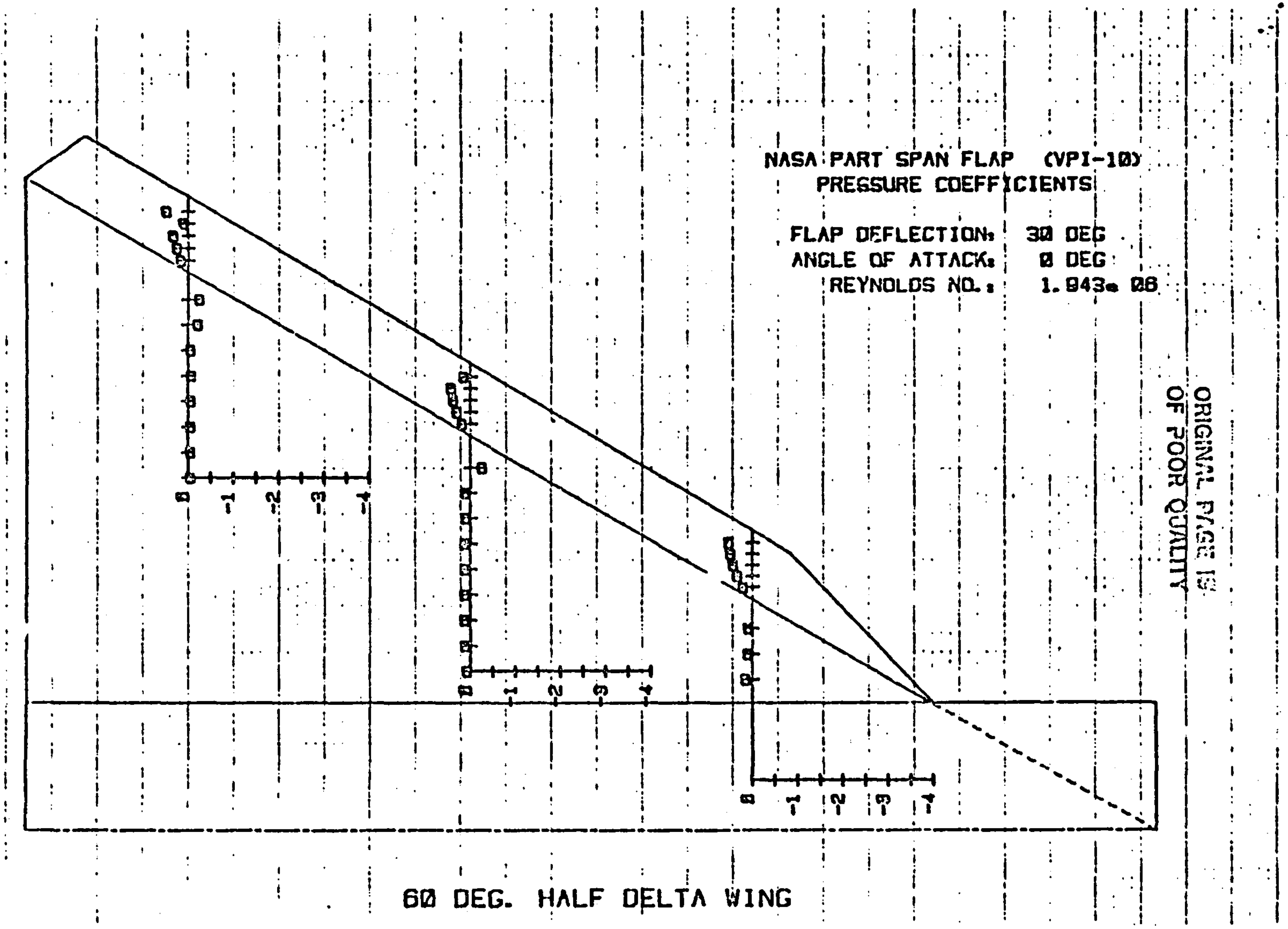

Figure 53 Pressures on VPI-10, with Fuselage, $\alpha = 0^0$, $\delta_f = 30^0$.

ORIGINAL PAGE IS OF POOR QUALITY

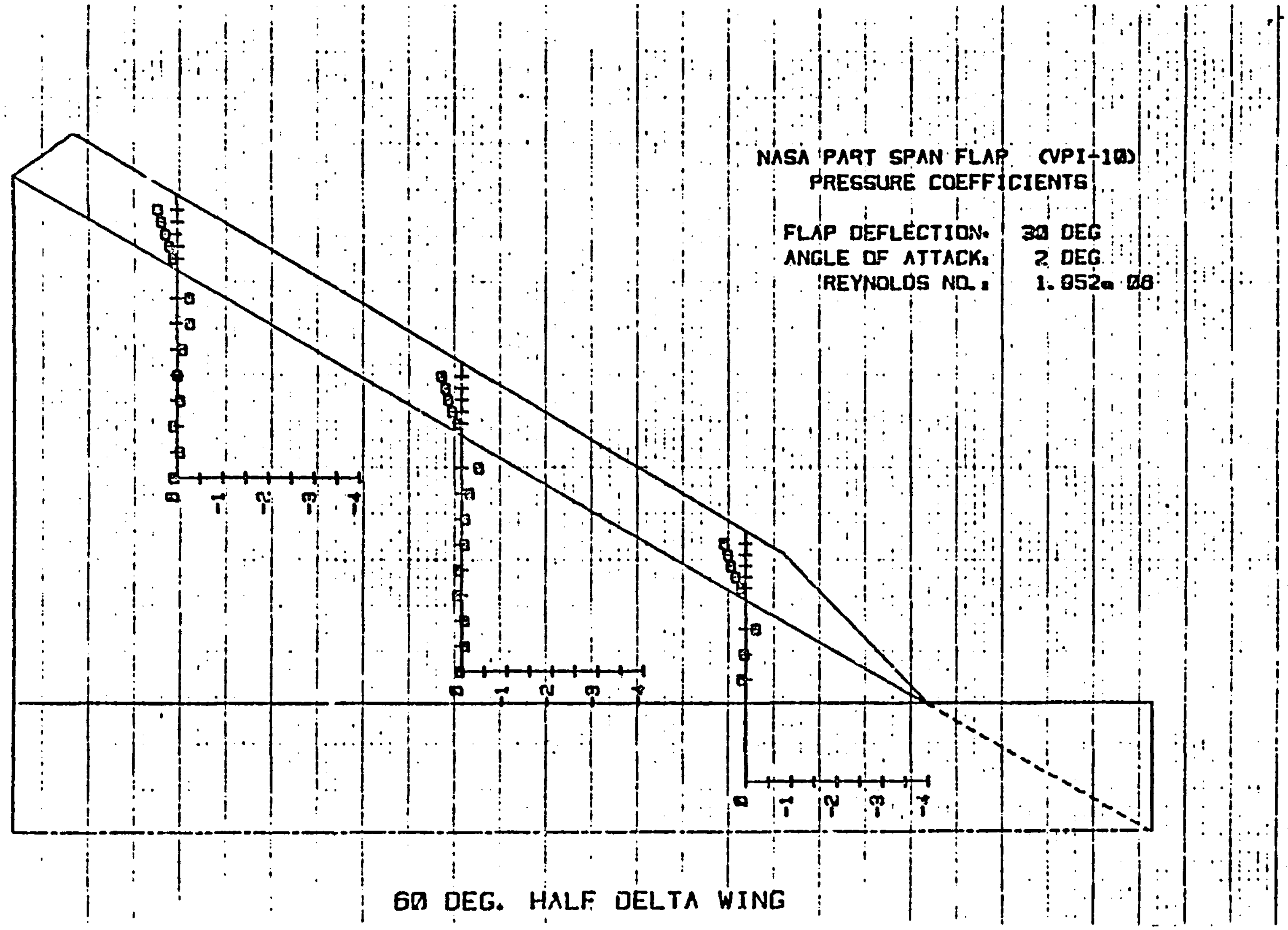

Figure 54 Pressures on VPI-10, with Fuselage, $\alpha = 2^0$, $\delta_f = 30^0$.

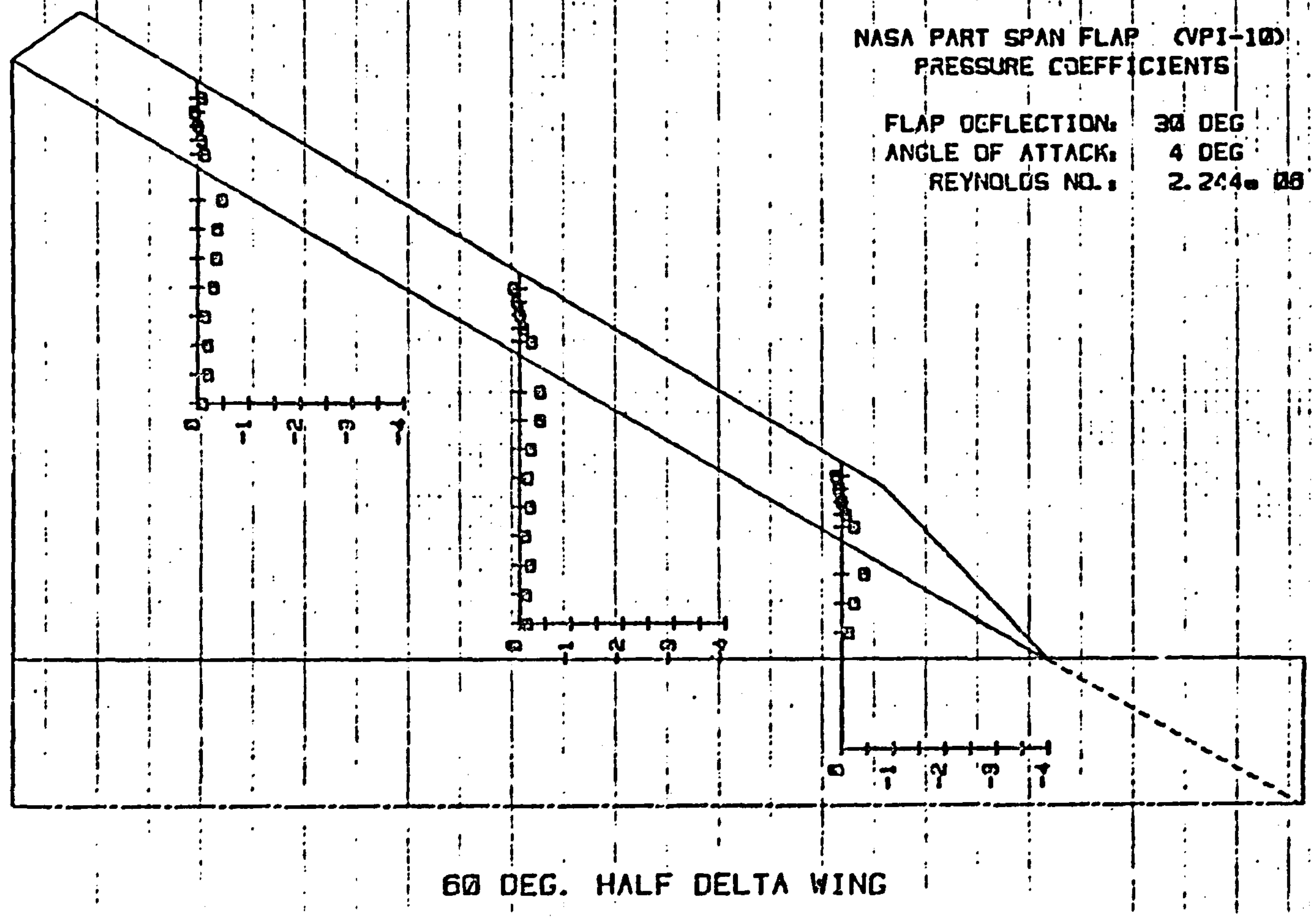

Figure 55 Pressures on VPI-10, with
Fuselage, α = 4^0, δ_f = 30^0.

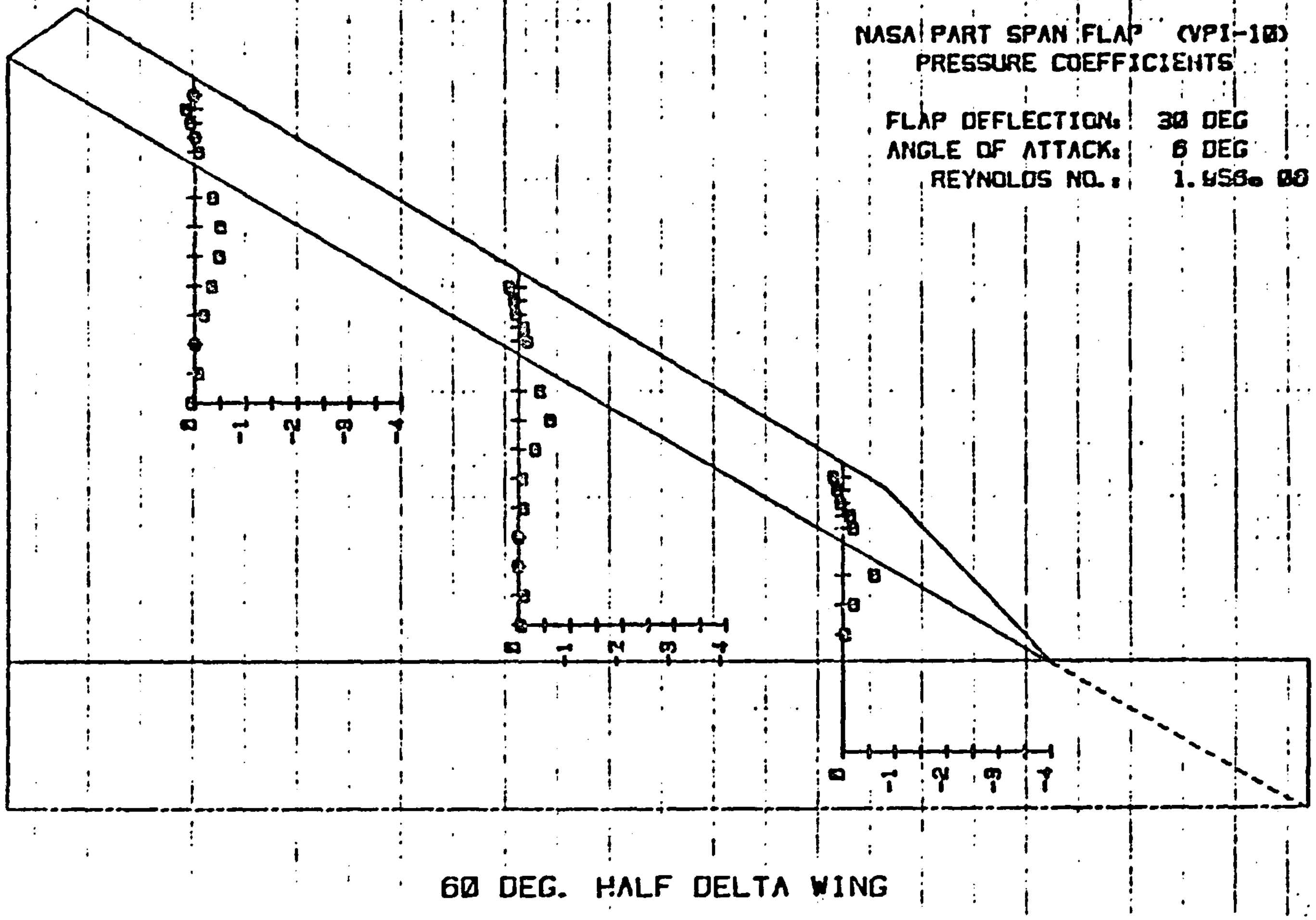

Figure 56 Pressures on VPI-10, with Fuselage, $\alpha = 6^0$, $\delta_f = 30^0$.

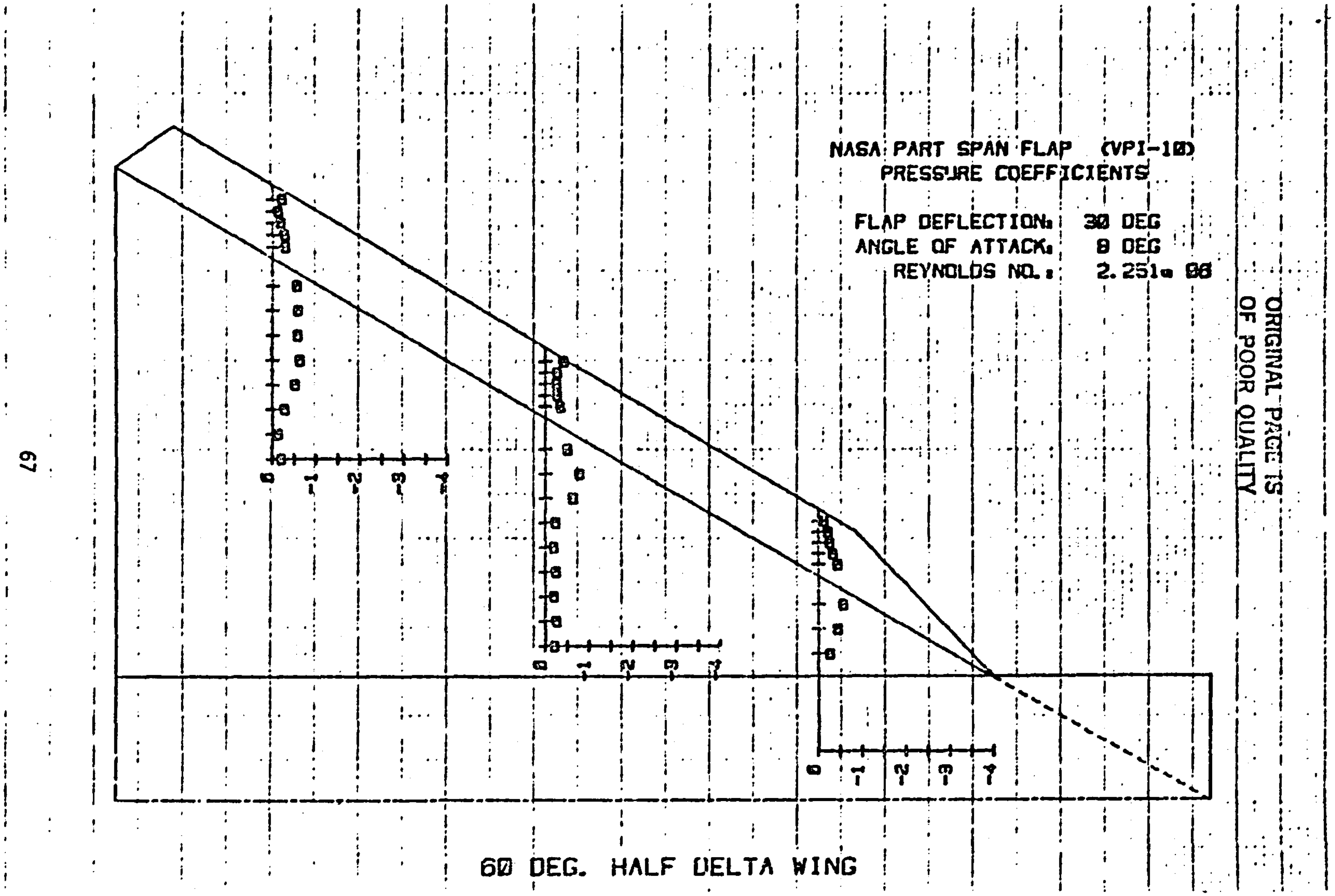

ORIGINAL PAGE IS OF POOR QUALITY

Figure 57 Pressures on VPI-10, with Fuselage, $\alpha = 8^o$, $\delta_f = 30^o$.

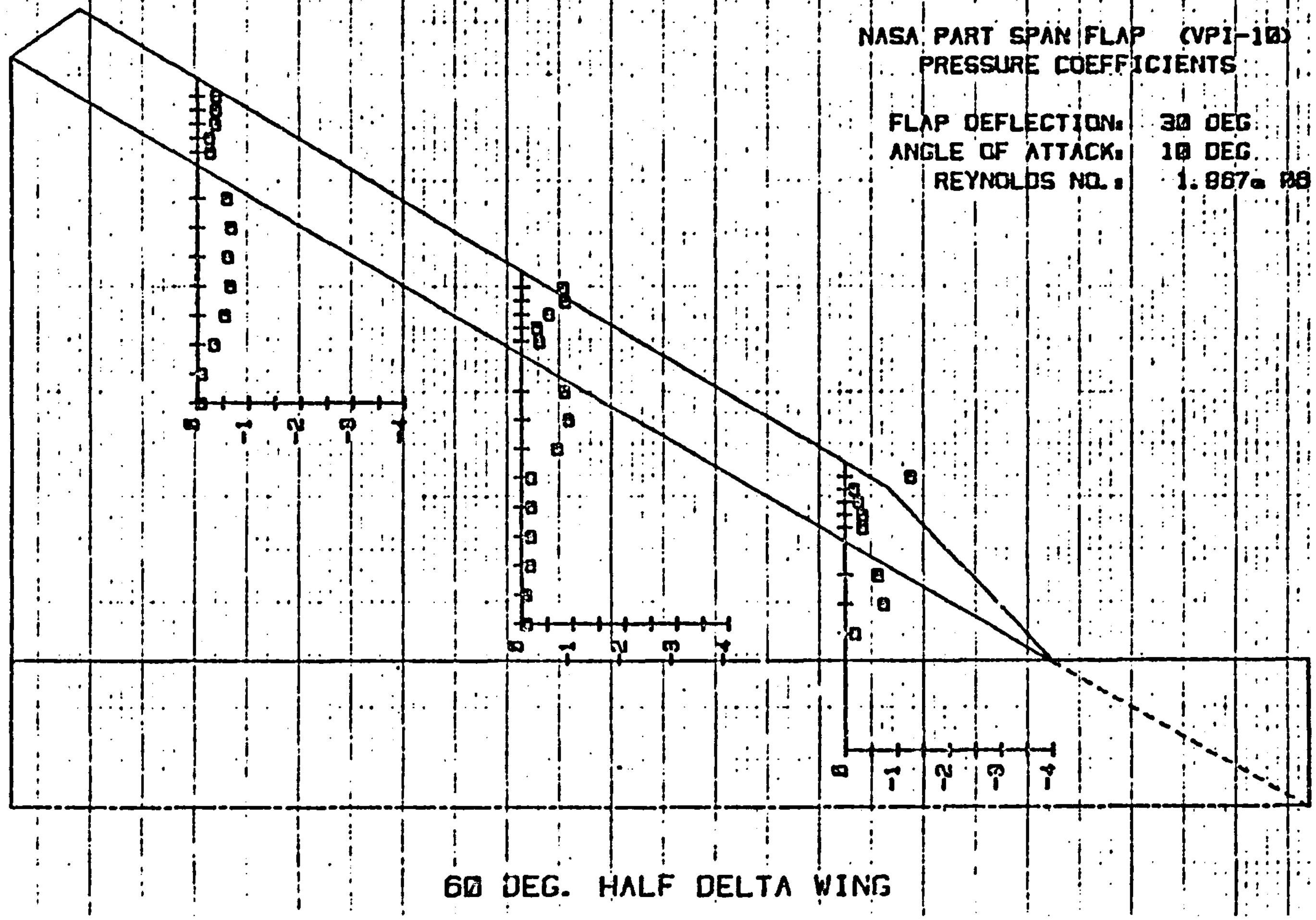

Figure 58 Pressures on VPI-10, with Fuselage, α = 10°, δ_f = 30°.

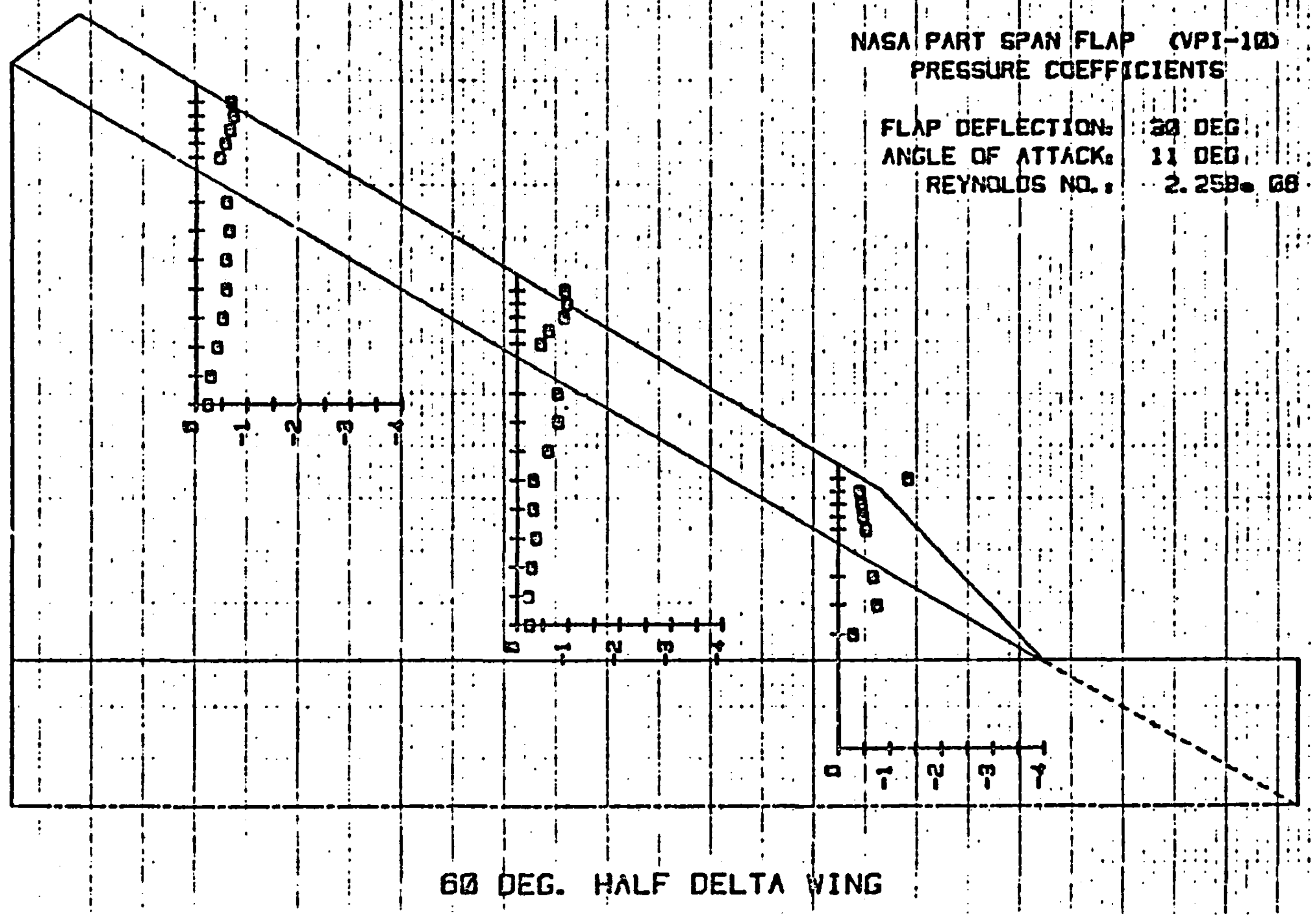

Figure 59 Pressures on VPI-10, with Fuselage, $\alpha = 11^{o}$, $\delta_f = 30^{o}$.

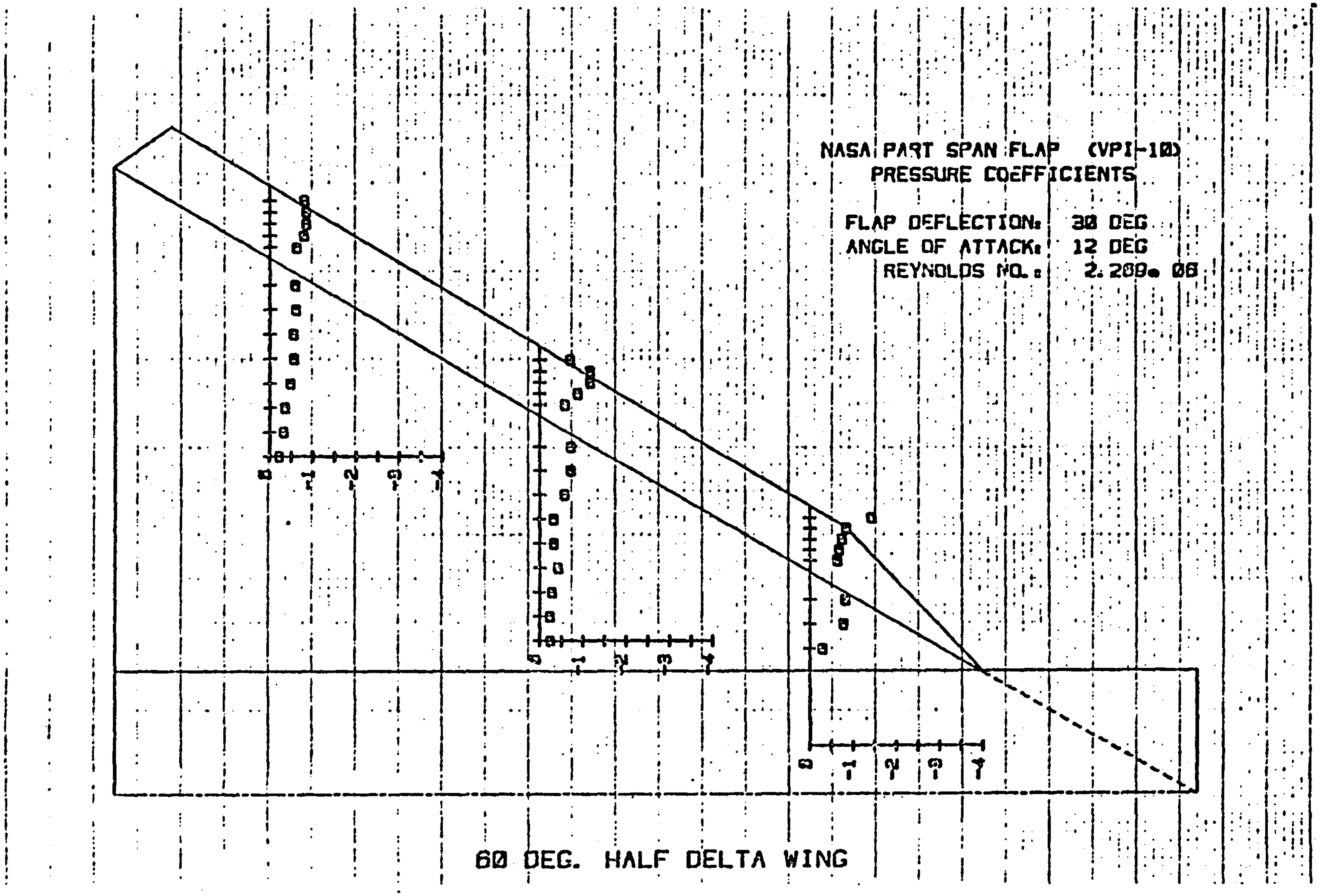

Figure 60 Pressures on VPI-10, with Fuselage, $\alpha = 12^o$, $\delta_f = 30^o$.

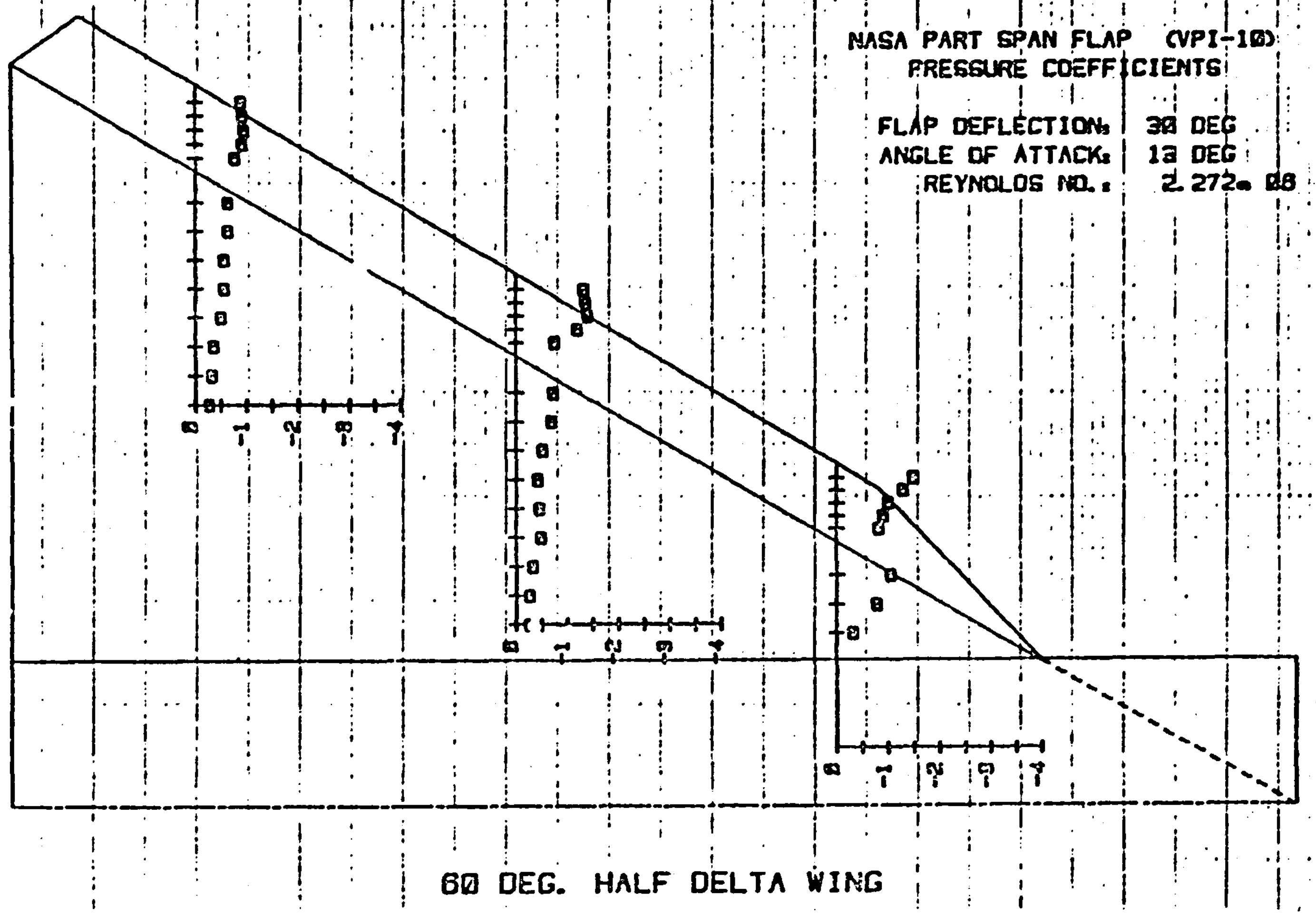

ORIGINAL PAGE IS
OF POOR QUALITY

Figure 61 Pressures on VPI-10, with
Fuselage, α = 13^{0}, δ_f = 30^{0}.

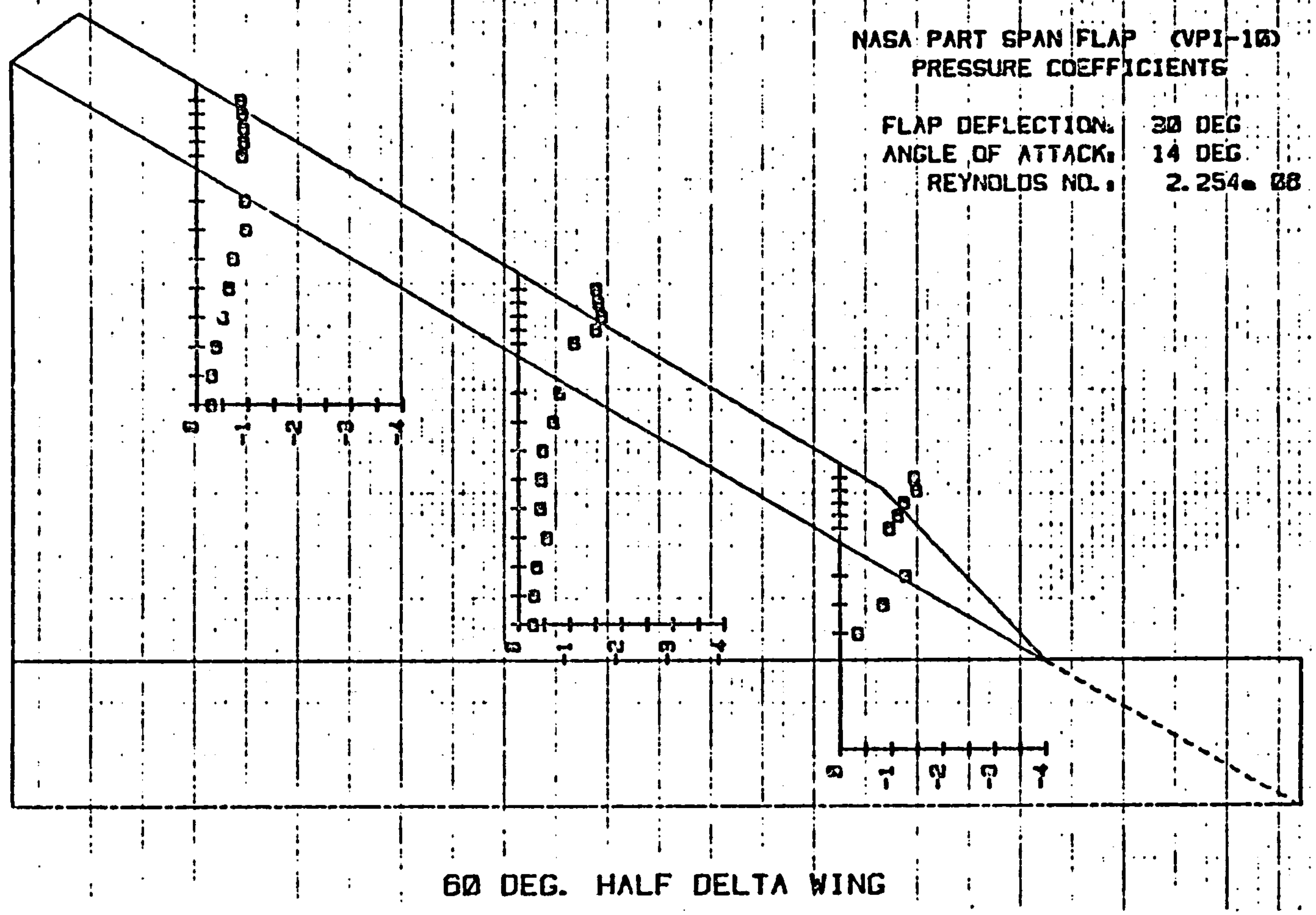

Figure 62 Pressures on VPI-10, with Fuselage, $\alpha = 14^{0}$, $\delta_f = 30^{0}$.

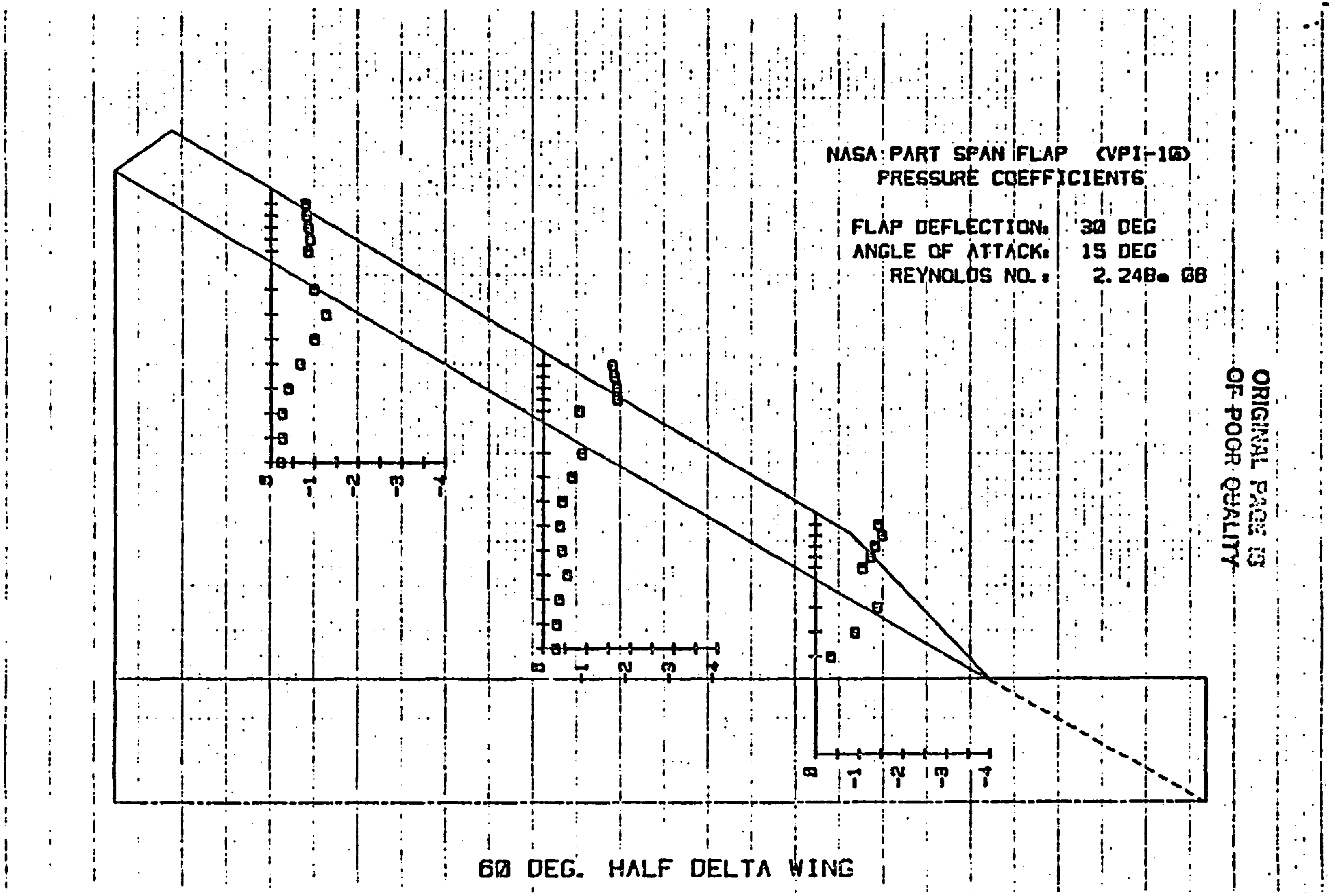

Figure 63 Pressures on VPI-10, with Fuselage, $\alpha = 15^0$, $\delta_f = 30^0$.

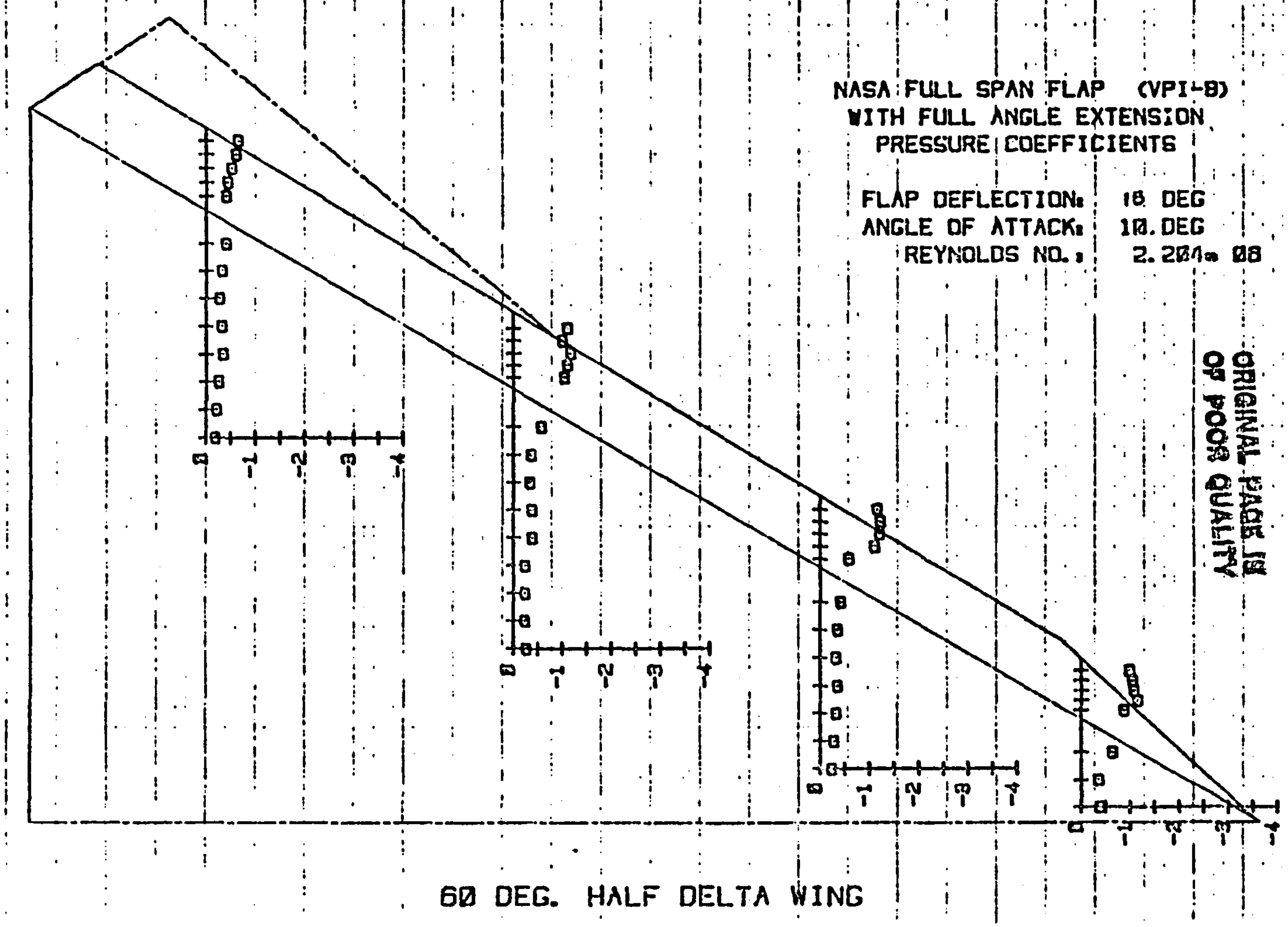

ORIGINAL PAGE IS OF POOR QUALITY

Figure 64 Pressures on VPI-8 with Extension Deflected Along Surface of Flap, $\alpha = 10^0$, $\delta_f = 15^0$.

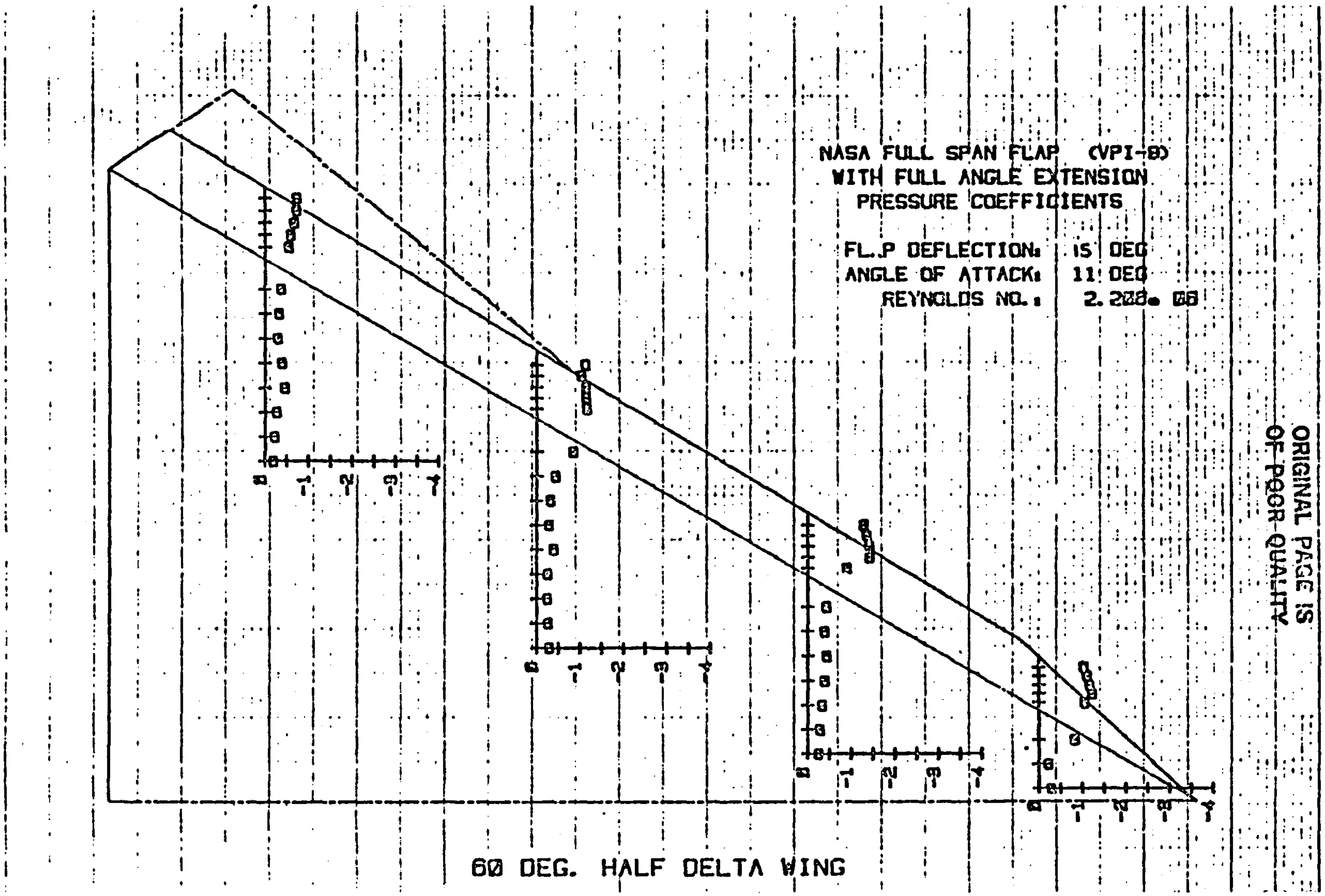

Figure 65 Pressures on VPI-8 with Extension Deflected Along Surface of Flap, $\alpha = 11^{0}$, $\delta_f = 15^{0}$.

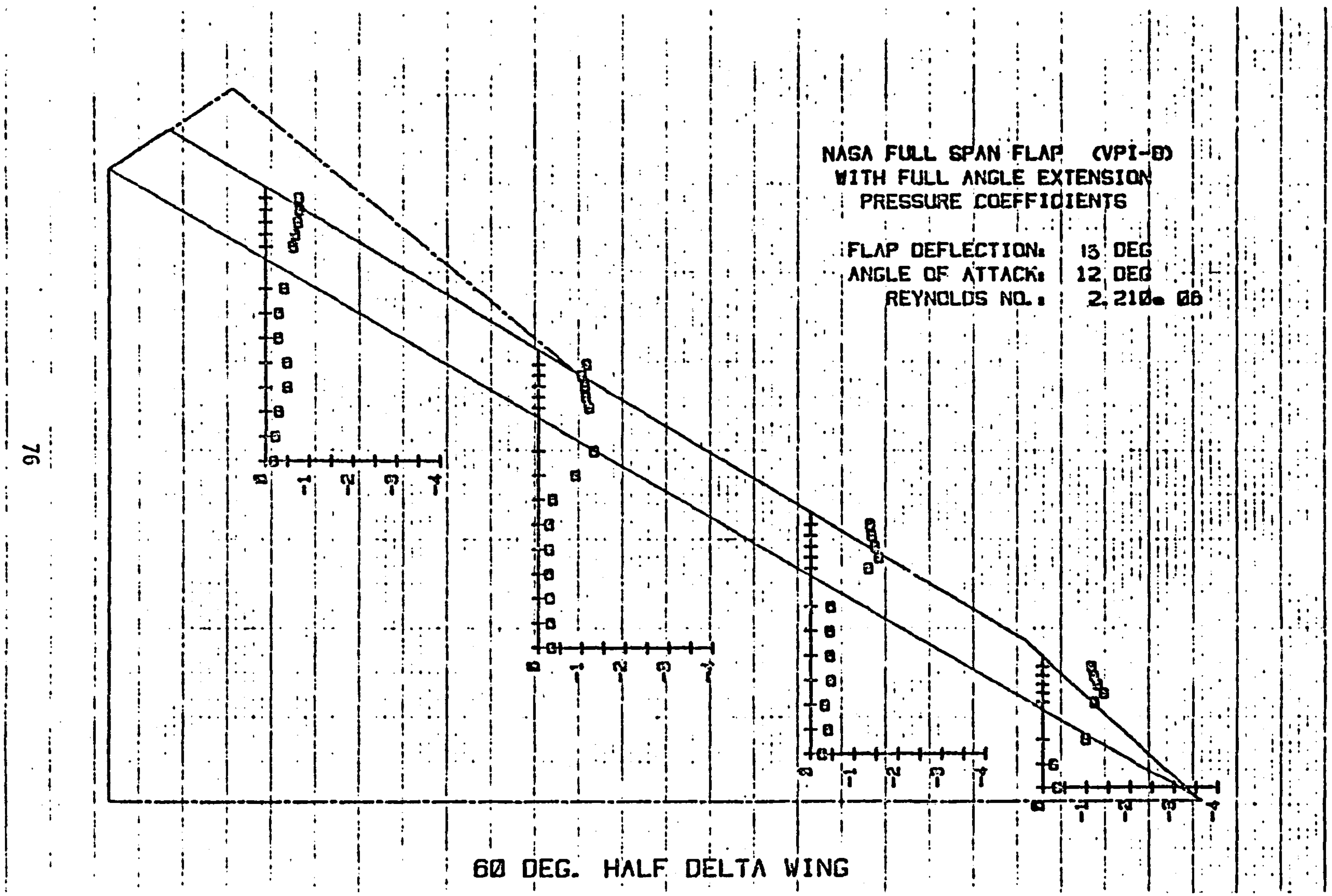

Figure 66 Pressures on VPI-8 with Extension Deflected Along Surface of Flap, $\alpha = 12^{0}$, $\delta_f = 15^{0}$.

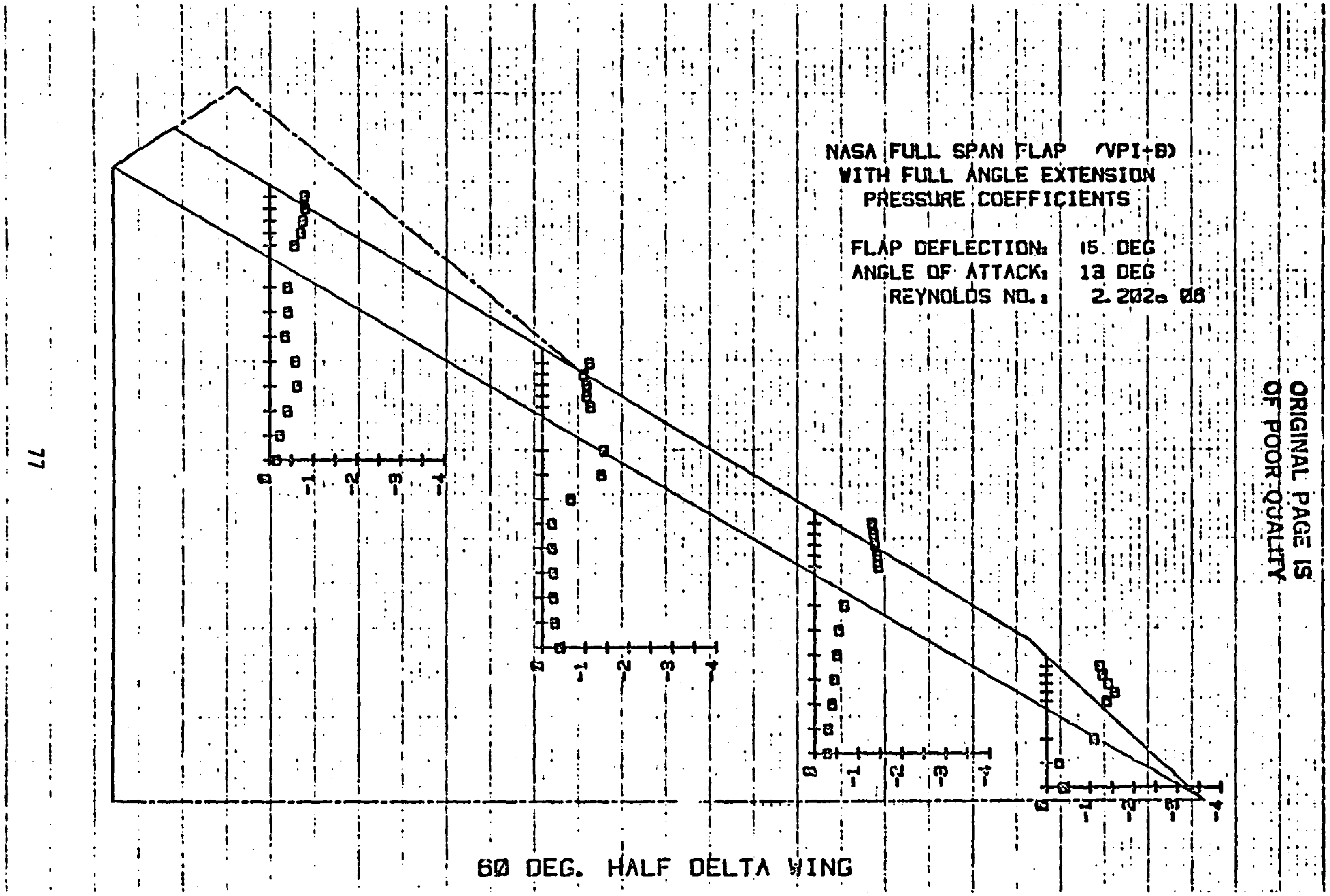

Figure 67 Pressures on VPI-8 with Extension Deflected Along Surface of Flap, $\alpha = 13^{o}$, $\delta_f = 15^{o}$.

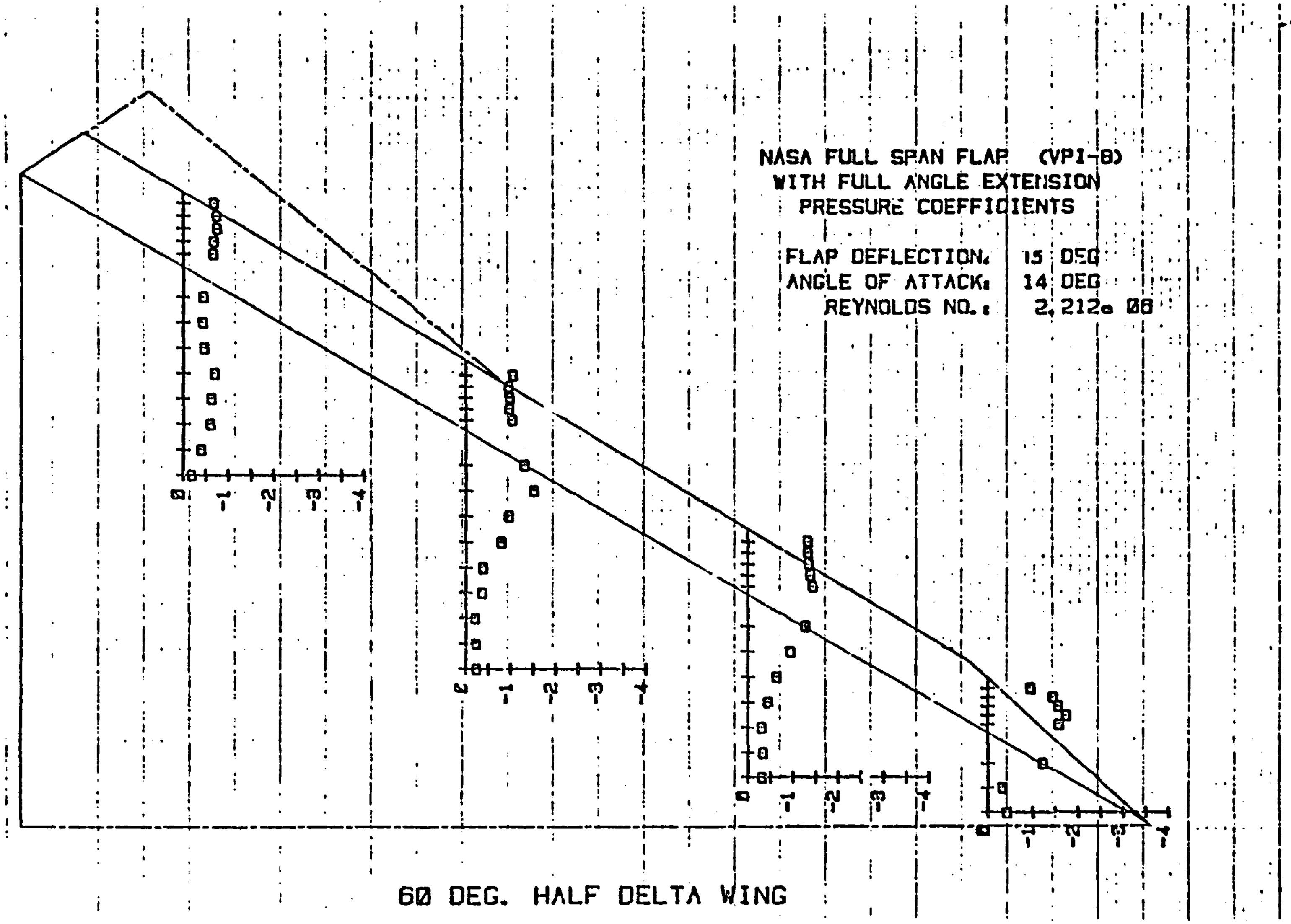

Figure 68 Pressures on VPI-8 with Extension Deflected Along Surface of Flap, $\alpha = 14^{0}$, $\delta_f = 15^{0}$.

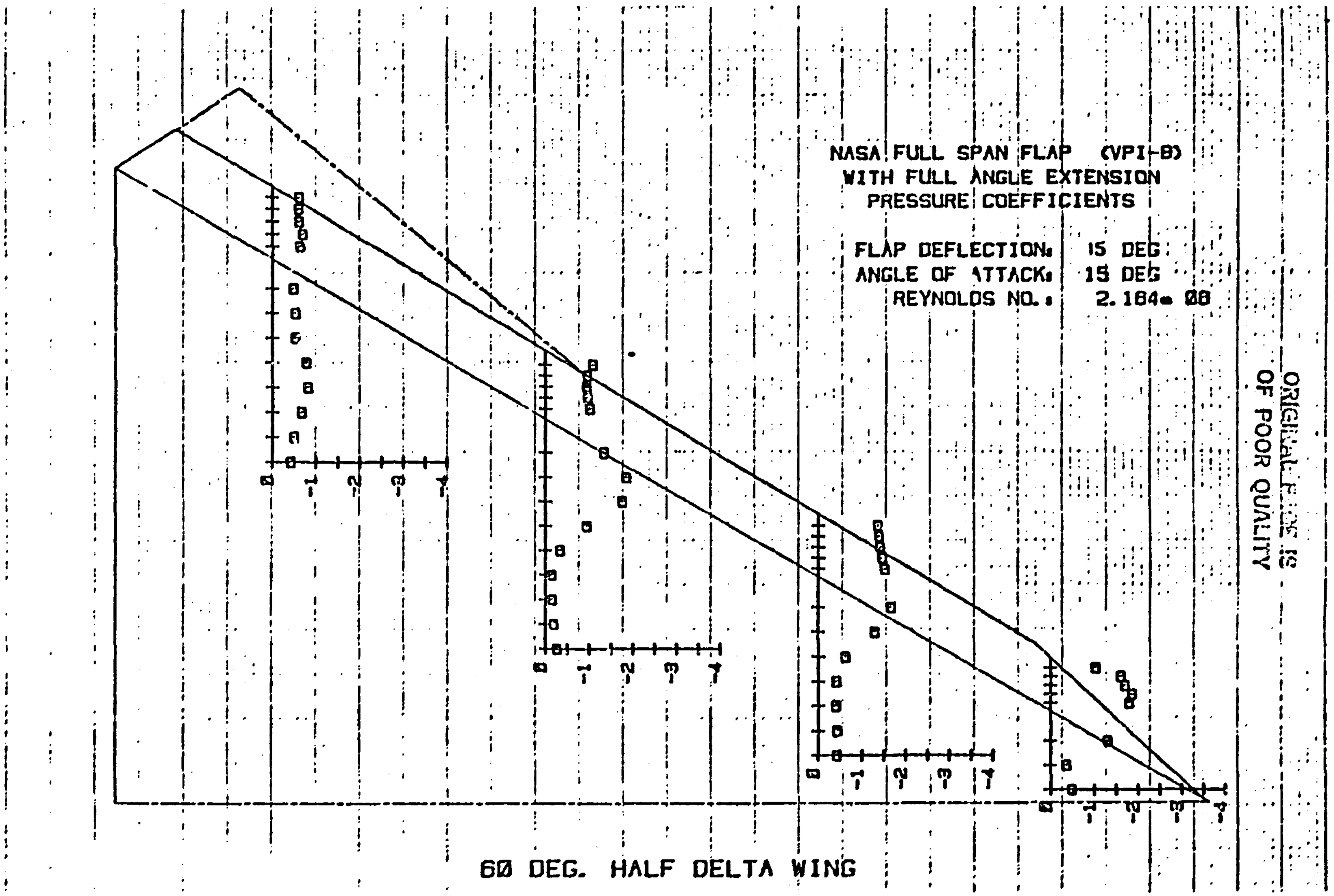

Figure 69 Pressures on VPI-8 with Extension Deflected Along Surface of Flap, $\alpha = 15^0$, $\delta_f = 15^0$.

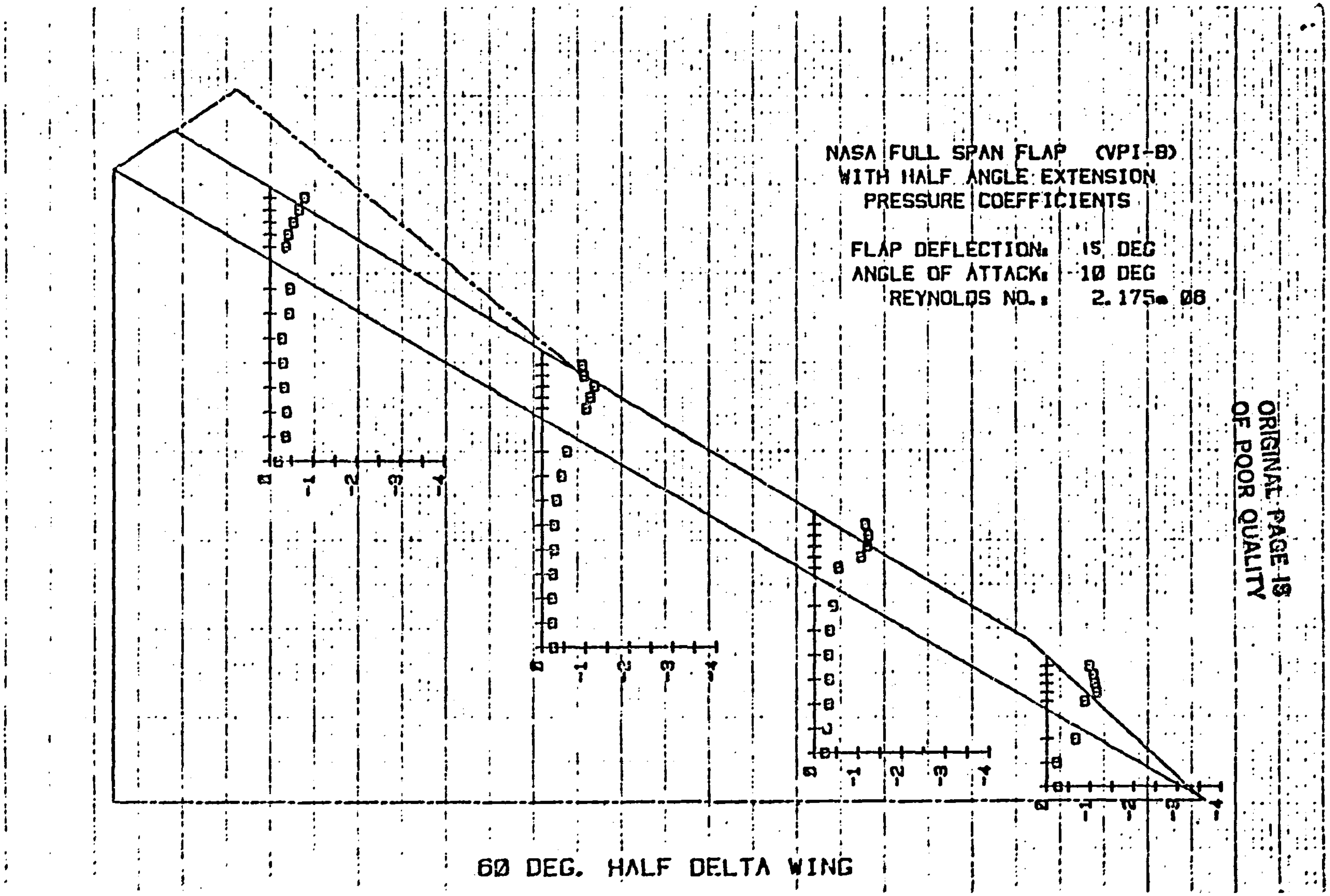

Figure 70 Pressures on VPI-8 with Extension Deflected Along Chordline of Flap, $\alpha = 10^o$, $\delta_f = 15^o$.

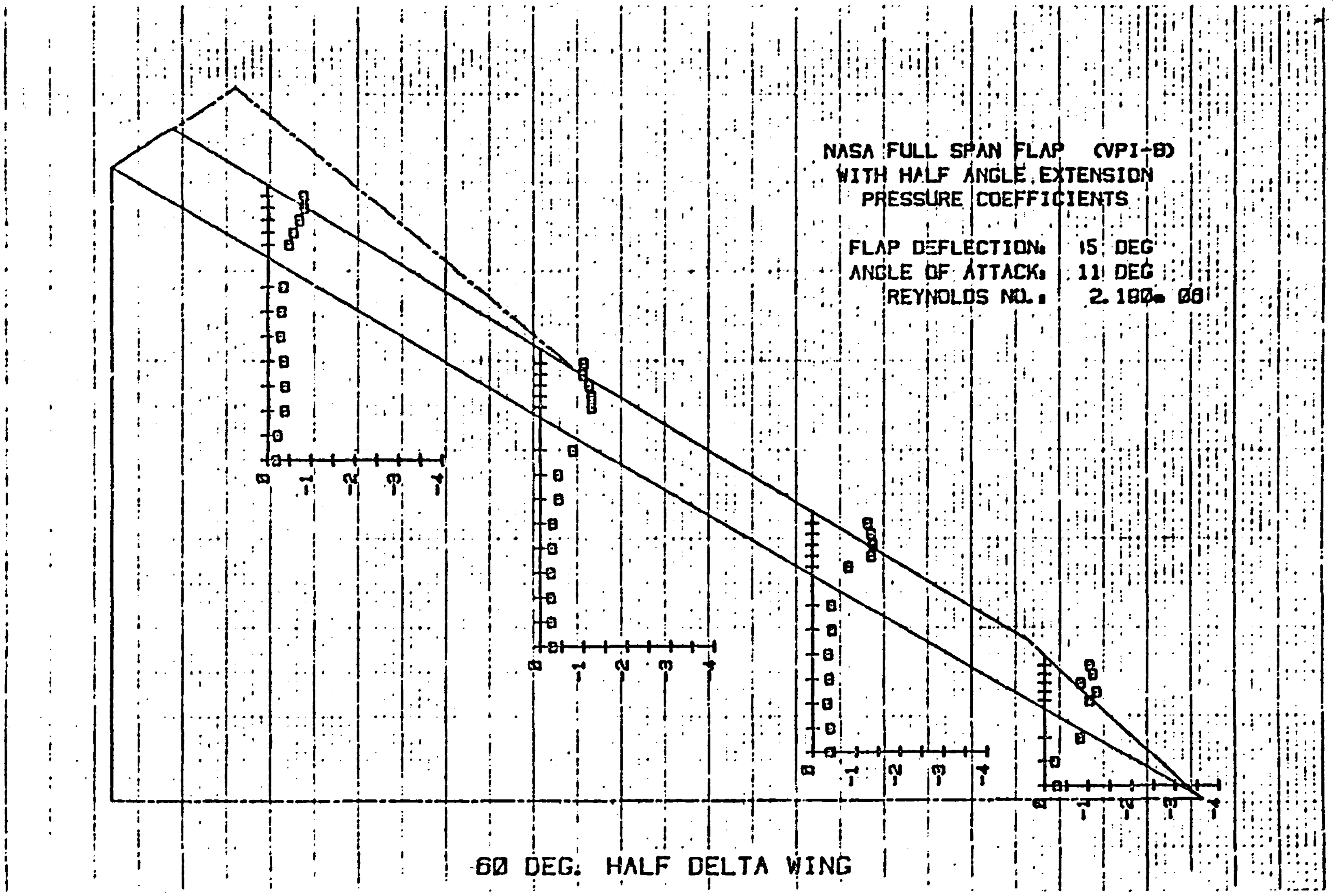

Figure 71 Pressures on VPI-8 with Extension Deflected Along Chordline of Flap, $\alpha = 11^{\circ}$, $\delta_f = 15^{\circ}$.

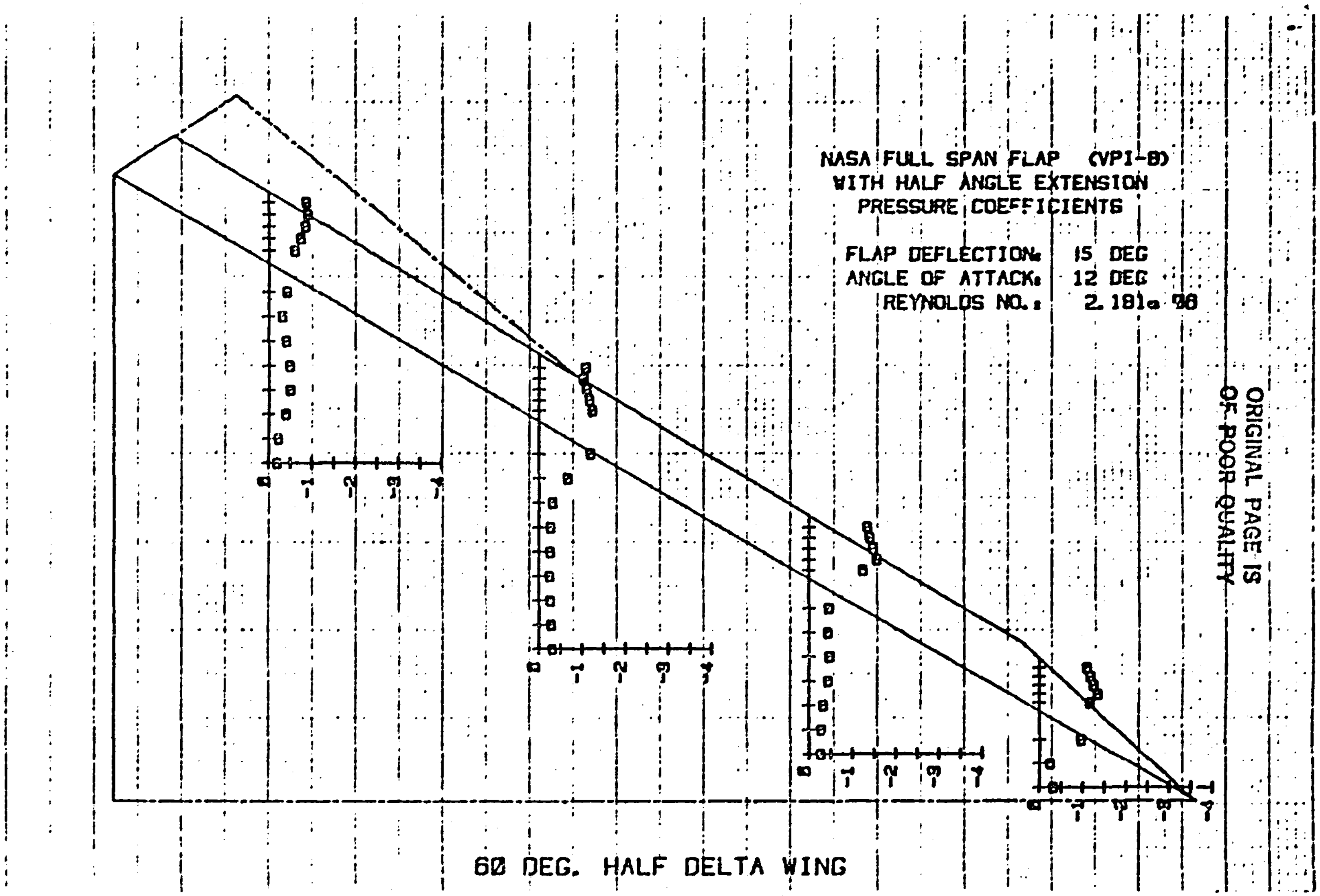

Figure 72 Pressures on VPI-8 with Extension Deflected Along Chordline of Flap, $\alpha = 12^{\circ}$, $\delta_f = 15^{\circ}$.

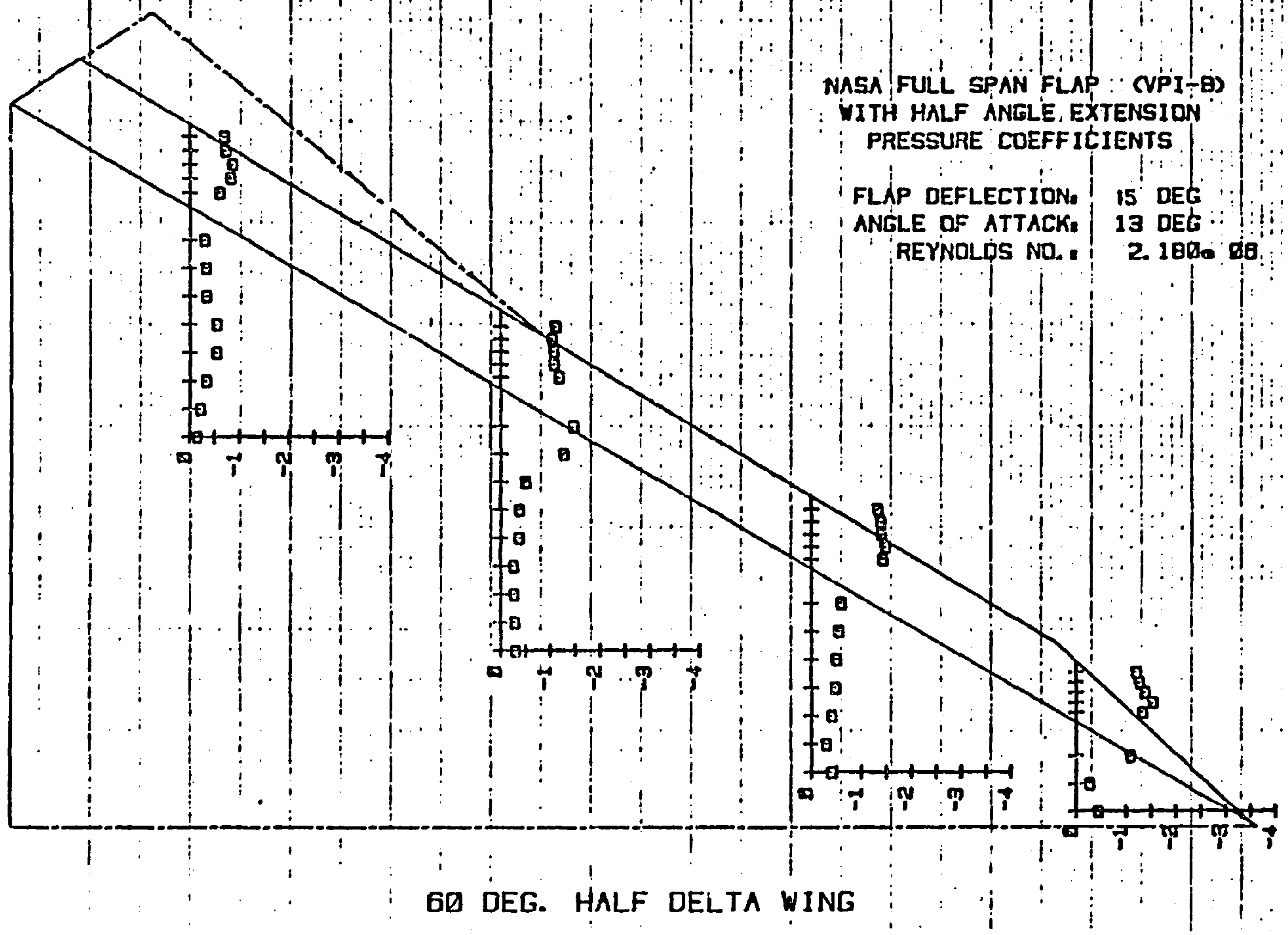

Figure 73 Pressures on VPI-8 with Extension Deflected Along Chordline of Flap, $\alpha = 13^{0}$, $\delta_f = 15^{0}$.

ORIGINAL PAGE IS
OF POOR QUALITY

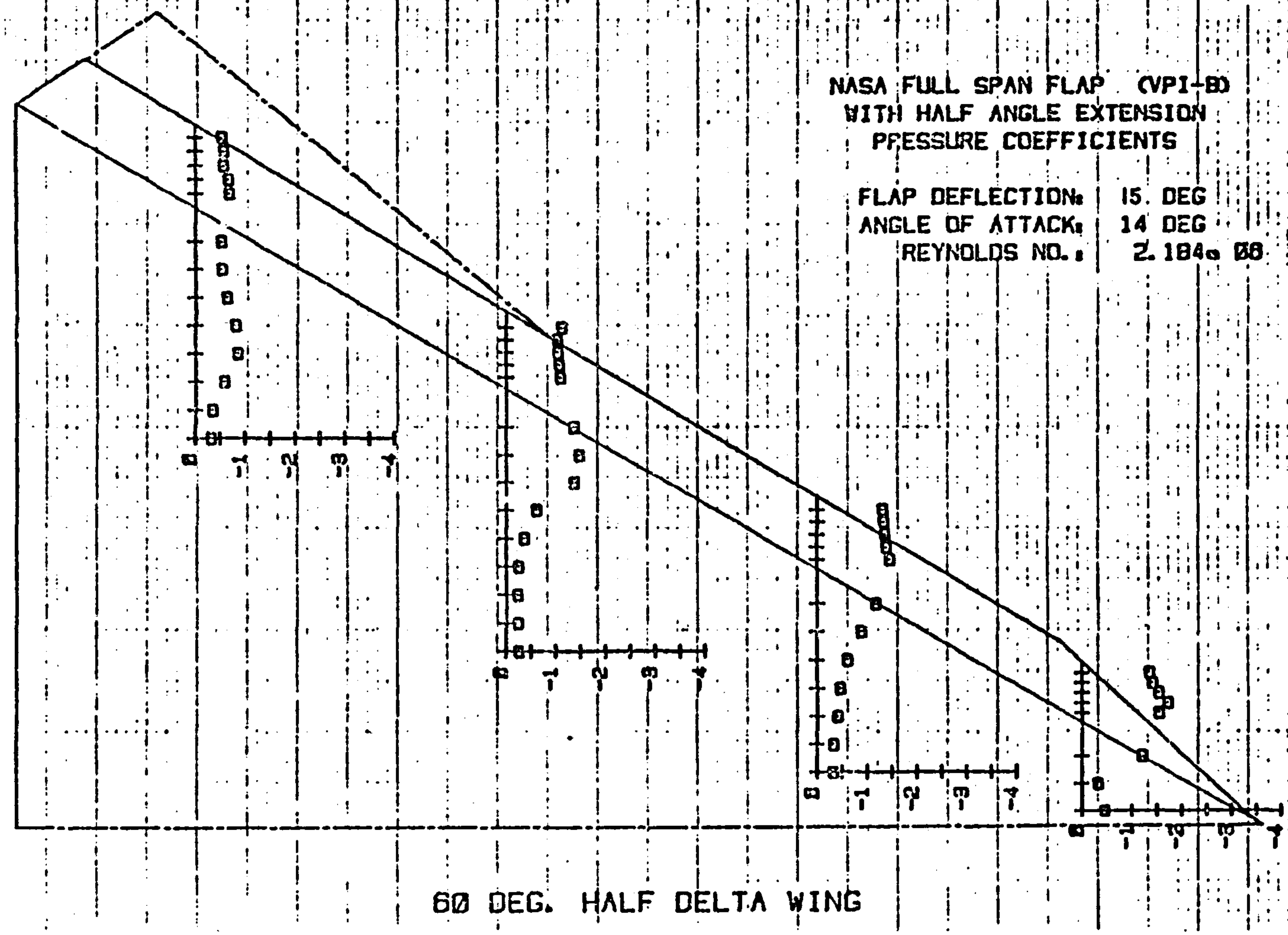

Figure 74 Pressures on VPI-8 with Extension Deflected Along Chordline of Flap, $\alpha = 14^{o}$, $\delta_f = 15^{o}$.

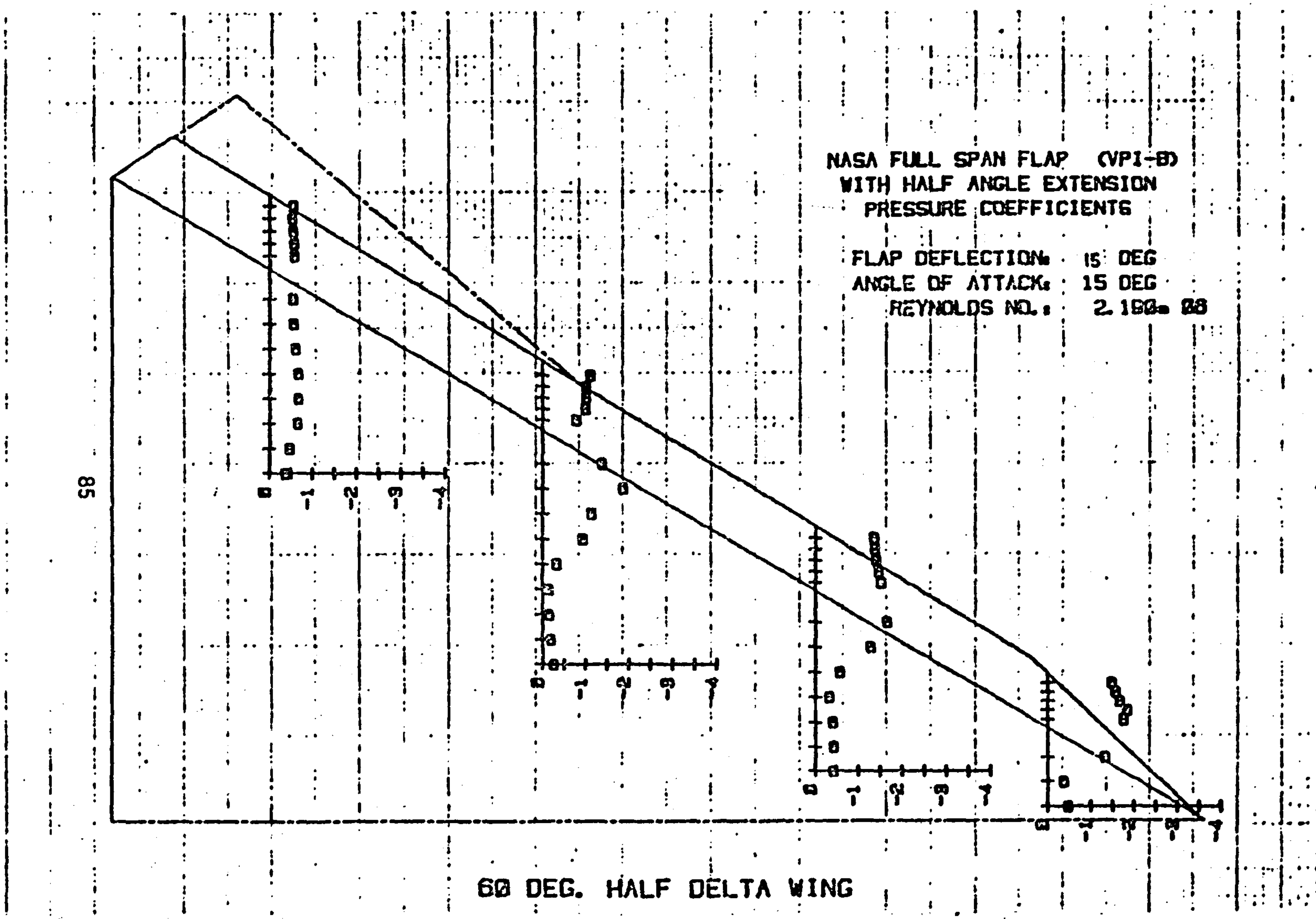

Figure 75 Pressures on VPI-8 with Extension Deflected Along Chordline of Flap, $\alpha = 15^o$, $\delta_f = 15^o$.

END

DATE

FILMED

APR 29 1983

End of Document